JPRS L/8227

17 January 1979

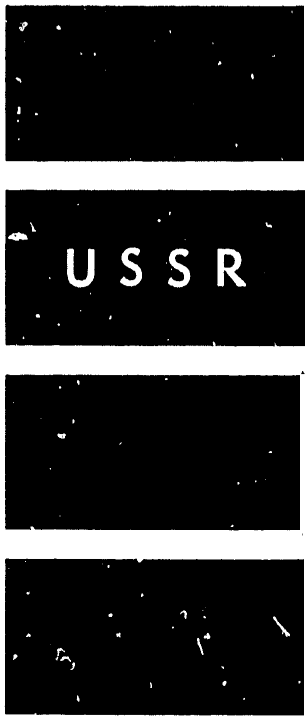

TRANSLATIONS ON USSR SCIENCE AND TECHNOLOGY
PHYSICAL SCIENCES AND TECHNOLOGY
(FOUO 4/79)

U. S. JOINT PUBLICATIONS RESEARCH SERVICE

NOTE

JPRS publications contain information primarily from foreign newspapers, periodicals and books, but also from news agency transmissions and broadcasts. Materials from foreign-language sources are translated; those from English-language sources are transcribed or reprinted, with the original phrasing and other characteristics retained.

Headlines, editorial reports, and material enclosed in brackets [] are supplied by JPRS. Processing indicators such as [Text] or [Excerpt] in the first line of each item, or following the last line of a brief, indicate how the original information was processed. Where no processing indicator is given, the information was summarized or extracted.

Unfamiliar names rendered phonetically or transliterated are enclosed in parentheses. Words or names preceded by a question mark and enclosed in parentheses were not clear in the original but have been supplied as appropriate in context. Other unattributed parenthetical notes within the body of an item originate with the source. Times within items are as given by source.

The contents of this publication in no way represent the policies, views or attitudes of the U.S. Government.

PROCUREMENT OF PUBLICATIONS

JPRS publications may be ordered from the National Technical Information Service, Springfield, Virginia 22151. In ordering, it is recommended that the JPRS number, title, date and author, if applicable, of publication be cited.

Current JPRS publications are announced in Government Reports Announcements issued semi-monthly by the National Technical Information Service, and are listed in the Monthly Catalog of U.S. Government Publications issued by the Superintendent of Documents, U.S. Government Printing Office, Washington, D.C. 20402.

Indexes to this report (by keyword, author, personal names, title and series) are available through Bell & Howell, Old Mansfield Road, Wooster, Ohio, 44691.

Correspondence pertaining to matters other than procurement may be addressed to Joint Publications Research Service, 1000 North Glebe Road, Arlington, Virginia 22201.

BIBLIOGRAPHIC DATA SHEET	1. Report No. JPRS L/8227	2.	3. Recipient's Accession No.
4. Title and Subtitle TRANSLATIONS ON USSR SCIENCE AND TECHNOLOGY - PHYSICAL SCIENCES AND TECHNOLOGY, (FOUO 4/79)			5. Report Date 17 January 1979 6.
7. Author(s)			8. Performing Organization Rept. No.
9. Performing Organization Name and Address Joint Publications Research Service 1000 North Glebe Road Arlington, Virginia 22201			10. Project/Task/Work Unit No. 11. Contract/Grant No.
12. Sponsoring Organization Name and Address As above			13. Type of Report & Period Covered 14.

15. Supplementary Notes

16. Abstracts

The report contains information on aeronautics; astronomy and astrophysics; atmospheric sciences; chemistry; earth sciences and oceanography; electronics and electrical engineering; energy conversion; materials; mathematical sciences; cybernetics, computers; mechanical, industrial, civil, and marine engineering; methods and equipment; missile technology; navigation, communications, detection, and countermeasures, nuclear science and technology; ordnance; physics; propulsion and fuels; space technology; and scientists and scientific organization in the physical sciences.

17. Key Words and Document Analysis. 17a. Descriptors

USSR
Aeronautics
Astronomy
Astrophysics
Atmospheric Sciences
Chemistry
Computers
Cybernetics
Earth Sciences
Oceanography
Electronics
Electrical Engineering
Energy Conversion
Materials
Mathematics
Mechanical Engineering
Civil Engineering
Industrial Engineering
Marine Engineering
Methods
Equipment
Missile Technology
Navigation and Communications
Detection and Countermeasures
Nuclear Science and Technology
Ordnance
Physics
Propulsion and Fuels
Space Technology

17b. Identifiers/Open-Ended Terms

17c. COSATI Field/Group 01,03,04,07,08,09,10,11,12,13,14,16,17,18,19,20,21,22

18. Availability Statement	19. Security Class (This Report)	21. No. of Pages
For Official Use Only. Limited Number of Copies Available From JPRS	UNCLASSIFIED	108
	20. Security Class (This Page) UNCLASSIFIED	22. Price

APPROVED FOR RELEASE: 2007/02/08: CIA-RDP82-00850R000100010034-2

JPRS L/8227

17 January 1979

TRANSLATIONS ON USSR SCIENCE AND TECHNOLOGY
PHYSICAL SCIENCES AND TECHNOLOGY

(FOUO 4/79)

CONTENTS

PAGE

ELECTRONICS AND ELECTRICAL ENGINEERING

Digital Detection of Incoherent Pulse Signals for the Case of a Changing Noise Power
(K.K. Vasil'yev; IZVESTIYA VUZ RADIOELEKTRONIKA, No 7, 1978) 1

Two-Stage Search for a Moving Target
(A.F. Terpugov, F.A. Shapiro; IZVESTIYA VUZ RADIOELEKTRONIKA, No 7, 1978) 10

PHYSICS

Surface Waves in Distributed-Coupling Integrated Optics Components (Review Article)
(Yu. A. Bykovskiy, et al.; KVANTOVAYA ELEKTRONIKA, Nov 78) 16

Radiation-Optical Stability of Low-Loss Glass Fiber Optical Waveguides
(A.N. Gur'yanov, et al.; KVANTOVAYA ELEKTRONIKA, Nov 78) 47

Fiber-Optic Data Link for Telecommunications Systems
(Zh. I. Alferov, et al.; KVANTOVAYA ELEKTRONIKA, Nov 78) 51

Feasibility of Developing Optical Memory Elements Based on GaAs MDP Structures
(V.A. Gaysler, et al.; KVANTOVAYA ELEKTRONIKA, Nov 78) 54

Thermal Radio Radiation From Clouds
(A.B. Akvilonova, B.G. Kutuza; RADIOTEKHNIKA I ELEKTRONIKA, No 9, 1978) 59

CONTENTS (Continued) Page

Amplifying Dynamic Holograms
(Ye. V. Ivakin, et al.; ZHURNAL PRIKLADNOY SPEKTROSKOPII, Jun 78) 80

SCIENTISTS AND SCIENTIFIC ORGANIZATIONS

Second International School of Semiconductor Electrooptics 'Cetniewo-1978'
(P.G. Yeliseyev, M.A. Herman; KVANTOVAYA ELEKTRONIKA, Nov 78) 87

PUBLICATIONS

Performance of Operating Systems
(E.A. Trakhtenberg; KAK RABOTAYUT OPERATSIONNYYE SISTEMY, 1978) 93

The Theoretical Principles of Radar
(A.A. Korostelev, et al.; TEORETICHESKIYE OSNOVY RADIOLOKATSII, 1978) 97

Transition Regions in Epitaxial Semiconductor Films
(L.N. Aleksandrov; PEREKHODNYYE OBLASTI EPITAKSIAL'NYKH POLUPROVODNIKOVYKH PLENOK, 1978) 104

ELECTRONICS AND ELECTRICAL ENGINEERING

UDC 621.391.2

DIGITAL DETECTION OF INCOHERENT PULSE SIGNALS FOR THE CASE OF A CHANGING NOISE POWER

Kiev IZVESTIYA VUZ RADIOELEKTRONIKA in Russian Vol 21 No 7, 1978 pp 11-18

[Article by K.K. Vasil'yev, manuscript received 29 Mar 77, following revision 21 Dec 77]

[Text] Optimal and quasioptimal algorithms are synthesized for the detection of signals in the case of a changing noise dispersion. The asymptotic effectiveness of the proposed processing rules is determined with respect to an optimal signal detector for the case of a known interference power.

Situations are frequently encountered when detecting radio signals against a background of interference in which the dispersion of the noise is unknown, and can vary during the time needed to make the observations. In this case, an effective solution of the detection problem can be found if in each j-th signal postion ($j = \overline{1, N}$) the observer positions a set of n independent readouts $\{x_{ij}\}_{i=1}^{n}$, made in the region of the interference (Figure 1), in addition to the readout of the input process x_{0j} in the region of the supposed signal. In this case, the difference ("contrast") between the noise and useful signal readouts is employed for the detection.

A large quantity of literature devoted to the problem considered here contains research on optimal algorithms for signal detection for the case of an unknown noise dispersion, but where the dispersion is constant within the limits of all of the reference readouts $\{\{x_{ij}\}_{i=1}^{n}\}_{j=1}^{N}$.

In this paper, the noise immunity of quasioptimal rules for processing signals having binary and multilevel amplitude quantization is synthesized and analyzed. The detectors which are found maintain their effectiveness even in the case where the dispersion of the interference remains constant only for the readouts $\{x_{ij}\}_{i=1}^{n}$, which correspond to one signal position.

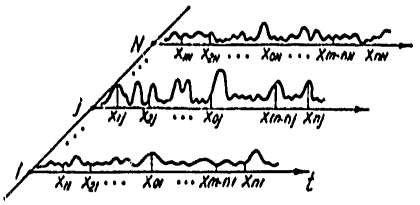

Figure 1. The realization of the input random process.

Optimal Algorithms

The synthesis of the detection rule in the problem considered here with unknown and changing values of the interference dispersion $\{\sigma_j^2\}_{j=1}^N$ can be accomplished in various ways, the most acceptable of which is the following: the method of maximum likelihood [1], the empirical theory of [2] or Bayyesovskiy's approach [3]. Considering the agreement in practice of the synthesis results using these methods, we shall consider a shorter path, which consists in using Bayyesovskiy's approach. In this case, the unknown values of the dispersions are treated as random quantities with distribution densities of $\{w(\sigma_j)\}$. By assuming the continuity of the true distribution laws, it is expedient to choose "nondistorting, improper" distributions as the a priori densities [3]: $\{w(\sigma_j) = 1,\ \sigma_j \geq 0\}_{j=1}^N$.

We shall likewise write the expressions for the combined distributions of the readouts $\{\{x_{ij}\}_{i=0}^n\}_{j=1}^N$ in the presence of a signal which fluctuates in amplitude:

$$w(x)=\prod_{j=1}^{N}\frac{x_{0j}}{\sigma_j^2(1+s)}\exp\left[-\frac{x_{0j}^2}{2\sigma_j^2(1+s)}\right]\prod_{j=1}^{n}\frac{x_{ij}}{\sigma_{ij}^2}\exp\left(-\frac{x_{ij}^2}{2\sigma_j^2}\right)$$

And for the case of a signal with a constant amplitude

$$w(x)=\prod_{j=1}^{N}\frac{x_{0j}}{\sigma_j^2}\exp\left(-\frac{x_{0j}^2}{2\sigma_j^2}-s\right)I_0\left(\frac{x_{0j}\sqrt{2s}}{\sigma_j}\right)\prod_{j=1}^{n}\frac{x_{ij}}{\sigma_j^2}\exp\left(-\frac{x_{ij}^2}{2\sigma_j^2}\right),$$

where s is the power signal to noise ratio; $I_0(\cdot)$ is a modified zero order Bessel function [4].

By writing the likelihood ratio $\Lambda = w_1(x;\ s)/w_1(x;\ s=0)$, where

$$w_1(x;s)=\int_0^\infty\ldots\int_0^\infty w(x)\prod_{j=1}^{N}w(\sigma_j)\,d\sigma_j,$$

following integration, we find a procedure for signal detection which is optimal in the sense of the Neumann-Pearson criterion:

$$T\begin{cases}>\Lambda_0 - \text{сигнал есть, Signal present}\\ <\Lambda_0 - \text{сигнала нет, Signal absent,}\end{cases}$$

where Λ_0 is a constant quantity, which is chosen from the specified false alarm probability. In this case, for the model of a signal with a random amplitude statistic:

$$T=\sum_{j=1}^{N}\ln\left(1+s\frac{\lambda_j}{\lambda_j+1+s}\right),$$

where $\lambda_j=x_{0j}^2/\sum_{i=1}^{n}x_{ij}^2$. (1)

For the model of a signal with a constant amplitude:

$$T=\sum_{j=1}^{N}\ln\left\{\exp\left(-\frac{s}{1+\lambda_j}\right)F_1\left[-(n-0{,}5);\,1;-\frac{s\lambda_j}{1+\lambda_j}\right]\right\}, \quad (2)$$

where $F_1[\alpha;\ \beta;\ \delta;]$ is a degenerate hypergeometric function [4].

The resulting formulas determine the critical regions of the local optimal algorithms, since in the case considered here, a uniform detection rule of the greatest power does not exist for any values of s, where $s \ll 1$ detectors for signals with random and constant amplitude coincide. It can be shown that in this case

$$T=\sum_{j=1}^{N}\lambda_j/(1+\lambda_j). \quad (3)$$

An important specific feature of the procedures found here is the monotonic dependence of the terms in formulas (1) - (3) on the value of the statistics λ_j. This permits writing a general detection rule with M-level amplitude quantization for the two signals models:

$$\sum_{j=1}^{N}\sum_{p=1}^{M-1}R_pU[\lambda_j-k_p]U[k_{p+1}-\lambda_j]\begin{cases}\geqslant k_0 & \text{Signal present сигнал есть,}\\ <k_0 & \text{сигнала нет, Signal absent}\end{cases} \quad (4)$$

where $\{k_p\}$ are the quantization levels; $k_M = \infty$; k_0 is the detection threshold; R_p is the weighting factor of the p-th level; $U[x] = 1$ when $x \geq 0$ and $U[x] = 0$ if $x < 0$.

The optimization of the derived rule (4) consists in finding a maximum of the correct detection probability for all values of the parameters $\{R_p;\ k_p\}$ and k_0 with the superimposed condition for false alarm probability that $F(\{R_p;\ k_p\}_{p=1}^{M-1},\ k_0) = \text{const}$. An investigation of this problem shows that the effectiveness of the algorithms will practically not change if values are chosen from the natural number series $\{R_p = p\}_{p=1}^{M-1}$ as the optimum set of weighting factors. In this case, detection rule (4) is simplified and can be written in the form:

$$\sum_{j=1}^{N}\sum_{p=1}^{M-1}U[\lambda_j-k_p]\gtrless K_0. \quad (5)$$

Quasioptimal Algorithms

The resulting digital signal detection algorithm (5) also makes it possible to find a number of simple quasioptimal procedures. For this, we shall consider the critical region of the p-th quantization level:

$$\lambda_j - k_p = 0 \quad \underset{\text{or}}{\text{или}} \quad x_{0j}^2 - k_p \sum_{i=1}^{n} x_{ij}^2 = 0.$$

It is not difficult to see that the latter formula is the equation of a cone in the n + 1 measurement space.

We shall construct a hyperpyramid, circumscribed around the cone, as the suboptimal critical region. For this, we draw n tangential planes, the intersection of which form the suboptimal region (Figure 2). Since the rotation of the system of coordinates about the general x_{0j} axis of the cone and the pyramid does not change the quality of the processing procedure, we shall choose that postion of the system $\{x_{ij}\}$, for which the planes contain the straight lines $\{x_{0j} = \sqrt{k_p}x_{ij};\ \{x_{kj} = 0\}_{k=1}^{n},\ k \neq i\}_{i=1}^{n}$, formed by the intersection of the coordinate surfaces $\{0x_{0j}x_{ij}\}$ with the surface of the cone (OA_1 and OA_2 in Figure 2). In this case, the conditions of the system of hyperplanes can be specified by the simpler equations $\{x_{0j} - \gamma_p x_{ij} = 0\}_{i=1}^{n}$, where $\gamma_p = \sqrt{k_p}$.

It is not difficult to convince oneself that the sample point $\{x_{ij}\}_{i=0}^{n}$ is located inside the pyramid if any of the following conditions are met:

$$x_{0j} > \gamma_p \sup_i x_{ij} \quad \underset{\text{or}}{\text{или}} \quad \{x_{0j} > \gamma_p x_{ij}\}_{i=1}^{n}, \quad \underset{\text{or}}{\text{или}} \quad \sum_{i=1}^{n} U[x_{0j} - \gamma_p x_{ij}] = n,$$

where $\sup_i x_{ij}$ is the value of the greatest of the readouts of $\{x_{ij}\}_{i=1}^{n}$.

Three comparatively simple quasioptimal signal detection rules follow directly from these relationships:

$$\sum_{j=1}^{N} \sum_{p=1}^{M-1} U[x_{0j} - \gamma_p \sup_i x_{ij}] \gtrless K_0, \tag{6}$$

$$\sum_{j=1}^{N} \sum_{p=1}^{M-1} \prod_{i=1}^{n} U[x_{0j} - \gamma_p x_{ij}] \gtrless K_0 \tag{7}$$

$$\sum_{j=1}^{N} \sum_{p=1}^{M-1} U\left[\sum_{i=1}^{n} U[x_{0j} - \gamma_p x_{ij}] - n\right] \gtrless K_0, \tag{8}$$

which are based on a pair by pair comparison of the readout in the region of the proposed signal x_{0j} with each of n reference readouts of the interference $\{x_{ij}\}$.

By noting that binary quantization of the statistic $v_\mu = \sum_{i=1}^{n} U[x_{0j} - \gamma_p x_{ij}]$ with respect to the level n is employed in the latter algorithm, one can write one more suboptimal detection algorithm, which was studied in the literature [5]:

$$\sum_{j=1}^{N}\sum_{p=1}^{M-1}\sum_{i=1}^{n} U[x_{0j} - h_p x_{ij}] \gtrless K_0, \tag{9}$$

in which supplemental quantization of the statistic v_p is excluded and new values of the quantization levels $\{h_p\}$ are introduced.

Shown in Figures 3a and 3b are block diagrams of the resulting algorithms (6) and (7) for the case of M-level amplitude quantization. As can be seen from the drawings, the main operation is binary quantization of the readout x_{0j}, multiplied by constant coefficients $\alpha_1 = 1/\gamma_1$, $\alpha_2 = \gamma_1/\gamma_2$, ... , $\alpha_{M-1} = \gamma_{M-2}/\gamma_{M-1}$, and of the readouts $\{x_{ij}\}_{i=1}^{n}$ by means of the comparators K. In this case, it is simplest to realize algorithm (6), the circuit of which contains an M-1 comparator and a *sup* block for segregating the largest of the interference readouts.

The block diagrams for algorithms (8) and (9) differ from the circuit of Figure 3b only in the changes of the elements of block L (Figure 3c and 3d). Nonetheless, it should be noted that to construct the detection rule (9), it is necessary to increase the volume of the memory n times, since the maximum number written into the adder at the j-th signal position is equal to n(M-1).

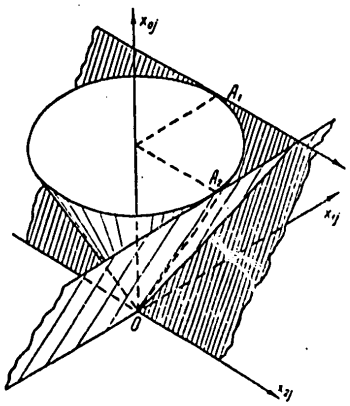

Figure 2. Optimal and quasi optimal critical regions in three-dimensional space (n = 2).

The method treated here for constructing suboptimal critical regions provides for invariance of the signal processing rules with respect to linear transformations $\{f(\bar{x}_j) = c_j x_j,\ c_j > 0\}$ of the small samples $\bar{x}_j = \{x_{ij}\}_{i=0}^{n}$ being analyzed.

Therefore, the derived algorithms (6) - (9), just as the optimal ones, are stable when the dispersion of the input process changes. Along with this, it is not difficult to show that the class of possible transformations of $\{f(x)\}$, which preserve the level of the threshold signal for quasioptimal algorithms is considerably broader than the class of linear transformations. In fact, if F(x) and $F(x_0)$ are one-dimensional distribution functions of the readouts x_{ij}; $i \geq 1$ and x_{0j}, then the probability of exceeding the threshold level γ_p for procedures (6) - (8) can be written in the form:

$$P = \int \left(\int_{x < \beta x_0} dF(x) \right)^n dF(x_0),$$

where $\beta = 1/\gamma_p$.

Correspondingly, the probability of exceeding the threshold γ_p', following the transformation $x = f(x)$, is:

$$P' = \int \left(\int_{z < z_0 \varphi} dF(z) \right)^n dF(z_0) = \int \left(\int_{f(x) < f(x_0)\varphi} dF(x) \right)^n dF(x_0),$$

where $\phi(\beta) = 1/\gamma_p'$.

Thus, $P = P'$ for all of the transformations which satisfy the functional equation $f(\beta x) = \phi(\beta) f(x)$. The resulting equation is easily reduced to the well-known one $g(\beta x) = g(\beta)g(x)$ by means of the substitution* $g(x) = f(x)/f(1)$, where the well-known equation has the unique solution $g(x) = x^{\mu}$ where $x > 0$. Since the analysis carried out here is justified for any (j-th) signal position, the class of transformations of the input process which preserve the level of the threshold signal can be written in the form $\{f_j(x) = c_j x^{\mu_j}$, $c_j > 0$, $\mu_j \neq 0\}$. Thus, suboptimal algorithms (6) - (8) have specified nonparametric properties which favorably distinguish them from optimal ones which are invariant only with respect to scale transformations.

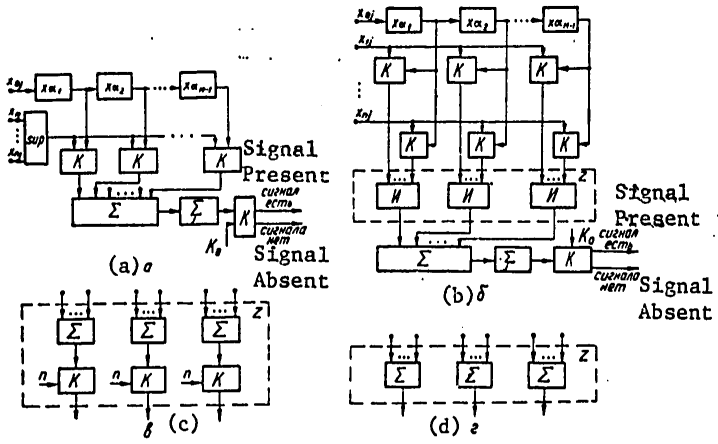

Figure 3. Structural configurations of quasioptimal algorithms.

* The presupposition $f(1) \neq 0$ does not narrow the class of transformations, since in the contrary case, $f(x1) = \phi(x)f(1)$, and consequently, $f(x) \equiv 0$.

The Effectiveness of Optimal and Quasioptimal Algorithms

To assess the quality of the algorithms which were found, for the case of a large number of signal postions N, we shall make use of the criterion of their asymptotic effectiveness (OAE) with respect to an optimal rule for signal detection for the case of completely known interference parameters. Since the law governing the distribution of the accumulated sums for all of the algorithms considered here approaches a normal law in step with an increase in N, the calculation of the OAE can be accomplished from the following formula [6]:

$$\rho = \lim_{N\to\infty} N_0/N = \lim_{N\to\infty} [\partial m_1\{T\}/\partial s]^2_{s=0}/N\sigma_T^2,$$

where N_0 is the number of signal postions being analyzed for an optimal detector for the case of a constant noise power; $m_1\{T\}$ is the mathematical mean value of the statistic T in the presence of a useful signal; σ_T^2 is the dispersion of T in the noise region. We shall find the OAE of the signal processing rules (4) - (9) for the extreme cases $M \to \infty$ and M = 2.

When $M \to \infty$, the effectiveness of all of the detectors considered here coincides with the OAE of optimal algorithms based on statistics (1) - (3). To find the magnitude of the effectiveness, we note that the statistic λ_j takes the form of the ratio of two random quantities x_{0j}^2 and $\sum_{i=1}^{n} x_{ij}^2$, which when $s \ll 1$, follows a gamma distribution. By using the well-known rules for the composition of probability laws, we find the following formula for the distribution density of λ_j:

$$w(\lambda_j) = n/(1+s)[1+\lambda_j/(1+s)]^{n+1},$$

which is justified for the model of a signal with an unknown amplitude where $s \ll 1$, while for a fluctuating signal, for any values of s. Following this, it is not difficult to compute the dispersion and the mathematical mean of the statistic (3) and to derive an expression for the OAE of optimal algorithms (1) - (3).

$$\rho = \frac{n}{n+2}.$$

when M = 2, the formulas for the OAE of optimal algorithms (4) and (5)

$$\rho_B = n^2k^4/(1+k^2)^2[(1+k^2)^n - 1]$$

And quasioptimal algorithms (6) - (8)

$$\rho_o = \left[\sum_{i=1}^{n} (\gamma^2/(i+\gamma^2))\right]^2 / \left[\prod_{i=1}^{n} (1+\gamma^2/i) - 1\right]$$

are found in a similar fashion. We will note that in the case considered here of binary quantization, when $\gamma = 1.0$, the resulting detection rules (6) - (8) coincide with the well-known nonparametric criterion of [7] which has an effectiveness of

$$\rho_D = \rho_0(\gamma = 1) = \frac{1}{n}\left(\sum_{l=1}^{n}\frac{1}{1+l}\right)^2,$$

and is substantially lower than ρ_V (Figure 4). A comparison of the optimal values of the threshold level γ (Table 1) with the values $\gamma = 1, 0$, used in paper [7], explains the small level of effectiveness ρ_D for large values of n.

Also shown in Figure 4 are the OAE's of the processing rules considered here calculated on a digital computer as a function of the number of reference readouts n in the interference region, for the corresponding values of the optimal threshold levels γ, k and h (Table 1). In this case, formulas derived in the literature [5] were used to calculate the effectiveness ρ_C of detection rule (9). An analysis of the results presented here allows the following conclusions.

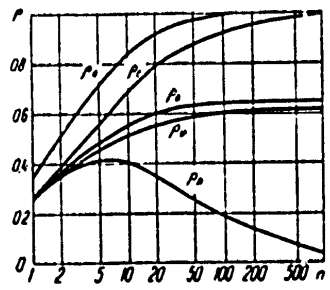

Figure 4. The asymptotic effectiveness of the optimal ρ_0, ρ_B and quasioptimal ρ_V, ρ_C and ρ_D algorithms as a function of the number of reference interference readouts.

1. The least amount of loss with respect to the case of completely known interference parameters is determined by the effectiveness of ρ_0 of rules (1) - (3). These same values of the effectiveness are achieved when using algorithms (5) - (9) with multiple amplitude quantization if $M \to \infty$.

2. A substantial simplification of the detectors can be achieved by using amplitude quantization with a small number of quantization with a small number of levels. In this case, the requisite increase in the sample volume with respect to the case of $M \to \infty$, even for the case of binary quantization, amounts to 1.31 - 1.56 times, depending on n. This loss falls off rapidly with an increase in the number of quantization levels. For example, when n = 1, the effectiveness of algorithms (5) - (9) is practically equal to the maximum amount, if the number of quantization levels is $M > 4$ (Table 2).

Table 1

n	1	2	3	5	10	20	50	100	∞
γ	1,00	0,91	0,86	0,79	0,72	0,65	0,59	0,55	0,00
k	1,00	0,79	0,67	0,54	0,39	0,28	0,17	0,14	0,00
h	1,00	1,10	1,19	1,27	1,45	1,67	1,95	2,24	∞

Table 2

M	2	3	4	5	6	7	∞
p	0,25	0,30	0,31	0,32	0,32	0,33	0,33

3. A comparison of the effectiveness of the optimal algorithms (4) and (5) and the simple quasioptimal algorithms with multilevel quantization shows that the amount of the losses does not exceed 9%. A comparatively high effectiveness ρ_c for detection rule (9) is achieved at the cost of somewhat of an increase in the memory volume.

BIBLIOGRAPHY

1. Wilks S., "Matematicheskaya statistika" ["Mathematical Statistics"], Moscow, Nauka Publishers, 1967.

2. Bogdanovich V.A., "Primeneniye printsipa nesmeshchennosti v zadachakh obnaruzhneiya s apriornoy neopredelennost'yu" ["The Application of the Principle of Empiricism to Problems of Detection with Apriori Ambiguity"], IZV. VUZOV - RADIOELEKTRONIKA [PROCEEDINGS OF THE HIGHER EDUCATIONAL INSTITUTES - RADIOELECTRONICS], 1972, 15, No 4, p 453.

3. De Groot M., "Optimal'nyye statisticheskiye resheniya" ["Optimal Statistical Solutions"], Moscow, Mir Publishers, 1974.

4. Gradshteyn I.S., Ryzhik I.M., "Tablitsy integralov, summ, ryadov, i proizvedeniy" ["Tables of Integrals, Sums, Series and Products"], Moscow, Nauka Publishers, 1971.

5. Vasil'yev K.K., Kramushchenko V.I., "Asimptoticheskaya effektivnost' nekotorykh algoritmov obnaruzheniya signalov v shumakh neizvestnoy moshchnosti" ["The Asymptotic Effectiveness of Certain Signal Detection Algorithms in Noise of an Unknown Power"], RADIOTEKHNIKA I ELEKTRONIKA [RADIO ENGINEERING AND ELECTRONICS], 1975, 20, No 5, p 1095.

6. Hansen, Olsen, "Neparametricheskoye obnaruzheniye signalov s ispol'zovaniyem obobshchennogo znakovogo kriteriya" ["Nonparametric Detection of Signals by Means of a Generalized Sign Criterion"], ZARUBEZHNAYA RADIOELEKTRONIKA [FOREIGN RADIOELECTRONICS], 1972, No 9, p 28.

7. Dillard, Entonyak, "Invariantnaya otnositel'no raspredeleniya signala protsedura obnaruzheniya dlya RLS" ["A Detection Procedure for Radars which is Invariant with Respect to the Signal Distribution"], ZARUBEZHNAYA RADIOELEKTRONIKA, 1971, No 8, p 3.

8225
CSO:8144/519

ELECTRONICS AND ELECTRICAL ENGINEERING

UDC 519.2

TWO-STAGE SEARCH FOR A MOVING TARGET

Kiev IZVESTIYA VUZ RADIOELEKTRONIKA in Russian Vol 21 No 7, 1978 pp 40-44

[Article by A.F. Terpugov and F.A. Shapiro, manuscript received 28 Mar 77, following revision, 10 Nov 77]

[Text] A modified algorithm for two-stage target search in a multichannel system, which takes into account the shifting of the target from channel to channel, is proposed and investigated.

For target search problems in a multichannel system, the most usual method is the sequential examination of the channels, where a decision is made concerning the presence or absence of a target in each of them. The appearance of inertialless switching devices and antennas with electrical beam sweep, which permit the practically instantaneous connection of the search device to the output of any channel, have made it possible to use more effective, even more complex algorithms for target search. Thus, a two-stage target search algorithm is proposed in [1] for a multichannel system, which consists in the following.

In the first stage, all of the channels are examined sequentially, one after the other for a certain time t_0, which is less than the time t_1 needed to make a decision concerning the presence or absence of a target in the channel. The value of the logarithm of the likelihood ratio is measured for each channel, and this ratio is stored.

All of the channels are ordered, based on the decline in the measured values of the logarithm of the likel hood ratio, i.e., the channel with the maximum logarithm of the likelihood ratio is given the number 1, while the channel with the minimum logarithm of the likelihood ratio is given the maximum number.

In the second stage, the channels are each examined the order of increase in their numbers for a time t_1, and in this case, a decision is made concerning the presence or absence of a target in each of them.

However, this method of target search, just as the algorithms, which are presented in [2, 3, 4], do not at all take into account the fact that over the

time between the preliminary and the final examination, the target can shift from one channel to another (for example, a radar target can move from one part of the scanning sector into another).

A modification of the algorithm presented in [1] is treated in this article, which permits accounting for the possible movements of the target from one channel to another during the time between the preliminary and final examination. For this, it is proposed that following the preliminary examinations stage, the values of the logarithm of the likelihood ratio be recomputed from the following formula:

$$u_j' = \sum_{k=1}^{N} q_{jk} u_k,$$

where u_k is the measured value of the logarithm of the likelihood ratio in the k-th channel; q_{jk} are certain coefficients, which depend on the rate at which the target shifts from one channel to another; u_j' is the recomputed value of the logarithm of the likelihood ratio in the j-th channel. The channels are to be ordered with respect to decreasing values of u_j', rather than the quantities u_j. The case studied in this paper is that where during the time between the preliminary examination of the channel and its examination in the second stage, there is a probability of 1 - p that the target can remain in the same channel where it was, and a probability of p/2 that it can go to the next channel to the left and a probability p/2 that it can shift to the next channel to the right, while the recomputation of the values of the logarithm of the likelihood ratio is carried out from the following formula:

$$u_j' = qu_{j-1} + (1-2q)u_j + qu_{j+1}, \quad 0 < q < 1/2. \tag{1}$$

It is apparent that this model of target motion corresponds to reality only for the case where it travels sufficiently slowly through the channels. For a more precise study, its transtion to channels removed by 2, 3, etc. channels from the initial channel would have to be taken into account. The formulas derived in this case will be similar to those given in the article, only in enormously more complex.

One of the most important characteristics of a detection system is the time transpiring between the start of the search and the selection of the channel with the target (the target detection time). Before moving on to finding the time for detecting the channel with the target, we shall introduce the requisite symbols. We shall assume that there are N channels in all ($N \gg 1$), and the target can be located only in one of them. We shall assume that there is one search device. Just as in [1, 4], we shall assume that the measured values of the logarithm of the likelihood ratio are normal random quantities with a dispersion of $2\mu t_0$ and a mathematical mean value of $\pm \mu t_0$ depending on whether the target is in the channel or is not there. Here μ is a quantity which characterizes the channel and has the sense of the signal to noise ratio, while t_0 is the time for the preliminary examination of each channel. Since the ordering is now carried out with respect to the quantities u_j' from

(1), the conditional average time for detecting the channel with the target, given the assumption that during the preliminary examination the target was in the channel with the number i, is equal to:

$$\bar{t}_i = Nt_0 + t_1\left[p_{ii}\sum_{j\neq i}\int_{u_i'=-\infty}^{+\infty}\int_{u_j'=u_i'}^{+\infty} p(u_i', u_j')\,du_i'du_j' + \right.$$

$$\left. + \sum_{k\neq i} p_{ik}\sum_{j\neq k}\int_{u_k'=-\infty}^{\infty}\int_{u_j'=u_k'}^{\infty} p(u_j', u_k')\,du_j'du_k'\right] + t_2, \qquad (2)$$

where $p(u_j', u_k')$ is the combined probability density for the quantities u_j' and u_k'. The first term in (2) is the time set aside for the preliminary examination. The second term, takes into account the shift of the target from one channel to another, represents the time needed to study those channels without the target, which proved to be in front of the channel with target following ordering. The first term in the square brackets appears if the target remained in the same channel where it was between the preliminary and the final inspection. The second term will appear in the square brackets in (2) if during the time between the preliminary and final inspection, the target moved from the channel with number i to the channel with the number k. The third term in (2) is the time which goes for studying the channel with the target in the second step.

We will note that it is assumed in the derivation of this formula that the second step is terminated with the correct decision on the presence of the target in one of the channels. In actual fact, if the probability of missing the target is equal to β, then the average time for detecting the target is $\bar{T}_i = \bar{t}_i + (1-\beta)T\sum_{n=0}^{\infty} n\beta^n$ where T is the time for a complete scan cycle. By transforming this expression to the form:

$$\bar{T}_i = \bar{t}_i + \frac{\beta}{1-\beta}T,$$

we see that a relative error on the order of β has been admitted in formula (2), which can be neglected for small values of β.

It follows from (1) that u_j' are normal random quantities

with the dispersion: $D\{u_j'\} = 2a(1-4q+6q^2) \quad \forall j,$

with the average value:

$$\bar{u}_j' = \begin{cases} a(1-4q) & \text{для } j=i, \\ -a(1-2q) & \text{» } j=i\pm 1, \\ -a & \text{» } j\neq i,\ i\pm 1 \end{cases}$$

and with the covariation:

$$cov(u'_j, u'_k) = 2a \begin{cases} 1-4q+6q^2 & \text{для } k=j, \\ 2q(1-2q) & \text{» } k=j\pm 1, \\ q^2 & \text{» } k=j\pm 2, \\ 0 & \text{for the remaining } k. \end{cases}$$

Taking these characteristics into account, in which $a = \mu t_0$, performing uncomplicated transformations and taking into account the fact that $p_{ii} = 1 - p\forall i$ while $p_{ik} = p/2$ for $|i-k| = 1$, we find that:

$$\bar{t} = Nt_0 + t_1\left\{(1-p)\left|2\Phi\left(-\sqrt{a}\frac{1-2q}{\sqrt{1-5q+6q^2}}\right)+\right.\right.$$
$$+2\Phi\left(-\sqrt{a}\frac{1-2q}{\sqrt{1-4q+5q^2}}\right)+(N-5)\Phi\left(-\sqrt{a}\frac{1-2q}{\sqrt{1-4q+6q^2}}\right)\Bigg]+$$
$$+p\left[\frac{1}{2}+\Phi\left(\sqrt{a}\frac{1-3q}{\sqrt{1-5q+8q^2}}\right)+\Phi\left(-\sqrt{a}\frac{q}{\sqrt{1-5q+8q^2}}\right)+\right.$$
$$\left.\left.+\Phi\left(-\sqrt{a}\frac{q}{\sqrt{1-4q+5q^2}}\right)+(N-5)\Phi\left(-\sqrt{a}\frac{q}{\sqrt{1-4q+6q^2}}\right)\right]\right\}+t_2, \qquad (3)$$

here $\Phi(t) = (2\pi)^{-1/2}\int_{-\infty}^{t} e^{-x^2/2}dx.$

Designating $\mu t_1 = a_1$, introducing the quantity $\mu\bar{t}/N$ in the analysis and going to the limit where $N \to \infty$ in (3), we find

$$\bar{\tau} = \lim_{N\to\infty}\mu t/N = a + a_1\left[(1-p)\Phi\left(-\sqrt{a}\frac{1-2q}{\sqrt{1-4q+6q^2}}\right)+\right.$$
$$\left.+p\Phi\left(-\sqrt{a}\frac{q}{\sqrt{1-4q+6q^2}}\right)\right]. \qquad (4)$$

We will note that the average detection time for the channel with the target using the algorithm presented in [1] is derived from (4) when $q = 0$, something which corresponds to the situation where the ordering is carried out in terms of decreasing values of u_j, and not u'_j. In this case:

$$\bar{\tau}_p = a + a_1[(1-p)\Phi(-\sqrt{a}) + p/2]. \qquad (5)$$

In the following, we will compare the algorithms studied here with the search procedure presented in [1], since it is a modification of the algorithm of [1].

We shall now move on to the minimization of the average detection time for the channel with the target. It is not difficult to see that the quantity $\bar{\tau}$ in (4), treated as a function of the parameters q and $a = c^2$, has a minimum with respect to this variable, and by choosing the value of the parameter q in the best fashion, one can achieve a decrease in the average detection time.

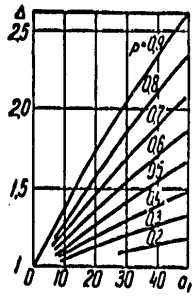

Figure 1.

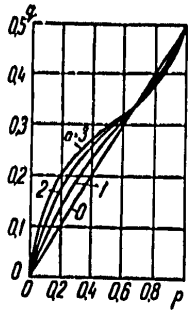

Figure 2.

The optimum values of the parameters q and c are derived from the equations $\partial\bar{\tau}/\partial q = 0$, $\partial\bar{\tau}/\partial c = 0$, which take on the form:

$$p = \frac{2q\varphi\left(\frac{c(1-2q)}{\sqrt{1-4q+6q^2}}\right)}{2q\varphi\left(\frac{c(1-2q)}{\sqrt{1-4q+6q^2}}\right)+(1-2q)\varphi\left(\frac{cq}{\sqrt{1-4q+6q^2}}\right)}, \tag{6}$$

$$a_1 = \frac{2c\sqrt{1-4q+6q^2}}{(1-p)(1-2q)\varphi\left(\frac{c(1-2q)}{\sqrt{1-4q+6q^2}}\right)+pq\varphi\left(\frac{cq}{\sqrt{1-4q+6q^2}}\right)}. \tag{7}$$

We shall compare the proposed algorithm with a two-step algorithm, which does not take into account target motion, and which is derived from our's if we set $q = 0$. In this case, the optimal value $c = c_1$ is found from the equation $\partial\bar{\tau}_p/\partial c = 0$, which has the form:

$$a_1 = \frac{2c_1}{(1-p)\varphi(c_1)}. \tag{8}$$

The advantage gained in the average detection time is equal to

$$\Delta = \frac{c_1^2 + a_1[(1-p)\Phi(-c_1)+p/2]}{c^2 + a_1\left[(1-p)\Phi\left(-\frac{c(1-2q)}{\sqrt{1-4q+6q^2}}\right)+p\Phi\left(-\frac{cq}{\sqrt{1-4q+6q^2}}\right)\right]}.$$

Equations (6) - (8) were solved numerically: by specifying $a = c^2$ and p, q was found from (6), and then a was found from (7) and c_1 was found from (8). Shown in Figure 1 are values of Δ as a function of a_1 for various values of p, from which it follows that because of the time optimization of the preliminary inspection, the average detection time is curtailed by an amount which can reach 60%. We will note that only is the average target detection time curtailed, but also the complete scanning cycle time. Shown in Figure 2 is q as a function of p for different values of $a = \mu t_0$, from which it can be seen that the quantity q increases monotonically with an increase in p, where the result is $q = 0$ at $p = 0$ (i.e., the original

algorithm presented in [1] is obtained for a stationary target), and when $p = 1$, $q = 0.5$. The dependence of q on p for various values of a does not deviate very sharply from the function $q = p/2$.

Thus, the algorithm modification proposed here, which takes into account the shifting of the target from channel to channel, can rather substantially curtail the average target detection time.

BIBLIOGRAPHY

1. Posner E.C., "Optimal Search Procedures", IEEE TRANS., 1963, IT-9, No 3, p 157.

2. Akindinov V.V., "Otnositel'naya effektivnost' optimal'nogo algoritma mnogoetapnogo poiska" ["The Relative Effectiveness of an Optimal Algorithm for Multistep Search"], IZV. AN SSSR, TEKHNICHESKAYA KIBERNETIKA [PROCEEDINGS OF THE USSR ACADEMY OF SCIENCES, ENGINEERING CYBERNETICS], 1964, No 4, p 34.

3. Bureyev V.A., Men'shikov A.V., "Analiz kharakteristik obnaruzheniya sistem s peremennoy razreshayushchey sposobnost'yu" ["An Analysis of the Characteristics of Detections Systems with a Variable Resolving Power"], RADIOTEKHNIKA I ELEKTRONIKA [RADIO ENGINEERING AND ELECTRONICS], 1965, 10, No 12, p 2091.

4. Terpugov, A.F., Shapiro F.A., "Dvukhetapnyy poisk signala v mnogokanal'noy sisteme s uporyadochivaniyem kanalov" ["Two-Step Signal Search in a Multichannel System with Ordering of the Channels"], IZV. AN SSSR, TEKHNICHESKAYA KIBERNETIKA, 1974, No 2, p 126.

8225
CSO:8144/0502

PHYSICS

UDC 621.372.8.09

SURFACE WAVES IN DISTRIBUTED-COUPLING INTEGRATED OPTICS COMPONENTS (REVIEW ARTICLE)

Moscow KVANTOVAYA ELEKTRONIKA in Russian Vol 5 No 11, Nov 78 signed to press 3 Apr 78 pp 2309-2331

[Article by Yu. A. Bykovskiy, V. L. Smirnov and A. V. Shmal'ko, Moscow Engineering-Physics Institute]

[Text] A survey of the literature devoted to the interaction and transformation of surface waves in distributed-coupling integrated optics elements is given. A general description of distributed coupling of surface waves in thin-film waveguides (TPV) is given and their interaction and transformation in waveguides with periodic modulation of parameters are considered in detail. The various types of periodic modulation of TPV parameters are considered and comparative analysis of them is conducted. The main components and devices of integrated optics circuits based on diffraction-grating periodic structures are considered. The possibilities of using "aperiodic" grating structures in integrated objects are shown and devices with tunnel distributed coupling are considered.

Many phenomena in physics and engineering can be regarded as coupled wave phenomena [1]. There is also a large number of phenomena of distributed coupling of surface waves in components and devices of various functional designation in integrated optics. They include radiation scattering on the irregularities of dielectric thin-film waveguides (TPV), diffraction transformations of surface waves on grating structures and directional branching of power, mode conversion and nonlinear interactions. Of greatest interest in integrated optics are devices and components developed on the basis of the phenomena of coupling and interaction of surface waves in TPV with periodic modulation of parameters which find application in development of active devices -- distributed-feedback (ROS) and distributed Bragg-mirror (RBZ) lasers -- and in development of various passive devices -- filters, radiation matching components, mode conversion components, diffraction

modulators and deflectors and also for spatial-selective radiation filtration in TPV. Many of the devices enumerated above may find extensive application in optical communications lines (OLS) based on fiber light guides.

A general description of distributed coupling of surface waves in TPV is given and the interaction and transformation of surface waves in waveguides with periodic modulation of parameters are considered in detail. The main components and devices of integrated optics circuits based on periodic grating structures are considered. The possibilities of using "aperiodic" grating structures in integrated objects are shown and devices with tunnel distributed coupling are corsidered.

1. General Description of Distributed Coupling of Surface Waves in TPV

Many problems of waveguide optics, primarily concerning exchange of power between TPV surface waves (modes), can be considered on the basis of coupled wave theory [2-5]. According to this approach, the resulting wave caused by perturbation of TPV parameters is written in the form of the sum of unperturbed modes whose amplitudes vary along the direction of propagation z due to some intermode coupling and it is assumed that variation of amplitudes by z are small at distances on the order of the wavelength. In the general case the theory of coupled waves considers the relationship between waveguide modes which form a complete orthogonal system, i.e., in the case of TPV their number also includes radiation modes. For most types of interaction of coupled waves, TPV are limited by two-wave approximation when the interaction of only two surface waves are taken into account for which the condition of phase synchronism is fulfilled and for which a significant exchange of power is provided, and other waveguide modes are disregarded. We shall subsequently distinguish the coupling of two waveguide modes from mode coupling with radiation modes and also homogeneous and heterogeneous coupling of waveguide modes.

Let us consider two electromagnetic surface waves of TPV, which are the natural modes of an unperturbed waveguide:

$$a_m(z, t)=A_m \exp [i(\omega t-\beta_m z)],$$
$$b_n(z, t)=B_n \exp [i(\omega t\pm\beta_n z)], \quad (1.1)$$

where A_m and B_n are complex wave amplitudes and β_m and β_n are their constant propagation. Coupling and exchange of power between modes a_m and b_n in the direction of their propagation occurs in the presence of perturbation in TPV and amplitudes A_m and B_n become dependent on z. In most cases of interest to us, perturbation in TPV may be represented in the form of a distributed polarization source, while the process of power coupling and exchange between modes itself may be regarded as interaction of surface waves with polarization waves. The propagated mode a_m interacts with the disturbance and gives polarization to the wave which acts on mode b_n. In similar fashion mode b_n acts on mode a_m.

For homogeneous interaction of waves (1.1) (the minus sign in the exponent in (1.1)) when their group velocities are directed in the same direction, the coupled wave equations may be represented in the following form [4, 5]

$$dA_m/dz = -ik_{mn}B_n \exp(-2i\delta z), \tag{1.2}$$

$$dB_n/dz = -ik_{nm}A_m \exp(2i\delta z), \tag{1.3}$$

where the coupling constant k is determined by the type of specific disturbance which leads to coupling of the waveguide modes and δ characterizes misalignment of the interacting waves from phase synchronism and depends on the difference $\beta_m - \beta_n$ and the spatial variations of the disturbance (rather on the difference of the constants of excited wave propagation and exciting polarizations $2\delta = g\Delta N$, $g = 2\pi/\lambda$, and ΔN is misalignment by the effective refractive index of TPV). It follows from the law of conservation of energy that in this case

$$k_{mn} = k_{nm}^{*}. \tag{1.4}$$

For boundary conditions $A_m(0) = 1$ and $B_n(0) = 0$, the coupled wave equations have the solutions

$$B_n(z) = -ik_{mn}\left[\sin(z\sqrt{k^2+\delta^2})/\sqrt{k^2+\delta^2}\right]\exp(-i\delta z), \tag{1.5}$$

$$A_m(z) = \left[\cos(z\sqrt{k^2+\delta^2}) + i\delta\sin(z\sqrt{k^2+\delta^2})/\sqrt{k^2+\delta^2}\right]\exp(i\delta z), \tag{1.6}$$

where $k^2 \equiv |k_{mn}|^2$.

Examples of single-direction interaction of surface waves may be mode converters and directional couplers, including the prism coupler used for TPV mode excitation [6]. This type of wave coupling in TPV also includes nonlinear optical interactions, phase synchronization by periodic disturbance and electrooptical and optical-acoustic switching and modulation [2].

Heterogeneous coupling of surface waves (the plus sign in the exponent in (1.1)) may occur when their group velocities are aligned in opposite directions. In this case the coupled wave equations (A_m -- direct and B_n -- reverse) assume the form [4]

$$dA_m/dz = -ik_{mn}B_n \exp(2i\delta z), \tag{1.7}$$

$$dB_n/dz = ik_{nm}A_m \exp(-2i\delta z), \tag{1.8}$$

where constants k_{mn} and k_{nm} satisfy relation (1.4).

By using ordinary boundary conditions for heterogeneous coupling of waves $A_m(0) = 1$ and $B_n(L) = 0$ (L is the length of the interaction zone), we find the solutions of equations (1.7) and (1.8) in the following form:

$$B_n(0) = -i\{(k_{mn}/k)/[\sqrt{k^2-\delta^2}\,\mathrm{cth}\,(L\sqrt{k^2-\delta^2}) + i\delta]\}\exp(i\delta z), \tag{1.9}$$

$$A_m(L) = \{\sqrt{k^2-\delta^2}/[\sqrt{k^2-\delta^2}\,\mathrm{ch}\,(L\sqrt{k^2-\delta^2}) + i\delta\mathrm{sh}\,(L\sqrt{k^2-\delta^2})]\} \times \exp(-i\delta z), \tag{1.10}$$

where $k \equiv |k_{mn}|$. An example of this type of interaction of surface waves may be waveguide filters formed by modulation of TPV parameters. We are also concerned with heterogeneous interaction of coupled waves in distributed feedback structures used for ROS and RBZ lasers, although there are some differences here related to amplification in the waveguide and the absence of an incident wave (the boundary conditions assume the form $A(0) = 0$ and $B(L) = 0$ in this case). More detailed discussion of this type of surface wave interaction is given in [7, 8].

The form of equations which describe the behavior of two coupled waves is independent of the numerical value of coupling constant k. However, the value of k determines the degree of interaction of the waves or in practice the distance at which given exchange of power between the interacting modes occurs. In the general case k depends directly on the type of the specific physical cause of disturbance in TPV which leads to coupling of the waveguide modes. The application of coupled wave theory to a disturbed waveguide [2, 3] shows that the value of k is determined by the overlap integral of electric field distribution of two coupled waves through the waveguide cross-section and by the value of polarization disturbance in the medium.

It is obvious from consideration of expressions (1.5), (1.6), (1.9) and (1.10) for the field amplitudes of interacting waves that there is a specific difference of the phases between their fields. The wave field whose power increases always lags by $\pi/2$ in phase from the wave field with decreasing power. Formally, this directly corresponds to selection of signs in coupling equations (1.2), (1.3), (1.7) and (1.8). The required phase relationship between polarization created by mode a_m and the field of mode b_n to which power should be pumped is the cause of the temporary lag from the physical viewpoint. It is well known [9] that power dissipation in the dielectric occurs when polarization lags behind the field. Consequently, in our case the field phase for excitation of mode b_n should lag behind the polarization phase which is generated by the field of mode a_m in phase with it.

Let us now consider some characteristics of waveguide mode coupling with radiation modes. Prismatic and diffraction radiation input devices [6] are characterized by the fact that power exchange occurs between the waveguide mode and the mode continuum. In the diffraction device the mode continuum

consists of the radiation mode of the waveguide itself and in the prismatic device it consists of a set of plane waves capable of propagating in the homogeneous material of the prism at different angles. The condition of phase matching of interacting waves is determined in this case by the equality of projections of the wave vectors of the radiation modes (for the prismatic device -- the plane waves in the prism material) and of the constants of the waveguide mode propagation onto waveguide axis Z. Coupling of the waveguide modes with the continuum leads to emission of electromagnetic energy from the waveguide to the substrate or to the surrounding medium. As indicated by the coupling equations for the waveguide mode and continuum [2, 3], due to radiation the amplitude of the waveguide mode decreases exponentially:

$$A_m = A_m(0) \exp(-\alpha_m z), \tag{1.11}$$

where α_m is the attenuation constant for the m-th waveguide mode, directly coupled with the value of coupling constant k [10]. By knowing the attenuation constant of the surface wave α_m, based on the reciprocity theorem, it is easy to analyze the effectiveness of the reverse process -- wave excitation by a given light beam impinging on the waveguide surface at the angle of phase synchronism (see, for example, [11]).

2. Interaction and Transformation of Surface Waves in TPV With Periodic Modulation of Parameters

Periodic modulation of the parameters of TPV (its thickness, the refractive indices of the waveguide material or of the surrounding medium) along the direction of propagation of a surface light wave in a waveguide is used extensively in integrated optics to develop and create diffraction-grating filters, coupling devices, ROS and RBZ lasers, for purposes of phase matching in electrooptical, optical-acoustic, nonlinear and other types of surface wave interaction in waveguides. The physical processes of surface wave propagation in these waveguides are light scattering on the periodic structure similar to scattering on a diffraction grating. Various diffraction transformations of surface waves to each other and to radiation modes are the basis for operation of many integrated optics components.

Periodic modulation of TPV parameters leads in the final analysis to modulation of the effective waveguide refractive index. In most practically important cases, one may limit oneself in analysis of the transformation and radiation of surface waves to relatively weak harmonic modulation of TPV parameters [12-15]. This not only simplifies analysis itself of the fields in these waveguides, but also makes it possible to avoid significant light losses due to redistribution to higher order diffraction waves. Calculation of the effects of the interaction of waveguide modes with slight modulation of TPV parameters is usually carried out on the assumption of the smallness of variation of the interacting wave amplitudes at distances comparable to the radiation wavelength. In this approximation, using boundary conditions for the corresponding field components in TPV [12-15] or coupled wave theory [2-5], the analytical expressions can be found for the coupling constants

which determine the effectiveness of one or another type of wave interaction in TPV. Since only first-order diffraction processes are taken into account in both cases in the first approximation, both methods of calculation yield completely identical results for the interaction constants both in the case of radiation [15] and in the case of resonance transformation of waves in TPV (see, for example, [13, 5]). However, when analyzing the process of resonance transformation and reflection of surface waves with simultaneous ejection of radiation on the corrugated section of the waveguide (with a period coincident with the light wavelength in the medium), one must also take into account second-order diffraction processes since the mutual resonance transformations of the waves in the second diffraction order correspond in their intensity to radiation (or excitation) processes of surface waves in the first order of diffraction [16-19].

Resonance transformation and reflection of surface waves in TPV. Resonance transformation and reflection of surface waves in TPV with periodic variations of the thickness and refractive index of the waveguide material are subordinate to the general principles determined by the direction of the interaction of the surface waves in the distributed coupling structures [12, 13]. However, waveguides with periodic modulation of the refractive index are preferable in some cases for some applications since deep spatial modulation of the waveguide modes and effective transformation of them can be ensured by using a volumetric diffraction grating due to selection of the slope of its optically homogeneous layers.

Let us assume that the refractive index of a TPV is slightly modulated by sine-wave law (Figure 1, a):

$$n=n_1+\delta n\cos \mathbf{K}\mathbf{r}, \tag{2.1}$$

where $|\delta n| \ll |n_1|$; r is the radius vector; $K = (2\pi/\Lambda)(-\cos\chi, 0, \sin\chi)$ is the grating vector; Λ is its period; and χ is the angle of inclination of the optically homogeneous layers of the grating with respect to the Z axis ($0 \leqslant \chi < \pi$). The surface wave being propagated in the waveguide plane alone the Z axis is sequentially transformed to diffraction waves of the corresponding orders which are then reflected from the TPV boundaries and are again diffracted on the grating structure and so on. Consequently, the self-congruent field of surface waves in this waveguide is the superposition of diffraction and reflection waves. With strong interaction of the two surface waves when one of the reflection waves excited by the initial surface wave is close to the other surface wave, mutual resonance transformation of them occurs, determined by the condition [13]

$$n_m^*+sN\sin\chi\approx\pm n_{m'}^*, \tag{2.2}$$

where n_m^* and $n_{m'}^*$ are the effective refractive indices of the interacting waves of order m and m'; $s = \pm1, \pm2, \ldots$ is the order of the diffraction

wave of reflection; and $N = K/g = \lambda/\Lambda$. The bottom sign in the right side of (2.2) corresponds to different-direction wave coupling in TPV.

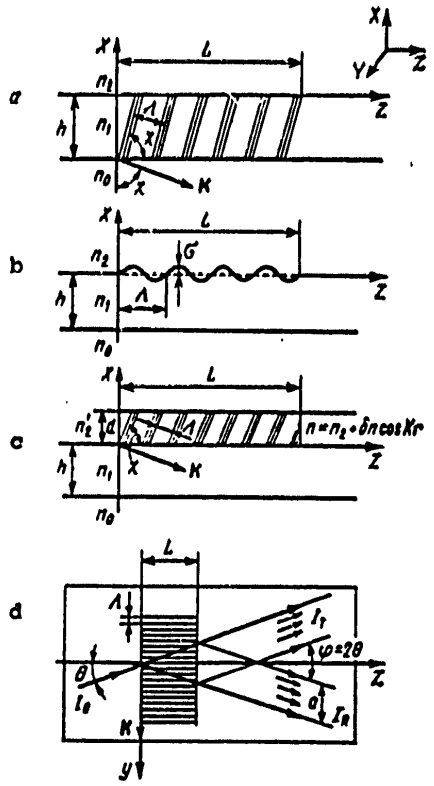

Figure 1. Schematic Representation of Various Types of Diffraction Grating Structures in TPV

If the parameters of a volumetric diffraction grating satisfy the condition of resonance (phase synchronism) (2.2), the surface wave impinging on it even with slight modulation of the refractive index of the film on sufficiently long sections of the grating, will be effectively transformed to another surface wave. With resonance reflection of the initial surface wave to an inverse wave of the same order ($m' = m$), determined by diffraction to the first reflective order ($s = -1$),

$$\chi = \pi/2, \quad N \approx 2n_m^*, \tag{2.3}$$

and for the case of a nonabsorbing waveguide (n_0, n_1, n_2 and δn are real numbers), the coefficient of reflection R_m of a surface wave of m-th order due to a phase grating of length L may be written in the form [13]

$$R_m = \mathrm{sh}^2(\gamma L)/[\mathrm{ch}^2(\gamma L) - (\Delta N/\tau)^2]. \qquad (2.4)$$

Here $\gamma = [\tau^2 - (\Delta N)^2]^{1/2} g/2$; $k = \tau g/2$ is the coupling constant; and $\Delta N = 2n_m^* - N$ is deviation from precise resonance ($\Delta N < \tau$). Coupling constant k for the case of TE-modes is determined by the expression

$$k_{TE} = \delta n (n_1/n_m^*)(h_m/h_m^*) g/2, \qquad (2.5)$$

where δn is the modulation amplitude of the refractive index of the waveguide material and h_m^* is the effective thickness of the waveguide (see [13] for the expressions for h_m^* and h_m). The coupling constant of the interacting waves k_{TE} approaches the value of $\delta ng/2$ with an increase of the film thickness (in the range that $gh \to \infty$).

Another possibility of accomplishing resonance transformation and reflection of surface waves in TPV is corrugation of the thin film (or substrate) surface by sine-wave law (Figure 1, b):

$$x = \sigma \sin(Kz), \qquad (2.6)$$

where σ is the modulation amplitude of the waveguide thickness h; $K = 2\pi/\Lambda$ and

$$(g\sigma)^2 \ll 1. \qquad (2.7)$$

Upon passage through this waveguide section, the surface wave is diffracted on the corrugated surface of the TPV. The diffraction waves excited in this case have projections of the wave vector onto the Z axis, equal to $gn_m^* + sK = g(n_m^* + sN)$ and the condition of resonance interaction of surface waves of orders m and m' is now reduced to the form

$$n_m^* + sN \approx \pm n_{m'}^*. \qquad (2.8)$$

It follows from stricter consideration with regard to condition (2.7) that upon resonance interaction of the two surface waves (s = 0 and ±1), their transformation to diffraction waves of other orders can be disregarded with relative accuracy of $(g\sigma)^2$ (approximation of strongly coupled waves) [12].

In the case of homogeneous wave coupling (the upper sign on the right side of (2.8)) when a surface wave or order m' is excited in the same direction as the initial wave of m-th order, the effectiveness of transformation η is equal to [12]:

$$\eta = \sin^2(\gamma z)/[1 + (\Delta N/\tau)^2]. \qquad (2.9)$$

Here $\gamma = [\tau^2 + (\Delta N)^2]^{1/2}\, g/2$; $\tau^2 > 0$; and $\Delta N = (n_m^* + sN) \mp n_{m'}^*$, characterizes deviation from precise resonance and the coupling constant for the case of TE-modes is equal to

$$k_{TE}^2 = \frac{g^2\sigma^2}{4h_m^* h_{m'}^*} \frac{(n_1^2 - n_m^{*2})(n_1^2 - n_{m'}^{*2})}{n_{m'}^* (n_m^* + sN)}. \qquad (2.10)$$

It is obvious from expression (2.9) that the maximum transformation of the power of interacting waves is reached at distances of $z = L_q$:

$$2\gamma L_q = \pi(1+2q), \quad q = 0, 1, 2, \ldots, \qquad (2.11)$$

and only under conditions of precise resonance ($\Delta N = 0$) can the initial wave of m-th order be completely transformed to a wave of order m' and in the case of $s = -1$ it can be transformed to a wave of higher order ($m' > m$) and in the case of $s = +1$ it can be transformed to a wave of lower order ($m' < m$).

In heterogeneous coupling of waveguide modes (the bottom sign on the right side of expression (2.8)) when the surface wave of m-th order passing along the grating resonantly excites the counter wave of given order m', the coefficient of reflection $R_{m,m'}$ from this distributed mirror of length L is described by an expression completely similar to expression (2.4), only in this case the values of γ and τ are taken by the absolute value and $|\gamma| = [|\tau^2| - (\Delta N)^2]^{1/2} g/2 \leq |\tau|$ (since now $n_m^* + sN \approx -n_{m'}^* < 0$). With an increase in the length of the "distributed mirror" kL, its coefficient of reflection approaches unity more rapidly, the more precisely the condition of resonance (2.8) is fulfilled.

The main parameter which characterizes the effectiveness of the considered resonance processes is the value of coupling constant k, which is significantly dependent both on the index of the interacting waves (mainly by n_m^* and h_m^*) and on their polarization. In the case of interaction of TM-waves [4]

$$k_{TM} = k_{TE} p, \qquad (2.12)$$

where factor $p = 1$ for TPV with $n_1 \approx n_0 \approx n_2 \approx n^*$ and at other waveguide parameters may cause a significant decrease in the value of k_{TM}. Moreover, with some quite specific periods of the grating and namely when the period of grating Λ satisfies the condition

$$n_m^*(n_m^* + sN) = -(n_1/n_2)^2 |N_2^0| \cdot |N_2^s|, \qquad s = -1, \qquad (2.13)$$

where $N = \lambda/\Lambda$ and $|N_2^s| = |[n_2^2 - (n_m^* + sN)^2]^{1/2}|$, the coupling constant k_{TM} approaches zero. This is physically related to the transverse nature of the

electromagnetic waves diffractionally excited in the TPV. A similar pattern is also observed with diffraction emission of surface waves in TPV since condition (2.3) is generally valid for total internal light reflection and diffraction on the corrugated surface of the interface of two homogeneous media [20, 21].

Diffraction emission and excitation of surface waves in TPV. Corrugation of the TPV surface by harmonic law (Figure 1, b) is one of the main methods of diffraction excitation of surface waves in it [14, 22]. As is known, a wave propagating along this waveguide may be emitted on its corrugated section due to diffraction to the media adjacent to the waveguide. A diffraction wave of -1 order (s = -1) makes the main contribution to emission in approximation of weak coupling (2.7) and the angles of emission to these media (with respect to the normal) are determined by the relation [22]

$$\sin\theta_j = (n_m^* - N)/n_j, \quad j = 0, 1, 2. \tag{2.14}$$

In this case the direction of light emission is not dependent on which surface of the film is corrugated -- the upper or lower, and varies slightly with variation of wave polarization (TE or TM). On the other hand, wave attenuation in the film is determined to a significant degree by its polarization and by the fact from which direction the waveguide is corrugated.

In view of the reversibility of optical phenomena in time, analysis of diffraction output of light emission from a film waveguide permits one to find the optimum conditions for the reverse process -- emission input to the TPV through its corrugated section. As already noted above, the main parameter which determines the optimum conditions of emission input to the waveguide is the attenuation constant α_m of an m-order surface wave during its emission along the corrugated section of the TPV. The expressions for constants α_m for TE- and TM-modes of TPV can be found, for example, in [14, 22, 23]. The value of α_m is usually greater when the film is corrugated from the direction of the air. This is related to the fact that the difference of the refractive indices on the film-air boundary is greater than that on the film-substrate boundary. On the other hand, with corrugation of the upper surface of the film waveguide, the interference effects manifested in the form of maximum and minimum values of $\alpha_m(\theta_j)$ are expressed to a lesser extent [2] and consequently the attenuation constant α_m becomes less critical to selection of the emission angles θ_j, i.e., to selection of the period of the grating structure Λ. In this sense corrugation of the upper boundary of the TPV is preferable. Those periods of corrugation Λ which would provide emission to one of the media adjacent to the waveguide (usually to the substrate) must be selected to accomplish optimum input of emission. Those periods to which "back" emission corresponds are more preferable since in the given case only the first order of diffraction is present in emission with any form of corrugation profile [22]. The periods Λ at which light is emitted only to the substrate satisfy the condition

$$(n_m^* - n_0) \leqslant N \leqslant (n_m^* - n_2), \tag{2.15}$$

which corresponds to "forward" emicsion in the direction of propagation of the surface wave and to condition

$$(n_m^* + n_2) \leqslant N \leqslant (n_m^* + n_0) \tag{2.16}$$

with "back" emission of light with respect to the direction of surface wave propagation.

There are some characteristics of diffraction excitation of diffuse optical waveguides related to the absence of interference effects and which lead to a smoother dependence of constant $\alpha_m(\theta_j)$ and to its smaller absolute value compared to TPV with sharp boundaries [20, 17].

With optimum periods of corrugation and with given value of α_m, the effectiveness of emission input into TPV η depends only on the distribution of the exciting light beam intensity along the length of coupling zone L and for homogeneous distribution of the incident beam field excitation is more effective at $\alpha_m L \approx 1.25$; then $\eta_{max} = 81$ percent [11]. If it is necessary to excite the waveguide from the direction of the air, it is better to use corrugation of the substrate since in this case a value of $\eta \sim 50$ percent can be achieved [22].

It should be noted that the large difference in the value of the attenuation constants for waves of different polarizations (α_{TE} and α_{TM}) at specific periods of corrugation Λ [20, 21, 23] can be used for selecting the surface waves by polarization and to create thin-film light polarizers based on diffraction emission of surface waves or on their resonance reflection.

Another possible method of diffraction excitation of TPV is the use of volumetric phase diffraction gratings applied to the waveguide surface or formed directly in the material of the waveguide itself [24, 25]. Investigation of the process of surface wave emission from a TPV with volumetric phase grating applied to its surface (Figure 1, c) shows [24] that only a -1-order diffraction wave with projection of the wave vector onto the Z axis equal to $gn_m^* - K \sin \chi$ makes the main contribution to emission in approximation of weak coupling ($|\delta n/n_2| \ll 1$).

Provided that

$$n_{0(2)} > |n_m^* - N \sin \chi| > n_{2(0)} \tag{2.17}$$

this wave is propagated in the substrate (or grating) at angle $\theta_{0(2)}$:

$$\sin \theta_{0(2)} = (n_m^* - N \sin \chi)/n_{0(2)}. \tag{2.18}$$

Provided that

$$n_1,\ n_2 > |n_m^* - N \sin\chi| \qquad (2.19)$$

this wave is emitted in both directions simultaneously. Moreover, the relations of the intensities with which a -1-order wave is emitted to a medium with grating and substrate adjacent to the TPV are considerably dependent on the angle of inclination of the homogeneous layers of the phase grating and may reach a value $\leqslant 10^{-2}$ ($\geqslant 10^2$). The expressions for the attenuation constants α_m for all these cases are found in [24]. The effectiveness of input (approximately 71 percent) achieved in experiment [26] approaches its theoretical limit (approximately 80 percent) to a significant degree.

The prevalent surface wave emission to one of the media adjacent to the waveguide is caused by Bragg scattering of this wave to a -1-order diffraction wave. In the general case the parameters of a volumetric grating should be selected to accomplish this Bragg scattering so that [24]

$$n_2 \approx n_1,\ N = 2n_m^* \sin\chi \left(\text{или } n_m^* = N \sin\chi = n_m^* \cos 2\chi\right). \qquad (2.20)$$

Two Bragg inclinations of homogeneous layers of the grating: $0 < \chi_1 < \pi/2$ and $\chi_2 = \pi - \chi_1$, are possible at each value of $N(< 2n_m^*)$. If $|\cos 2| < n_0/n_m^*$ and n_2/n_m^*, then the surface wave is essentially completely emitted to the medium with a grating at $\chi = \chi_1$ and is Bragg-scattered to the substrate at $\chi = \chi_2$. If $n_{2(0)} > n_m^* |\cos 2\chi_1| > n_{0(2)}$, the surface wave is emitted to the grating (or substrate).

It should be noted with regard to the use of a volumetric diffraction grating for input of light emission to the TPV that the condition of phase synchronism for a diffraction wave and for the m-th waveguide mode excited by it is incompatible with the condition of precise Bragg resonance of the diffraction grating. Therefore, some slight misalignment of the Bragg grating structure from resonance is required to ensure effective excitation of the given waveguide mode [11].

Diffraction of light beams on periodic structures in TPV. Diffraction of emission on periodic structures in the TPV plane is of interest not only for division or deflection of light beams in film waveguides [27] but also for spatial-selective filtration of them [28-30]. To do this, Bragg type grating structures can be formed in TPV both as the result of modulation of thickness and of the refractive index of the waveguide material. For definiteness, let us consider a TPV with volumetric sine-wave phase grating formed due to weak modulation of the refractive index of the waveguide material ($|\delta n/n_1| \ll 1$). The diffraction-grating structure on which noncolinear interaction of the surface waves in the TPV can be accomplished when the directions of propagation of the interacting waves do not coincide with the vector of grating K, is shown schematically in Figure 1, d. In

this case the Wolf-Bragg condition with regard to waveguide propagation of emission has the form [31, 32]

$$N=2n_m^* \sin\theta, \tag{2.21}$$

where θ is the Bragg diffraction angle. In the considered configuration, the phase grating operates in the transmission mode and its diffraction effectiveness η in approximation of the interaction of plane waves in the absence of losses in the TPV may be described by an expression totally similar to (2.9) [33] where the effective length of the grating $L^* = L/\cos\theta$ and $\Delta N = (2n_m^* \times \sin\theta - N)\sin\theta$ is introduced instead of z. As one should also expect, the constant k is significantly dependent on the index and polarization of the waveguide modes. In the case of a volumetric phase grating for TM waveguide modes, it can be written in the form

$$k_{TM}\approx\delta n(n_1/n_m^*)g/2. \tag{2.22}$$

The absolute value of k_{TE} for the TE-modes is less and is determined by the value of the angle of deflection $\varphi = 2\theta$ (see Figure 1, d):

$$k_{TE}\approx-\delta n(n_1/n_m^*)(g/2)\cos\varphi. \tag{2.23}$$

When the grating structure operates in the reflection mode [33], its diffraction efficiency (coefficient of reflection) can be determined by using expression (2.4).

All that considered above also remains valid in general features for Bragg diffraction-grating structures formed by modulation of the TPV thickness. However, the form of the coupling constants k in this case will apparently be more complex (unlike expressions (2.10) and (2.12)) since Bragg diffraction on this grating structure may be accompanied by transformation of the incident wave to a wave or orthogonal polarization and this problem requires further investigation [32, 34].

It should be noted that the sloping impingement of emission on the grating structure during Bragg diffraction leads to distortion of the spatial shape of the diffracted and transient light beams and it is stronger, the broader the incident beam spectrum compared to the band of Bragg diffraction angles (frequencies) [29, 35]. Specifically, the total width of the diffracted band transient beams is always not less than $a = 2L\sin\theta$. Distortion of the spatial shape of the signal is usually manifested to a greater extent for grating structures formed by corrugation of the TPV surface, which is related to a smaller value of the achieved values of the coupling constant k.

The high spatial-angular and frequency-selective characteristics of Bragg type diffraction-grating structures permits highly effective spatial-selective filtration of emission in the TPV during its inclined impingement on the grating structure. These spatial-selective filters may find application

for multichannel OLS with channelling [28, 30]. The frequency-selective selectivity of a filter is related to its angular selectivity by the simple relation [33]

$$\Delta\lambda/\lambda = -\Delta\theta \operatorname{ctg}\theta, \quad \Delta\theta \ll \theta, \tag{2.24}$$

which determines the dependence between variations of wavelength and the angle of incidence of emission, leading to the same detuning from Bragg resonance. For homogeneous and symmetrical distribution of the value of the coupling constant k by the effective length of the grating structure L*, the shape of its spectral characteristic is symmetrical [36] and the total spectral width of its resonance $\Delta\lambda/\lambda$ during inlcined incidence of emission on the grating may be written in the form [37]

$$\Delta\lambda/\lambda \approx 2(\Lambda^*/L^*)[1+(kL^*/\pi)^2]^{1/2}, \tag{2.25}$$

where their effective values instead of Λ and L are introduced in the direction of propagation of the incident light beam ($\Lambda^* = \Lambda/\sin\theta$) and the value of kL* for ensuring a minimum value of $\Delta\lambda/\lambda$ does not exceed $\pi/2$ (or π) for grating structures operating to transmission (or reflection). This approach to determining the selective and diffraction properties of grating filters is related to the use of approximation of the plane wave [33, 37] and is justified when the angular divergence of emission in the TPV is significantly less than the angular width of the Bragg resonance of the grating. In the opposite case when calculating the spectral characteristics and diffraction effectiveness of a grating filter, the entire set of spatial components of the wave vectors of plane waves impinging on the grating must be taken into account. The field distribution in the diffracted and transient beams are then determined by Fourier transformation of the product of the spectrum of incident plane waves by the amplitude coefficients of reflection or transmission [29, 35].

Comparative analysis of different types of modulation of TPV parameters. It is of interest to carry out comparative analysis of the various types of modulation of TPV parameters for selecting the preferable type of modulation of film waveguide parameters (if there is this type of modulation).

It is obvious from the previous consideration that the effectiveness of surface wave interaction in TPV on a grating structure is determined by the value of the coupling constant k which in the most general case is proportional to the absolute value of the modulation amplitude of the effective waveguide refractive index Δn^*. Actually, limiting ourselves to the case of weak modulation of thickness h and the refractive index of the waveguide material n_1 and taking into account the expressions for derivatives $\partial n_m^*/\partial h$ and $\partial n_m^*/\partial n_1$ [38], it is easy to show that

$$k = (\pi/\lambda)\Delta n_m^*, \tag{2.26}$$

where Δn_m^* for the TE-modes of TPV upon modulation of thickness h is equal to

$$(\Delta n_m^*)_\sigma = \sigma(n_m^*/h_m^*)[(n_1/n_m^*)^2 - 1], \tag{2.27}$$

and upon modulation of the refractive index of the material n_1 is equal to

$$(\Delta n_m^*)_{\delta n} = \delta n(n_1/n_m^*)(h_m/h_m^*). \tag{2.28}$$

For simplicity it was implicitly assumed here that colinear interaction of the modes with identical indices (m' = m) is considered. Comparing expressions (2.27) and (2.28) and assuming that $h_m \approx h$, which occurs in most real cases, we find

$$(\Delta n_m^*)_\sigma/(\Delta n_m^*)_{\delta n} = (\sigma/h)[1-(n_m^*/n_1)^2]/(\delta n/n_1). \tag{2.29}$$

Let us introduce the parameter $\Delta_m = n_1 - n_m^*$ and, since $n_m^* \sim n_1$, we finally find

$$(\Delta n_m^*)_\sigma/(\Delta n_m^*)_{\delta n} \approx 2(\Delta_m/n_1)(\sigma/h)/(\delta n/n_1) \tag{2.30}$$

Since usually $\Delta_m \ll n_1$, it follows from expression (2.33) that considerably less relative modulation of the refractive index of the waveguide material is required compared to the relative modulation of its thickness to ensure an identical value of the modulation amplitude of the effective refractive index Δn_m^* or, which is the same thing, of the value of coupling constant k. Moreover, the indicated difference is manifested more strongly for the lower waveguide modes and is amplified with an increase of its thickness h. This is physically related to the lesser contribution of the modulation of waveguide thickness to disturbance of the surface wave field compared to modulation of the refractive index of its material, which makes a contribution to the value of the coupling constant k through the entire TPV cross-section. One may also arrive at a similar conclusion on the basis of analyzing the results of numerical calculations obtained for various types of periodic structures in TPV [39]. This comparison is valid only for the TE-modes of TPV. In the case of a TM waveguide mode, as was already noted above, the coupling constant k depends in a more complex manner on the TPV parameters and returns to zero during some quite specific periods of corrugation of its surface (see (2.13)). Consequently, modulation of the waveguide thickness does not lead in this case to coupling and mutual transformation of surface waves.

Absolute comparison of the effectiveness of one or another type of modulation of TPV parameters may also be carried out for specific TPV materials. Thus, for example, analyses show that the maximum possible modulation of the effective refractive index Δn^* due to variation of the refractive index of the waveguide material n_1 is approximately an order or more higher for such a

TPV material as amorphous chalcogenide semiconductor film [40, 41] than (depending on h) in the case of a corrugated surface.

For definiteness let us consider a TPV based on As_2S_3 films on $LiNbO_3$ substrates ($\lambda \approx 0.63$ micron, $n_0 \approx 2.29$ and $n_1 \approx 2.48$). Absolute comparison for real TPV parameters ($h \sim \lambda$) shows that the coupling constant due to modulation of the refractive index of the waveguide material n_1 is more than fivefold higher than k for a corrugated surface for the TE_0 waveguide mode ($n_0^* \approx 2.476$, $h \approx 0.6$ micron; $\delta n_{max} \approx 0.06$ and we assume that the maximum depth of the corrugation $2\sigma_{max}$ is equal to 0.2 micron). The efficiency of corrugated grating structures may be comparable to that of a structure with modulated refractive index and is higher than this efficiency for sufficiently thin single-mode waveguides when working near the cut-off, but in this case the condition of weak coupling is usually not fulfilled and the losses in the TPV increase significantly; moreover, the thinnest possible waveguide layer does not exhaust all the possibilities of interest from the practical viewpoint. There is a sharp decrease of the operating efficiency of the corrugation with an increase of waveguide thickness h, whereas the coupling constant, beginning at some value of h ($h < \lambda$) is essentially independent of waveguide thickness in the case of modulation of the refractive index of the material n_1. One should also bear in mind that corrugation of the TPV surface is possible on a wider range of materials and realization of modulation of the refractive index of the waveguide material itself requires a search for special materials for TPV.

With regard to periodic structures in the substrate (the surrounding medium), they operate much less efficiently compared to periodic variation of the refractive index of the waveguide material itself since the values of derivatives $\partial n_m^*/\partial n_j$ ($j = 0, 2$) are usually much less than $\partial n_m^*/\partial n_1$. With the same parameters of the grating structures and real parameters of TPV, their efficiency in the sense of the possibility of providing a given value of k is approximately 50-100 times less. It should be noted that a similar conclusion also remains valid for relief type grating structures. Thus when a thin corrugated layer of another material with refractive index $n < n_1$ is applied to the TPV surface, the coupling constant decreases $|(n^2 - n_2^2)/(n_1^2 - n_2^2)|$ times for TE-modes and is somewhat greater for TM waveguide modes (compared to corrugation of the waveguide surface itself) [21, 45].

3. Integrated Optics Components and Devices Based on Diffraction-Grating Structures

In this section we shall consider some applications of diffraction-grating structures in integrated optics. Most attention is devoted to periodic grating structures as the most investigated; the possibilities of using grating structures with variable period ("aperiodic" grating structures) are also considered.

Periodic grating structures. The use of periodic grating structures in integrated objects led to the development of many thin-film waveguide devices such as emission input and output devices, band filters and mode

converters, diffraction type modulators and deflectors and ROS and RBZ lasers; phase matching and spatial-selective filtration of surface waves in TPV are accomplished by using them.

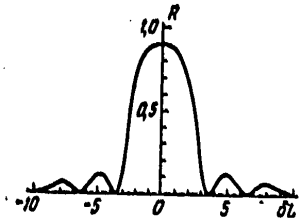

Figure 2. Spectral Characteristics of Reflecting Filter

The operation of band reflecting filters and mode converters is based on resonance reflection or on transformation of surface waves on the diffraction-grating structure in TPV. The condition of resonance surface wave reflection (2.3) and (2.8) assigns the working length of the reflecting filter wave and expression (2.4) (where $\Delta N = 2\delta/g$) gives the dependence of the coefficient of reflection R_m of an m-order surface wave on detuning from resonance δ. In practice δ may be varied due to variation of the emission frequency or wavelength. The dependence of the coefficient of reflection R_m on the value of $\delta L \approx [(\omega - \omega_0)Ln_m^*/c]$ for $kL = 1.84$, which corresponds to $R_{max} \approx 0.9$ (here ω_0 is the resonance frequency of the filter), is shown in Figure 2. The band width of the main maximum reflection of the lattice structure by wavelength $\Delta\lambda/\lambda$ may be determined from expression (2.25), where $\Lambda^* \equiv \Lambda$ and $L^* \equiv L$, while the maximum coefficient of reflection of the filter R_{max} corresponds to precise resonance ($\Delta N = 0$ in (2.4)). Moreover, the value of R_{max} is different (Figure 3) for different wavelengths with fixed length of the grating structure L. Filters with a narrower band should have a value of $kL \leqslant \pi$. At $kL > \pi$ the side lobes become comparable to the main lobes [33].

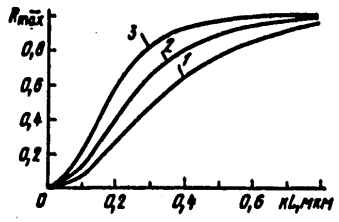

Figure 3. Maximum Coefficient of Reflection of Filter R_{max} as a Function of Parameter kL for Different Wavelengths: 1 -- 1.15 microns; 2 -- 0.86 micron; 3 -- 0.63 micron

Development of narrowband grating filters for a given wavelength λ places specific restrictions both on the permissible value of deviation from resonance ΔN, caused by the inaccuracy of being given the period of the grating Λ, and also on the permissible variations of the effective refractive index of the waveguide n_m^* caused by the inhomogeneity of its thickness along the length of the grating structure. Deviations in the period of the grating $\Delta\Lambda$ lead to a change in the resonance wavelength of the filter [42]

$$\Delta\lambda_1 \approx \lambda(\Delta\Lambda/\Lambda), \tag{3.1}$$

while the inhomogeneities in the thickness of the film waveguide Δh cause changes in the position of the maximum reflection of the filter along the wavelength and consequently lead to broadening of its band by the value [37]

$$\Delta\lambda_2 = \lambda(\Delta h/h_m^*)[(n_1/n_m^*)^2 - 1]. \tag{3.2}$$

Experimental investigation of narrowband reflecting filters with half-width of resonance on the order of fractions and units of angstroms and with coefficient of reflection of approximately 0.8-0.9, achieved due to a corrugated TPV surface [37, 42] and modulation of the refractive index of the waveguide material [40], shows good agreement of the calculated and experimental results. This justifies development of methods of synthesizing optical waveguide filters with given frequency characteristics operating in the reflection and transmission mode [43, 44]. It is proposed in [45] that selection of the incident wave by means of a thin-film mode selector be used to create narrowband frequency-selective filters operating due to mode conversion during single-direction interaction of them on grating structures in TPV. Interesting possibilities for various applications in integrated optics are opened up by mode conversion in TPV on a grating structure with non-sine-wave profile during noncolinear interaction of surface waves [46]. However, additional investigations are still apparently required in this direction.

Experimental investigations devoted to spatial-selective filtration of emission in TPV by using periodic grating structures [28-30], although they are few, now indicate new possibilities of using integrated-optics circuits in OLS with channelling. We would especially like to emphasize the prospects of using for these purposes such TPV material as amorphous chalcogenide semiconductor films which permit creation of various phase-relief structures in the waveguide itself both by optical methods [30, 40] and by using electron beam processing [41]. The conducted investigations [40] show that the actually achieved characteristics of Bragg grating structures permit development of highly efficient frequency-selective devices based on them for combination (mixing) and separation of optical data channels with different carrier frequencies. Comparitive analysis of spatially-selective filters based on Bragg grating structures formed in the waveguide and due to corrugation of its surface permits one to conclude that the least distortion of

the spatial shape of the signal may be achieved in TPV based on amorphous chalcogenide semiconductors when the grating structures are formed in the waveguide itself.

The possible variants of constructing optical channel mixers are shown schematically in Figure 4. The simplest are devices based on a set of deflecting grating structures with different periods and scanning gradient channel waveguide (Figure 4, a and b). They are suitable in a small number of data channels (approximately up to 10). More complex grating structures which utilize the principle of superposition of three-dimensional phase holograms (Figure 4, c) permit one to realize a mixer with a considerably larger number of packed channels. This mixer based on superimposed three-dimensional phase grating structures is more universal due to its reversibility and the possibility of operating in the channel-separation mode and provides considerably greater compactness of the device as a whole. The wave tracks of separated channels in an optical waveguide are shown on the right in the photograph in Figure 4, c. The nearest optical carriers were separated from each other by approximately 15-20 nm, which, however, is not maximum. In real OLS circuits, this mixer may operate, as indicated by analyses, with considerable greater channelling (on the order of 50) with building up adjacent optical carriers on the order of several angstroms.

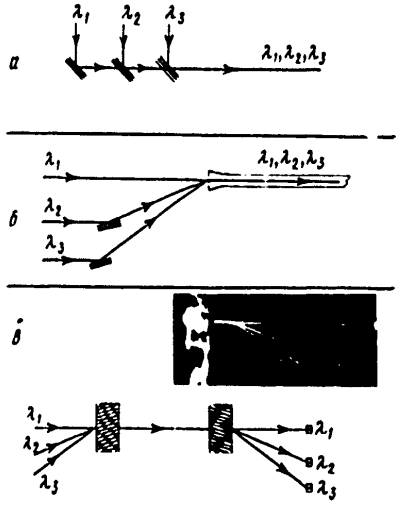

Figure 4. Schematic Diagram of Different Variants of Spatial-Selective Filters for Channel Mixers Based on Periodic Diffraction-Grating Structures in TPV

Periodic modulation of TPV parameters is also possible by using the electro-optical effect when the modulating voltage is applied to a periodic system of antipin electrodes or by using the optical-acoustic effect which utilizes acoustic waves of the appropriate frequencies. Since the refractive index of the TPV may now be varied due to the effect of the modulating voltage or the amplitude of the acoustic wave, this type of thin-film diffraction devices may serve as amplitude modulators, switches or deflectors. Thin-film diffraction type optical-acoustic devices may also be used in optical signal processing devices. The most significant parameters in this case are the efficiency of diffraction, the working frequency band, the speed and number of resolved light beam positions.

A large number of both original [47-51] and survey papers [52-53] is devoted to theoretical analysis of the various aspects of optical-acoustic interactions in TPV. Single-direction interaction of coupled surface light waves during colinear [54, 55] and noncolinear [56-58] interaction of them with a surface acoustic wave (PAV) is used in diffraction type modulators and deflectors. Bragg diffraction [56, 57] when only one diffraction order occurs is usually employed to achieve the greatest efficiency. Channelling of the optical and acoustic beams leads to high power densities, to an increase of the interaction length and, because of this, to more effective interaction at low levels of control power. Thus, an optical-acoustic deflector-modulator with working frequency above 200 MHz and control acoustic power not exceeding 7 mW was developed on the basis of lithium niobate waveguides [59]. Thin-film variants of optical-acoustic convolvers which utilize light diffraction in TPV on PAV and which accomplish the operation of convolution of optical signals, have higher efficiency than their volumetric analogs [60, 61]. They apparently find broad application in development of various optical data processing devices.

The speed of optical-acoustic diffraction devices is limited both by the converter frequency band and by the transit time of the acoustic wave through the optical beam. These principal restrictions are eliminated in electrooptical diffraction modulators in which the phase diffraction grating is induced by an electric field applied by a system of pin electrodes. Their potentially possible bandwidth is restricted only by the natural capacity of the device itself and may be brought up to several gigahertz [59]. In this case the control voltage is corresponding to the percentage modulation close to 100 percent do not exceed a value on the order of 10 V [59, 62]. The characteristics of electrooptical modulators of this type can be optimized by proper selection of the TPV parameters and of the corresponding electrode structure.

By utilizing the respnance properties of periodic grating structures, one can also modulate the emission intensity in TPV by controlling the diffraction efficiency of a stationary phase grating structure. The possibility of this type of emission modulation by using ROS and RBZ electrooptically controlled structures are discussed theoretically in [63]; light modulation in semiconductor TPV by using stationary phase diffraction gratings with

resonance excitation of the acoustic wave in them was investigated experimentally in [64]. Modulators of this type expand the capabilities of known thin-film diffraction modulators and apparently find application in integrated optics.

Along with diffraction type electrooptical and optical-acoustic thin-film devices, deflectors and modulators are beginning to be developed and investigated in which the magnetooptical effect is used to control the parameters of the phase grating formed by the periodic structure of the magnetic domains [65, 66].

We will not dwell in detail on the problems devoted to experimental investigation of diffraction-grating emission input and output devices since many practical aspects of their application in integrated optics were considered in the previous section; moreover, there is a special survey paper on this problem [67]. We shall note only the more significant aspects related to the new possibilities which grating structures with an asymmetrical profile [68, 69] open up for integrated optics, which make it possible to achieve single-direction emission from TPV to one of the media adjacent to the waveguide with sufficiently long period of them (and, consequently, high efficiency of TPV emission input), and volumetric phase gratings formed both on the surface of and in the TPV itself [24, 25] in which high efficiency is combined with new functional capabilities.

With regard to ROS and RBZ lasers, many papers, including those of a survey nature [5, 8, 16, 70-72] have been devoted to their theoretical and experimental investigations and the practical aspects of applications in integrated optics, which are of independent interest and go far beyond the framework of the given survey.

Aperiodic grating structures. Almost periodic grating structures with a period, varying monotonically along the length of the grating ("aperiodic" grating structures), are of great interest to integrated optics and open up broad possibilities for development and creation of a number of new spatially-selective thin-film waveguide devices [73-76]. These grating structures with variable period can be achieved by corrugation of the TPV surface (as in the case of strictly periodic structures) when recording an interference pattern of two laser beams with plane and cylindrical wave fronts on a photoresistor surface applied to a waveguide (Figure 5). In the considered configuration, the period of the grating structure is a monotonic function of coordinate $\Lambda(z) = \lambda_e/[2n_2 \sin((\theta_0 + \theta)/2)]$, where λ_e is the wavelength of the irradiating emission [73]. By introducing $N(z) = \lambda/\Lambda(z)$ (here λ is the working wavelength of emission propagated in the TPV, one can show that in paraxial approximation (when $(z - z_0) \ll \ll (a^2 + b^2)^{1/2}$, see Figure 5)

$$N(z) \approx N(z_0) + A(z - z_0), \tag{3.3}$$

where parameter A characterizes variation of the period of the grating which decreases in our case with an increase of z and depends on the recording

conditions and wavelength λ [74]. An aperiodic grating on a TPV surface with parameters which satisfy the condition of emission output $|n_m^* - N| < n_0, n_2$, will operate as an output focusing device with focal distance F_m (in a medium with refractive index of n_2), dependent on the emission wavelength, mode index m and parameter A [74]:

$$F_m \approx |n_2^2 - (n_m^* - N(z_0))^2| / A n_2. \qquad (3.4)$$

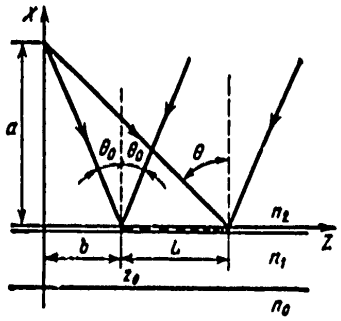

Figure 5. Diagram of Achieving Aperiodic Grating Structures on TPV Surface

One of the important applications of aperiodic grating structures in integrated optics may be the emission input device into TPV, the emission having significant divergence, for example, from a semiconductor laser, or a fiber light guide TPV matching device [74], but there are still many unresolved problems here. Aperiodic grating structures may also find application in development of wideband reflecting filters [36], whose response (i.e., the coefficient of reflection as a function of wavelength) may vary due to variation of the aperiodicity of the grating structure. Spatial-selective filtration of emission in TPV may be accomplished by using them, frequency-selective devices for combination and separation of optical data channels with different carrier frequencies (multiplexers and demultiplexers) may operate on their basis [75] and multichannel ROS and RBZ lasers may also be realized on their basis [76].

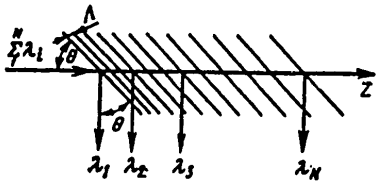

Figure 6. Schematic Diagram of Spatial-Selective Filter Based on Aperiodic Grating Structure in TPV

A diagram of a spatial-selective filter based on an aperiodic grating structure in a TPV is shown in Figure 6. Its operation is based on selective Bragg reflection of emission with different wavelengths from different sections of the grating structure so that spatial separation or combination of them in the general transmitting channel is accomplished. The obvious design and technological advantage of this channel mixer compared to the variant shown in Figure 4, a should be noted, but it is also suitable for operation with a small number of data channels. Expressions (2.4) or (2.9), which correspond to the resonance case where the effective length L_{ef} of the corrugated section within the range of the resonance width of Bragg reflection $(\Delta\Lambda)_0$ by period Λ should be taken instead of L*, may be used as a function of the operating mode to analyze the coefficient of reflection [75]. Assuming that variation of the period along the length of the grating structure is linear, i.e., limiting oneself to approximation (3.3), one can find that

$$L_{э\phi}=\lambda(\Delta\Lambda)_0/(A\Lambda). \tag{3.5}$$

There is no doubt that further investigation of grating structures with variable period for purposes of integrated optics will lead to new advances.

4. Devices With Tunnel Distributed Coupling

Two regular closely arranged dielectric waveguides may efficiently exchange power due to tunnelling of the electromagnetic wave energy from one waveguide to another, thus providing directional power branching [77, 78]. The condition of phase synchronism for the interacting waves ($\beta_m = \beta_n$) must be fulfilled to accomplish effective coupling. The coupling constant k is real in a medium without losses and if the waveguides have identical distribution of the refractive indices, the constants k_{mn} and k_{nm} in equations (1.2) and (1.3) are equal. For waveguides with different propagation constants ($\beta_m \neq \neq \beta_n$), coupling may be improved by periodic disturbance of the waveguide parameters, thus ensuring the condition of phase synchronism ($\delta = 0$) which for sine-wave disturbance may be written in the form

$$\delta=\beta_m\pm\beta_n\pm q(2\pi/\Lambda), \tag{4.1}$$

where Λ is the period of disturbance in the direction of wave propagation z and q = 1, 2, ... (usually operation at q = 1 is most efficient). In this case power transfer both in the forward and reverse directions is possible [78, 79]. Couplers with smooth variation of parameters along the length of the coupling zone were proposed and investigated in [79] to provide noncritical phase matching of waves to selection of waveguide parameters.

An important example of accomplishing tunnel type coupling is a prismatic coupler which is used for excitation of waveguide modes in TPV. Although laser emission rather than the waveguide mode is used for excitation in a

prismatic coupler, its operating principle is similar to the mechanism of coupling between regular waveguides. In both cases "disturbance" of total internal reflection from the waveguide boundaries and tunnelling of the electromagnetic energy occur, which also ensures coupling of the interacting waves. Coupling of this type by using an exponentially attenuating field has the advantage of directionality and is used for directional shunting of power. Detailed analysis of the operation of a prismatic device, although based somewhat differently from coupled wave theory, is carried out in [11]. The processes of tunnel and diffraction emissions of surface waves in diffusion waveguides with arbitrary transverse distribution of the refractive index were investigated in [80] and the optimum conditions of effective excitation of diffusion waveguides were formulated in universal form. Expressions for the attenuation constants α_m for both considered cases are presented in the same paper. The main conclusions of this paper were checked experimentally in [81] where the dependence of the attenuation constants on the mode index were determined and it was shown that the effective input of emission to diffusion waveguides is possible only through a small gap of special profile. The greatest difficulties are encountered during tunnel excitation of TPV having high refractive index, for example, based on GaAs; the effectiveness of excitation is usually low in this case (approximately 10-15 percent) [82]. However, a significant increase of emission input efficiency is possible for these TPV when using combined devices consisting of a coupling prism and a diffraction grating applied to its base [83].

Realization of monolithic and combined integrated optics circuits with effective coupling of the emitter and the TPV [84, 85] is possible on the basis of an optical tunnel device under conditions of providing phase synchronism due to the appropriate design version of the emitter. The effectiveness of coupling may practically reach its theoretical limit in this case. Tunnel coupling of a semiconductor laser with a TPV due to an exponentially attenuating field may also be accomplished in the absence of phase matching but in this case, as indicated by experiments, efficiency does not exceed 25 percent [86]. Direct coupling of a RBZ laser to a TPV with corresponding selection of the grating structure and waveguide parameters is also possible [87].

Upon an exchange of power between two identical coupled waveguides (the condition of phase synchronism is fulfilled, $\delta = 0$), the total power from the first waveguide is transmitted to the second at some coupling wavelength L_1, determined from expression (1.8) and equal to

$$L_1 = \pi/(2k). \qquad (4.2)$$

If the interaction length is greater than L_1, reverse pumping of power to the first waveguide occurs. The value of L_1 is determined by the coupling constant k and depends on the distance between the waveguides and the parameters of the waveguides themselves [77]. Waveguide systems in which power is pumped with very small gaps between coupled waveguides usually find application [88]. This places serious technological requirements on

manufacture of these directional couplers based on channel waveguides, the distance between which does not exceed units and tens of microns at values of L_1 on the order of several millimeters. An increase of the gap at this length of the coupling zone can be achieved by using complex profiles of the refractive index of the waveguides themselves, which provide great depth of penetration of the directed emission field [89]. By changing the value of the coupling constant, for example, by electrooptical or other methods, coupling between two waveguides can be controlled at a given value of L_1 and thus emission can be modulated. A large number of directional controlled couplers [90] and switches, the typical control voltages of which comprise approximately 20 V, has been constructed on this principle [91].

Further improvement of OLS systems is impossible without extensive introduction of integrated optics components. Practical use of integrated optics components in combination with fiber light guides is limited by the absence of highly efficient coupling devices between film and fiber waveguides. The same three main types of matching devices -- tunnel, diffraction and those with beveled edge of the waveguide -- are used to accomplish coupling, but the efficiency of these devices is usually low and they are not all universal. The greatest number of developments is devoted to devices based on the light energy tunnelling effect. Devices for joining integrated optics circuits by using complex ribbon optical fibers have been proposed [92]. Both input and output of laser emission to TPV is possible by using these devices and their operating principle is the same as in a directional coupler. The maximum luminous energy transfer coefficient reaches 97 percent. TPV coupling with ordinary fiber light guides is also possible on this principle [93], but effective coupling is possible only in the case of single-mode fibers. Another method of matching TPV and an optical fiber is light emission tunnelling from a TPV to a fiber cut at some angle [94] and return [95] with the end of the fiber being arranged parallel to the waveguide surface. The use of this device in combination with the beveled edge of the TPV made it possible to accomplish emission input into the fiber with an efficiency of approximately 80 percent [96]. Many pattents [97] have been devoted to problems of tunnel matching of fiber light guides with TPV, but no actually existing systems and coupling components having acceptable parameters have yet been developed. Different variants of realizing combined TPV-fiber light guide coupling devices are also possible when diffraction output of emission directly to the optical fiber [98] or the holographic method of matching [99] is used when recording a hologram on the surface or in the volume of the TPV; aperiodic grating structures may also be used for this.

It should be noted in conclusion that the limits of the applicability of results which describe the considered diffraction processes of transformation of surface waves are closely related to the maximum permissible relative value of modulation of the effective refractive index of TPV $\Delta n^*/n^*$. Based on comparison of the results of numerical solution of the equations of first- and second-order coupled waves for spatially periodic media [100], one may conclude that the results presented in this survey are valid for $\Delta n^*/n^* \lesssim$ $\lesssim 0.012$, which almost always occurs in most real cases.

Unfortunately, the limited scope of the survey did not permit consideration of the various methods of achieving diffraction-grating structures for purposes of integrated optics. The methods of their manufacture are closely related to the technology of producing TPV themselves [101, 102] and are usually based on the use of holographic methods and photolithography methods with subsequent etching of the treated surface [8, 103, 104]. One of the most promising methods of producing grating structures on a TPV surface based on semiconductor compounds is the method of photoselective etching of their surface [105, 106].

BIBLIOGRAPHY

1. Elashi, TRUDY IIER, Vol. 64, No. 12, 1976.
2. Yariv, A., IEEE J, QE-9, 1973; Yariv, A., in "Vvedeniye v integral'nuyu optiku" [Introduction to Integrated Optics], edited by M. Barnoski, Moscow, Mir.
3. Marcuse, D., Theory of Dielectric Optical Waveguides, New York, Academic Press, 1974.
4. Kogelnik, H., in Integrated Optics, edited by T. Tamir, New York, Springer-Verlag, 1975.
5. Yariv, A. and M. Nakamura, IEEE J, QE-13, 1977.
6. Kogel'nik, H., UFN, Vol. 121, 1977.
7. Kogel'nik, H. and C. V. Shank, J. APPL. PHYS., Vol. 43, 1972.
8. Luk'yanov, V. N., A. T. Semenov, N. V. Shelkov and S. D. Yakubovich, KVANTOVAYA ELEKTRONIKA, Vol. 2, 1975.
9. Landau, L. D. and Ye. M. Lifshits, "Elektrodinamika sploshnykh sred" [The Electrodynamics of Compact Media], Moscow, Fizmatgiz, 1959.
10. Taylor and Yariv, TRUDY IIER, Vol. 62, No. 8, 1974.
11. Zolotov, Ye. M., V. A. Kiselev and V. A. Sychugov, UFN, Vol. 112, 1974.
12. Kiselev, V. A., KVANTOVAYA ELEKTRONIKA, Vol. 1, 1974.
13. Kiselev, V. A., KVANTOVAYA ELEKTRONIKA, Vol. 1, 1974.
14. Kiselev, V. A., KVANTOVAYA ELEKTRONIKA, Vol. 1, 1974.
15. Rigrod, W. W. and D. Marcuse, IEEE J, QU-12, 1976.
16. Zlenko, A. A., V. A. Kiselev, A. M. Prokhorov, A. A. Spikhal'skiy and V. A. Sychugov, KVANTOVAYA ELEKTRONIKA, Vol. 2, 1975.

17. Prokhorov, A. M., A. A. Spikhal'skiy, V. A. Sychugov and G. P. Shipulo, KVANTOVAYA ELEKTRONIKA, Vol. 3, 1941 (1976).

18. Kazarinov, R. F., Z. N. Sokolova and R. A. Suris, ZHTF, Vol. 46, 1976; Z. N. Sokolova and V. B. Khalfin, PIS'MA V ZHTF, Vol. 3, 1977.

19. Gudzenko, A. I., RADIOTEKHNIKA I ELEKTRONIKA, Vol. 21, 1976.

20. Prokhorov, A. M., A. A. Spikhal'skiy and V. A. Sychugov, KVANTOVAYA ELEKTRONIKA, Vol. 3, 1976.

21. Kiselev, V. A. and A. M. Prokhorov, KVANTOVAYA ELEKTRONIKA, Vol. 4, 1977.

22. Zlenko, A. A., V. A. Kiselev, A. M. Prokhorov, A. A. Spikhal'skiy and V. A. Sychugov, KVANTOVAYA ELEKTRONIKA, Vol. 1, 1974.

23. Zlenko, A. A., A. M. Prokhorov, A. A. Spikhal'skiy and V. A. Sychugov, KVANTOVAYA ELEKTRONIKA, Vol. 3, 1976.

24. Kiselev, V. A., KVANTOVAYA ELEKTRONIKA, Vol. 1, 1974.

25. Bozhevol'nyy, S. I., Ye. M. Zolotov, V. A. Kiselev, V. M. Pelekhatyy, A. M. Prokhorov and Ye. A. Shcherbakov, DAN SSSR, Vol. 235, 1977.

26. Kogelnik, H. and T. P. Sosnovskiy, BELL SYSTEMS TECHNICAL JOURNAL, Vol. 49, 1970.

27. Chang, W. S. C., IEEE TRANS, MTT-21, 1973.

28. Bykovskiy, Yu. A., V. L. Smirnov and A. V. Shmal'ko, Republic Scientific-Technical Conference "Integrated and Fiber Optics Components in Communications Systems" (Report Topics), Kiev, Ukrainian NIINTI, 1977.

29. Baranov, L. I., V. N. Luk'yanov, A. T. Semenov and N. V. Shelkov, KVANTOVAYA ELEKTRONIKA, Vol. 4, 1977.

30. Andriyesh, A. M., Yu. A. Bykovskiy, V. L. Smirnov, M. R. Cherniy and A. V. Shmal'ko, KVANTOVAYA ELEKTRONIKA, Vol. 5, 1978.

31. Kenan, R. P., J. APPL. PHYS., Vol. 46, 1975.

32. Gudzenko, A. I., RADIOTEKHNIKA I ELEKTRONIKA, Vol. 21, 1976.

33. Kogelnik, H., BELL SYSTEMS TECHNICAL JOURNAL, Vol. 48, 1969.

34. Noel, G., M. Jacques and T. Guy, C. R. ACAD. SCI., Vol. 284B, 1977.

35. Sotin, V. Ye., All-Union Scientific-Technical Conference "Further Development of Electrooptics," Report Topics, Moscow, 1977.

36. Kogelnik, H., BELL SYSTEMS TECHNICAL JOURNAL, Vol. 55, 1976.

37. Flanders, D. S., H. Kogelnik, R. V. Schmidt and C. V. Shank, APPL. PHYS. LETTS., Vol. 24, 1974.

38. Tien, P. K., APPL. OPTICS, Vol. 10, 1971.

39. Elachi, C. and C. Yen, APPL. PHYS., Vol. 44, 1973.

40. Andriyesh, A. M., Yu. A. Bykovskiy, E. P. Kolomeyko, A. V. Makovkin, V. L. Smirnov and A. V. Shmal'ko, KVANTOVAYA ELEKTRONIKA, Vol. 4, 1977.

41. Remesnik, V. G., V. A. Fatayev and V. G. Tsukerman, KVANTOVAYA ELEKTRONIKA, Vol. 4, 1977.

42. Schmidt, R. V., D. C. Flanders, C. V. Shank and R. D. Standley, APPL. PHYS. LETTS., Vol. 25, 1974.

43. Matsuhara, M., K. O. Hill and A. Watanabe, J. OPT. SOC. AMER., Vol. 65. 1975.

44. Cross, P. S. and H. Kogelnik, OPT. LETTS., Vol. 1, 1977.

45. Zlenko, A. A., V. A. Kiselev, A. M. Prokhorov and V. A. Sychugov, KVANTOVAYA ELEKTRONIKA, Vol. 1, 1974.

46. Zolotov, Ye. M., A. M. Prokhorov and Ye. A. Shcherbakov, KVANTOVAYA ELEKTRONIKA, Vol. 2, 1975.

47. Ohmachi, Y., APPL. PHYS., Vol. 44, 1973.

48. Schmidt, R. V. and I. P. Kaminow, IEEE J., QE-11, 1975.

49. Lin, Ye., "Vvedeniye v integral'nuyu optiku" [Introduction to Integrated Optics], edited by M. Barnoski, Moscow, Mir, 1977.

50. Gudzenko, A. I., I. L. Zubarev and O. A. Kurdyumov, RADIOTEKHNIKA I ELEKTRONIKA, Vol. 22, 1977.

51. Gudzenko, A. I. and L. N. Deryugin, IZV. VUZOV. SER. RADIOELEKTRONIKA, Vol. 20, 1977.

52. Lin, E., D. White and K. Wilkinson, TRUDY IIER, Vol. 64, No. 5, 1976.

53. Gudzenko, A. I., O. A. Kurdyumov and L. A. Osadchev, ZARUBEZHNAYA RADIOELEKTRONIKA, No. 9, 1976.

54. Gudzenko, A. I., O. B. Gusev, L. N. Deryugin, S. A. Zabuzov, V. V. Kludzin, L. A. Osadchev, B. P. Razzhivin, G. F. Sirotin, V. Ye. Sotin and N. N. Chernyshov, RADIOTEKHNIKA I ELEKTRONIKA, Vol. 21, 1976.

55. Gudzenko, A. I., L. N. Deryugin, S. A. Zabuzov, V. V. Kludzin, L. A. Osadchev, G. F. Sirotin, V. Ye. Sotin, B. P. Razzhivin and A. A. Tishchenko, RADIOTEKHNIKA I ELEKTRONIKA, Vol. 22, 1977.

56. Lemanov, V. V., B. V. Sukharev, V. V. Kludzin and S. V. Kulakov, PIS'MA V ZHTF, Vol. 2, 1976.

57. Zolotov, Ye. M., V. M. Pelekhatyy, A. M. Prokhorov, Ye. V. Rakova, S. A. Semiletov, S. M. Shkornyakov and Ye. A. Shcherbakov, KVANTOVAYA ELEKTRONIKA, Vol. 4, 1977.

58. Smolenskiy, G. A., M. A. Garsia, S. A. Mironov, A. N. Ageyev, B. P. Trubitsyn and O. P. Obrubov, PIS'MA V ZHTF, Vol. 3, 1977.

59. Zolotov, Ye. M., V. M. Pelekhatyy, A. M. Prokhorov and Ye. A. Shcherbakov, PIS'MA V ZHTF, Vol. 3, 1977.

60. Chang, W. S. C., S. Tsai Chen, R. A. Becker and I. W. Yao, IEEE J., QE-13, 1977.

61. Smolenskiy, G. A., M. A. Garsia, S. A. Mironov and A. N. Ageyev, PIS'MA V ZHTF, Vol. 3, 1977.

62. Yermolayev, V. M., F. A. Logachev, N. M. Lyndin, B. B. Meshkov, A. M. Prokhorov, V. A. Sychugov and G. P. Shipulo, KVANTOVAYA ELEKTRONIKA, Vol. 3, 1976.

63. An, J. C., Y. Cho and Y. Matsuo, IEEE J., QE-13, 1977.

64. Bykovskiy, Yu. A., V. L. Smirnov and A. V. Shmal'ko, PIS'MA V ZHTF, Vol. 3, 1977.

65. Hepner, G., J. P. Castera and B. Desormiere, APPL. OPTICS, Vol. 15, 1976.

66. Sauter, G. F., M. M. Hanson and D. L. Fleming, APPL. PHYS. LETTS., Vol. 30, 1977.

67. Tamir, T., in "Integrated Optics," 1975.

68. Peng, S. T. and T. Tamir, OPTICS COMMS., Vol. 11, 1947.

69. Takashi, A., A. Yoshinobu and N. Susumu, APPL. PHYS. LETTS., Vol. 29, 1976.

70. Prokhorov, A. M., A. A. Spikhal'skiy and V. A. Sychugov, KVANTOVAYA ELEKTRONIKA, Vol. 4, 1977.

71. Alferov, Zh. I., FTP, Vol. 11, 1977; Alferov, Zh. I., S. A. Gurevich, M. N. Mizerov and Ye. L. Portnoy, PIS'MA V ZHTF, Vol. 3, 1977.

72. Wang, S., IEEE J., QE-13, 1977.

73. Katzir, A., A. C. Livanov, J. B. Shellan and A. Yariv, IEEE J., QE-13, 1977.

74. Bozhevol'nyy, S. I., Ye. M. Zolotov, V. A. Kiselev, A. M. Prokhorov and Ye. A. Shcherbakov, PIS'MA V ZHTF, Vol. 3, 1977.

75. Livanov, A. C., A. Katzir, A. Yariv and C. S. Hong, APPL. PHYS. LETTS., Vol. 30, 1977.

76. Matsuda, A. and S. Iizima, APPL. PHYS. LETTS., Vol. 31, 1977.

77. Somekh, S., in "Vvedeniye v integral'nuyu optiku," edited by M. Barnoski, Moscow, Mir, 1977.

78. Markuze, D., "Opticheskiye volnovody" [Optical Waveguides], Moscow, Mir, 1974.

79. Yamamoto, Y., Y. Naruse, T. Kamiya and H. Yanai, ANNUAL REPORT OF ENGINEERING RESEARCH INSTITUTE "FAC. ENG., UNIV. TOKYO,", Vol. 34, 1975.

80. Kiselev, V. A. and A. M. Prokhorov, KVANTOVAYA ELEKTRONIKA, Vol. 2, 1975.

81. Zolotov, Ye. M., V. M. Pelekhatyy and A. M. Prokhorov, KVANTOVAYA ELEKTRONIKA, Vol. 4, 1977.

82. Bykovskiy, Yu. A., A. V. Makovkin, V. L. Smirnov and A. V. Shmal'ko, KVANTOVAYA ELEKTRONIKA, Vol. 2, 1975.

83. Boud, J. T. and C. S. Kuo, APPL. OPTICS, Vol. 15, 1976.

84. Zlenko, A. A., V. A. Kiselev, A. M. Prokhorov, A. A. Spikhal'skiy and V. A. Sychugov, KVANTOVAYA ELEKTRONIKA, Vol. 2, 1975.

85. Bykovskiy, Yu. A., A. V. Makovkin, V. I. Molochev, V. L. Smirnov and A. V. Shmal'ko, OPTIKA I SPEKTROSKOPIYA, Vol. 41, 1976.

86. Campbell, J. G. and D. W. Bellavance, IEEE J., QE-13, 1977.

87. Bykovskiy, Yu. A., Yu. P. Zakharov, A. V. Makovkin, V. K. Malyshev, V. I. Molochev, V. L. Smirnov, O. N. Talenskiy and A. V. Shmal'ko, KVANTOVAYA ELEKTRONIKA, Vol. 4, 1977.

88. Kuz'minov, Yu. S., N. M. Lyndin, A. M. Prokhorov, A. A. Spikhal'skiy, V. A. Sychugov and G. P. Shipulo, KVANTOVAYA ELEKTRONIKA, Vol. 2, 1975.

89. Kersten, R. Th., OPTICS COMMS., Vol. 17, 1976.

90. Auracher, F., R. Th. Kersten, H. H. Witte and G. Ziedler, SIEMENS FORSH. UND ENTWICK. LAUGSBER., Vol. 5, 1976.

91. Schmidt, R. V. and H. Kogelnik, APPL. PHYS. LETTS., Vol. 28, 1976.

92. Millar, C. A. and P. J. R. Laybourn, OPTICS COMMS., Vol. 18, 1976.

93. Hsu, H. P. and A. F. Milton, IEEE J., QE-13, 1977.

94. Bykovskiy, Yu. A., A. V. Makovkin and V. L. Smirnov, KVANTOVAYA ELEKTRONIKA, Vol. 2, 1975.

95. Heidrich, P. F. and C. G. Powell, U. S. Patent, cl. 350-96c, No. 3967877, published 6 July 76.

96. Zolotov, Ye. M., V. M. Pelekhatyy and A. M. Prokhorov, KVANTOVAYA ELEKTRONIKA, Vol. 3, 1976.

97. Oleynik, A. A. and V. P. Red'ko, ZARUBEZHNAYA RADIOELEKTRONIKA, No. 2, 1978.

98. Hammer, J. M., R. A. Bartolini, A. Miller and C. C. Neil, APPL. PHYS. LETTS., Vol. 28, 1976.

99. Bykovskiy, Yu. A., A. V. Makovkin and V. L. Smirnov, OPTIKA I SPEKTROSKOPIYA, Vol. 37, 1974.

100. Kong, J. A., J. OPT. SOC. AMER., Vol. 67, 1977.

101. Goncharenko, A. M. and V. P. Red'ko, "Vvedeniye v integral'nuyu optiku" [Introduction to Integrated Optics], Minsk, Nauka i tekhnika, 1975.

102. Volkov, V. G., RADIOELEKTRONIKA ZA RUBEZHOM, No. 12, 1977.

103. Somekh, S. and H. C. Casey, APPL. OPTICS, Vol. 16, 1977.

104. Labunov, V. A., G. I. Mel'yanets, B. I. Val'kov, Yu. A. Rodionov and V. M. Tel'nov, ZARUBEZHNAYA ELEKTRONNAYA TEKHNIKA, No. 17, 1977.

105. Belyakov, L. V., D. N. Goryachev, M. N. Mizirov and Ye. L. Portnoy, ZHTF, Vol. 44, 1974.

106. Alferov, Zh. I., D. N. Goryachev, S. A. Gurevich, M. N. Mizerov, Ye. L. Portnoy and B. S. Ryvkin, ZHTF, Vol. 46, 1976.

6521
CSO: 1870

PHYSICS

UDC 535.8.666.189.2;666.11:621.039.553

RADIATION-OPTICAL STABILITY OF LOW-LOSS GLASS FIBER OPTICAL WAVEGUIDES

Moscow KVANTOVAYA ELEKTRONIKA in Russian Vol 5 No 11, Nov 78 signed to press 26 May 78 pp 2484-2486

[Article by A. N. Gur'yanov, G. G. Devyatykh, Ye. M. Dianov, L. S. Korniyenko, Ye. P. Nikitin, A. M. Prokhorov, A. O. Rybaltovskiy, P. V. Chernov and A. S. Yushin, Physics Institute imeni P. N. Lebedev of the USSR Academy of Sciences, Moscow, and the Institute of Chemistry of the USSR Academy of Sciences, Gor'kiy]

[Text] The great advances of the past few years in development of low-loss glass fiber waveguides and fiber-optic cables led to the possibility of extensive use of them in optical communications systems during the next few years. In this regard the question arises of the effect of the surrounding medium, specifically of ionizing radiation, on glass fiber waveguides. The effect of gamma-radiation on optical losses in quartz glass and glass fiber waveguides (SVS) of various types (see, for example, [1-3]) has already been reported in the literature. It was shown that the effect of gamma-radiation leads to a significant increase of optical losses and in this case the induced absorption depends on the composition of the glass, its purity, the hydroxyl group content, irradiation doses and a number of other factors. The spectral dependence of induced absorption is of special interest. The absorption bands induced by ionizing radiation in pure and alloyed quartz glass are usually located in the UV and visible regions of the spectrum. Therefore, one should expect an increase of radiation-optical stability (ROU) of waveguides made from this glass with transition from the visible to the near IR band of wavelengths. Most experiments on study of low-loss ROU of SVS were conducted in the range of wavelengths of 0.8-1.1 microns, which is now of greatest interest for fiber-optics communications. And actually, an increase of ROU with an increase of wavelength was observed [1, 2]. An even greater increase of ROU may be expected in the region of the spectrum of 1.1-1.7 microns, promising for fiber-optics communications [4-6]. However, we know of no papers on investigation of low-loss ROU of SVS in this spectral region.

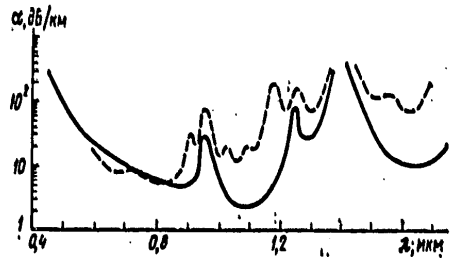

Figure 1. Spectra of Optical Attenuation α of SVS of First (Solid Curve) and Second (Dashed Curve) Types

Some results of investigating the effect of gamma-radiation on the extent of optical losses in low-loss SVS of two types: type I -- core of SiO_2 + + GeO_2 (diameter of 45 microns) and shell of SiO_2 (diameter of 110 microns) and type II -- core of SiO_2 (diameter of 200 microns) and shell of silicone rubber (outer diameter of 500 microns) -- are reported in the present paper. The measurements were made in the spectral range of 0.45-1.7 microns. The initial losses of the investigated waveguides are presented in Figure 1.

The waveguides were irradiated on a source of Co^{60} gamma-radiation with dose rates of 250 and 2 rad/s. The induced absorption spectra were taken every 1 hour after irradiation. Moreover, the induced absorption in the waveguides was measured immediately during irradiation at fixed wavelengths. The induced absorption spectra of waveguides of the first type for various doses of gamma-radiation are presented in Figure 2. It is obvious that the induced absorption decreases monotonically with wavelength and is apparently determined by the long-wave edge of the absorption band whose maximum lies outside this range.

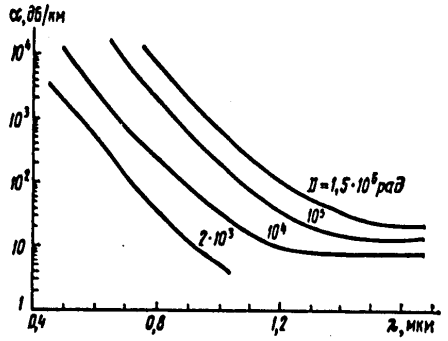

Figure 2. Induced Absorption Spectra of SVS First Type Measured Every Hour After Exposure to Various Doses of Gamma-Radiation. The radiation dose rate was 250 rad/s

The dose dependence of induced absorption in waveguides of the first type are presented in Figure 3, a. The growth kinetics of the induced radiation α with dose D is nonlinear and is described by the law $\alpha \sim \sqrt{D}$ in the range of approximately 1.3-1.7 microns. A similar law of accumulation of radiation defects was observed in alkali-halide crystals and is interpreted in [7]. Radiation defects which determine induced absorption in waveguides of this type are stable at room temperature: the induced absorption drops by a total of 5 percent within the first 5 minutes after the end of exposure. Comparison of the dose dependence of induced absorption at different wavelengths shows that the ROU of waveguides of the first type increases sharply with an increase of wavelength.

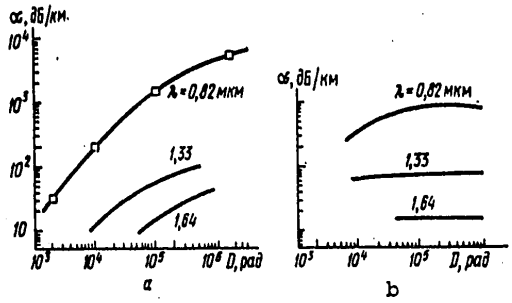

Figure 3. Dose Dependence of Induced Absorption of SVS of First (a) and Second (b) Types at Different Wavelengths. The dependence for 0.82 micron in Figure a corresponds to measurements every hour after irradiation and the remaining dependences correspond to measurements during irradiation

A similar increase of ROU with wavelength was also observed for waveguides of the second type. The dose dependences of the induced absorption of these waveguides are presented in Figure 3, b. These waveguides differ sharply from those of the first type by the kinetics of the increase of induced absorption with irradiation dose: the induced absorption emerges to saturation at doses of 10^3-10^4 rad. Therefore, the dose dependences have a plane section in the dose range of 10^4-10^6 rad. The radiation defects of these waveguides are unstable and recombine at room temperature: the induced absorption drops several times within 5 minutes after the end of exposure. The process of radiation defect recombination significantly affects the dose dependence of induced absorption of waveguides of the second type. Thus, the same radiation dose of 10^4 rad received by a waveguide at dose rate of 2 rad/s induces an order less absorption than that at a dose rate of 250 rad/s.

Thus, it was shown experimentally for the first time that low-loss ROU of SVS based on quartz glass increases sharply upon transition to the spectral region of 1.3-1.7 microns. This circumstance and also the fact that SVS

based on quartz glass have absolute minimum losses and zero material dispersion in this region [4-6] make the spectral region of 1.3-1.7 microns very promising for fiber-optics communications.

It should be noted that the kinetics of induced absorption for $\lambda < 1$ micron deviates from the law $\alpha \sim \sqrt{D}$. This permits one to state that absorption in the region of 1.3-1.7 microns is determined not only by the limb of the UV band, but also by the presence of a second (IR) absorption band.

BIBLIOGRAPHY

1. Friebele, E. J., G. H. Sigel and R. E. Jaeger, A Digest of the Topical Meeting on Optical Fiber Transmission II, TUD-9, February 22-24, 1977, Williamsburg, Virginia.

2. Boganov, A. G. et al., KVANTOVAYA ELEKTRONIKA, Vol. 4, 1977.

3. Friebele, E. J. et al., APPL. PHYS. LETTS., Vol. 32, 1978.

4. Belov, A. V., A. N. Gur'yanov et al., KVANTOVAYA ELEKTRONIKA, Vol. 4, 1977.

5. Kobayashi, S. Shibata, N. Shibata and T. Izawa, Proceedings of the International Conference on Integral Optics and Optical Fibers Communications, Tokyo, 1977.

6. Belovi, A. V., KVANTOVAYA ELEKTRONIKA, Vol. 5, 1978.

7. Durand, P., Y. Farge and M. Lambert, J. PHYS. CHEM. SOL., Vol. 30, 1969.

6521
CSO: 1870

PHYSICS

UDC 621.372.8.09

FIBER-OPTIC DATA LINK FOR TELECOMMUNICATIONS SYSTEMS

Moscow KVANTOVAYA ELEKTRONIKA in Russian Vol 5 No 11, Nov 78 signed to press 26 May 78 pp 2486-2488

[Article by Zh. I. Alferov, M. I. Belovolov, A. T. Gorelenok, A. N. Gur'yanov, G. G. Devyatykh, Ye. M. Dianov, A. Ya. Karasik, V. I. Kolyshkin, P. S. Kop'yev, A. M. Prokhorov and A. S. Yushin, Physics Institute imeni P. N. Lebedev of the USSR Academy of Sciences, Moscow, Institute of Chemistry of the USSR Academy of Sciences, Gor'kiy, and Physicotechnical Institute imeni A. F. Ioffe of the USSR Academy of Sciences, Leningrad]

[Text] The region of wavelengths of 0.8-1.1 microns is now used extensively for fiber-optics communications. This is related to the presence of a well-developed base of efficient radiation sources and detectors and also to the sufficiently low level of optical losses (several dB/km) in glass fiber waveguides (SVS) in this range of wavelengths.

However, a more promising spectral region for development of maximum wide-band fiber-optics communications lines (VOLS) over great distances is the region of wavelengths of approximately 1.3 microns since the material dispersion of pure and alloyed germanium or boron of quartz glass passes through zero in a narrow range of 1.3±0.05 microns* and the total optical losses in this band may be reduced to a level of approximately 1 dB/km [1-3]. Moreover, a very important circumstance for a number of applications is the fact that the radiation stability of SVS increases significantly upon transition to the spectral region greater than 1 micron [4].

Testing of a 2-km VOLS in which specially developed new semiconductor lasers operating at wavelength of 1.3 micron were used as the sources and the possibility of data transmission over great distances was investigated, is reported in this paper. SVS with core and shell diameters of 40 and 120 microns, respectively, numerical aperture of 0.28 and losses of 2-4 dB/km in the region of 1.3 micron were used [2].

*The mode dispersion may be minimized or completely eliminated by selecting the corresponding profile of the refractive index.

The characteristics of the components used and the capabilities of VOLS as a whole were measured on an experimental data link. The line was assembled by the typical scheme and its characteristic feature is the possibility of conducting investigations with signals from different data sources and also from a digital data pulse simulator (G5-48 generator). The low-noise wide-band pre-amplifier and main amplifier provided data transmission at a speed up to 10 Mbits/s. The signal was recorded by germanium photodetectors with standard characteristics: dark current of approximately 10^{-7} A and sensitivity of approximately 0.5 A/W at a wavelength of 1.3 microns. Thus, the minimum detectable output of the optical signal at the input of the receiver (compared to noise) does not exceed $1 \cdot 10^{-7}$ W.

(1) Тип источника	(2) Длина волны излучения, мкм	(3) Потери в СВС, дБ/км	(4) Энергетический потенциал П, дБ	(5) Потери на ввод $П_{\eta}$, дБ	(6) Динамический диапазон D, дБ	(7) Допустимое расстояние между ретрансляторами, км
ПГЛ	1,30	2—4	45—50	≤ 2	>40	10—20

KEY:

1. Type of source
2. Radiation wavelength, microns
3. Losses in SVS, dB/km
4. Energy potential P, dB
5. Input losses P_{η}, dB
6. Dynamic range d, dB
7. Permissible distance between repeaters, km

A lot of semiconductor heterolasers (PGL) of band configuration on a system of solid solutions of In-Ga-As-P with maximum emission in the region of 1.3 micron at room temperature was manufactured for use as sources in the investigated VOLS. The method of preparing these lasers and their parameters was reported previously [5]. The PGL had low thresholds ($\lesssim 0.5$ A), which considerably facilitated combination of the laser modulation circuit with the data sources.

An excess of optical signal output of the PGL above the minimum detectable by the receiver determines the energy potential P in the data link and is one of the most important characteristics of VOLS. Measurements on 10 PGL models showed that potential P comprises 45-50 dB in our system and is limited mainly by the natural noise level at the receiver input.

The dimensions of the PGL emitting area comprise 1 x 16 microns, while emission divergence comprises 50 x 2°, which permitted efficient use of various macrooptical devices in the PGL-SVS adapter subassembly. Radiation losses of the PGL to the input P_{η} in SVS with the parameters indicated above with direct joining comprised 7 ± 0.5 dB. The low losses to the input ($\lesssim 2$ dB) are achieved by using microoptical devices on the ends of waveguides (spherical and cylindrical lenses and the cone-shaped sections of waveguides), but the requirements on adjustment of the joined elements

increased significantly in this case. The monitored shaping of the microlenses and welding of the segments of the SVS (the fiber channel consisted of three SVS segments 1, 0.5 and 0.5 km long) was accomplished on a special electric-arc unit. The losses at the joints of the SVS with each other did not exceed 0.5 dB.

The value of the dynamic range D of the permissible attenuation of the optical signal in the fiber channel (without regard to losses to the radiation input into the SVS) is dependent on the rate and type of modulation (amplitude, pulse-code and so on) and is equal to $D \approx P - P_{\eta} - P_m$, where P_m (in dB) characterizes the required excess signals above the noise level which provide the required signal-noise ratio in the VOLS or which give an error probability (usually approximately 10^{-8}) during digital data transmission. We investigated the dependence of D on the type of informative modulation and its rate up to 10 Mbits/s and the derived dependences were close to those in [6]. The value of D comprised more than 40 dB during data transmission with pulse-code modulation (IKM) which we tested.

The energy characteristics of VOLS on PGL and the possibilities of using it for telecommunications during data transmission with IKM are presented in the table.

It should be noted that the use of low-noise photodiodes or avalanche photodiodes with amplification in VOLS permits an increase in the value of D by at least 10-10 dB.

Thus, the energy characteristics of the developed semiconductor heterolasers at wavelength of 1.3 microns permits data transmission by SVS with the parameters indicated above over a distance of tens of kilometers without using intermediate amplifiers.

BIBLIOGRAPHY

1. Horigushi, M. and H. Osanai, ELECTRONICS LETTS., Vol. 12, 1976.

2. Belov, A. V. et al., KVANTOVAYA ELEKTRONIKA, Vol. 4, 1977.

3. Belov, A. V. et al., KVANTOVAYA ELEKTRONIKA, Vol. 5, 1978.

4. Gur'yanov, A. N., G. G. Devyatykh, Ye. M. Dianov, L. S. Korniyenko, Ye. P. Nikitin, A. M. Prokhorov, A. O. Rybaltovskiy, P. V. Chernov and A. S. Yushin, KVANTOVAYA ELEKTRONIKA, Vol. 5, 1978.

5. Alferov, Zh. I., A. T. Gorelenok, P. S. Kop'yev, V. N. Mdivani and V. K. Tibilov, PIS'MA V ZHTF, Vol. 3, 1977.

6. Kao, C. K. and J. E. Goell, ELECTRONICS, Vol. 49, 1976.

6521
CSO: 1870

PHYSICS

UDC 681.327.68

FEASIBILITY OF DEVELOPING OPTICAL MEMORY ELEMENTS BASED ON GAAS MDP STRUCTURES

Moscow KVANTOVAYA ELEKTRONIKA in Russian Vol 5 No 11, Nov 78 signed to press 14 Mar 78 pp 2495-2497

[Article by V. A. Gaysler, A. F. Kravchenko, V. F. Solov'yev and A. S. Terekhov, Institute of Semiconductor Physics of the Siberian Department of the USSR Academy of Sciences, Novosibirsk]

[Text] Metal-dielectric-semiconductor structures find broad application in development of the component base of optical computer technology, specifically in development of media for optical data recording and storage. The data in MDP [Metal-dielectric-semiconductor] structures is stored in the form of a potential relief created by the trap charge in the dielectric layer of the structures [1-4]. The storage time may reach several tens of thousands of hours. A method of data storage in MDP-structures based on charge capture by the dielectric states and on the final relaxation time of the nonequilibrium region of the space charge (OPZ) in MDP-structures is considered in the given paper. The data recording-readout cycle begins with transmission of a voltage pulse with polarity corresponding to ejection of the main charge carriers from the semiconductor to the metal electrode of the MDP-structure. In this case a nonequilibrium depletion zone is formed and the greater part of the applied voltage drops in the semiconductor. The data is recorded by light with photon energy $\hbar\omega$ which is greater than the width of the forbidden zone E_g; light generation of electron-hole pairs leads to rapid relaxation of nonequilibrium OPZ. The potential in the MDP-structure is redistributed and the greater part of the applied voltage drops in the dielectric. Information is read by the light with photon energy $\hbar\omega$ somewhat less than E_g. The reading light, passing through the MDP-structure, is amplitude-modulated due to the Frantz-Keldysh effect. The data storage time in an ideal MDP-structure is determined by the relaxation time of non-equilibrium OPZ. The bias is not tapped from the metal electrode of the structure during the record-readout cycle. One of the advantages of this type of data storage in MDP-structures is the possibility of data transmission from one memory element to another (transmission may be accomplished the same as in PZS-structures).

A similar operating principle is considered in [5, 6], where the possibility of creating a dynamic optically controlled transparency (OUT) was investigated [7]. The possibility of creating an OUT with memory based on GaAs MDP-structure is studied in the given paper.

The basis for manufacturing the structures was the epitaxial layer of gallium arsenide approximately 10^{-3} cm thick with free electron concentration of $n \approx 10^{14}$ cm^{-1}, grown by the gas-transport method in an open chloride system on a strongly alloyed substrate ($n \approx 10^{18} cm^{-3}$). An Si_3N_4 dielectric approximately 100 nm thick was applied to the surface of the epitaxial layer. The dielectric was applied by pyrolytic decomposition of silicon tetrachloride $SiCl_4$ and hydrosine N_2H_4. This permitted a significant decrease of the silicone nitride production temperature and made it possible to avoid thermal dissociation of the GaAs [8]. A semitransparent aluminum electrode was sputtered onto the dielectric surface. The volt-farad characteristics were measured on the produced structures. These measurements made it possible to determine the relaxation time of nonequilibrium OPZ [9], which comprised several hours at T = 77 K in the absence of illumination. The width of the hysteresis loop of the volt-farad characteristics did not exceed 1 V, i.e., the concentration of the charge-exchange slow traps in the investigated structures was low. The electric strength of the dielectric layers comprised $(4-5) \cdot 10^6$ $V \cdot cm^{-1}$. The installation described in [10] was used for optical measurements. The spectral and time functions of the modulation coefficient m and contrast k of the structure were measured.

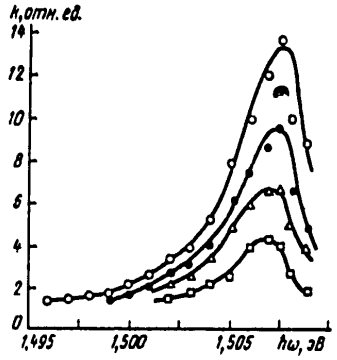

Figure 1. Spectral Dependence of Contrast $k(\hbar\omega)$; Amplitude of the Voltage Pulses Applied to the Structure Was V_m = = 50 V: O -- Δt = 0 ms; ● -- Δt = 0.5 ms; Δ -- Δt = 3 ms; □ -- Δt = 9 ms

The measurements were made in the following manner. Square-wave negative polarity voltage pulses were fed to the metal electrode. A data record light pulse and within time Δt a data read light pulse were fed to the MDP-structure during the effect of the pulse. A helium-neon laser beam with photon energy of 1.96 eV was used to record the data. Since the data

are read with partial destruction of it caused by absorption of the reading light, it is necessary that the reading light pulse energy be much less than the data record energy when making the optical measurements. Analyses showed that the energy density of the data record pulse comprises approximately 10^{-6} J·cm^{-2} and that of the reading light pulse does not exceed approximately 10^{-7} J·cm^{-2}. All the measurements were made at T = 77 K. This was determined by the following factors: the coefficient and efficiency of Frantz-Keldysh modulation [10] increases with a decrease of temperature due to an increase of the curvature of the edge of natural absorption and, which is also significant, the relaxation time of nonequilibrium OPZ increases. The spectral dependence of the modulation coefficient $m = |\Delta T(v)/T(0)|$, whose maximum value comprised 93 percent at $\hbar\omega = 1.507$ eV, was measured. The amplitude of the voltage pulses applied to the structure was equal to 50 V. The spectral functions of the contrast of the device, which is determined by the following relation, are presented in Figure 1:

$$k(\hbar\omega, v) = T_3(\hbar\omega, v)/T(\hbar\omega, v),$$

where $T_3(\hbar\omega, v)$ is the transmission of the structure during data recording and $T(\hbar\omega, v)$ is the transmission of the structure without data recording. The maximum contrast (like the maximum modulation coefficient) is reached at $\hbar\omega = 1.507$ eV. As can be seen from Figure 1, the contrast decreases with time. The functions $k(\Delta t)$ at fixed values of $\hbar\omega$ were constructed to determine the data storage time. These functions are presented in Figure 2. The data storage time, which we determined as the time during which $k \geqslant 2$, comprises approximately 10^{-2} s. It was established that a decrease of contrast occurs due to a decrease of $T_3(\hbar\omega, v)$. The value of $T(\hbar\omega, v)$ does not vary in the investigated range of Δt from 0 to 9 ms. The most probable cause of data destruction (decrease of contrast) is leakage of holes from the inversion channel through the dielectric to the metal; these currents were observed on some structures during measurement of the volt-farad characteristics and the area of structures during measurement of C-V characteristics comprised 0.5 mm^2, while it comprised approximately 30 mm^2 during measurement of the optical parameters, i.e., the probability of a hole in the MDP-structure increases by almost a factor of 2. The currents flowing through the dielectric break down the inversion hole layer, the width of the OPZ increases in this case, the transmission of the structure $T_3(\hbar\omega, v)$ decreases and consequently the contrast also decreases. The data storage time is determined in the given case by the currents flowing through the dielectric rather than by the time of nonequilibrium OPZ.

Thus, the possibility of using GaAs MDP-structures for development of optical memory devices with data storage time of approximately 10^{-2} s, having high modulation coefficient and low data recording energy, is shown on the basis of experimental data in the paper. It was established that the data storage time in the investigated structures is determined by the hole concentration. It can apparently be increased to the relaxation time of nonequilibrium OPZ by improving the technology.

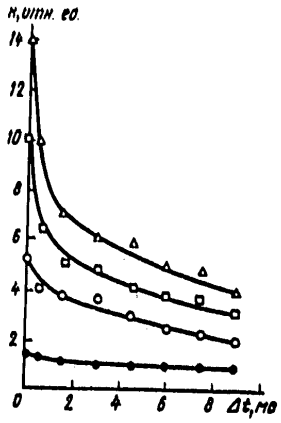

Figure 2. Time Function of Contrast $k(\Delta t)$: ● -- $\hbar\omega$ = 1.495 eV; O -- $\hbar\omega$ = 1.504 eV; △ -- $\hbar\omega$ = 1.507 eV; □ -- $\hbar\omega$ = = 1.508 eV

BIBLIOGRAPHY

1. Bulan'kov, N. I., V. D. Zhuravov, A. F. Plotnikov, V. N. Seleznev, D. N. Tokarchuk and G. P. Ferchev, KVANTOVAYA ELEKTRONIKA, Vol. 3, 1976.

2. Plotnikov, A. F., V. N. Seleznev, V. E. Shubin and A. B. Kravchenko, KRATKIYE SOOBSHCHENIYA PO FIZIKE, No. 10, 1973.

3. Kravchenko, A. B., A. F. Plotnikov, Yu. M. Popov, V. N. Seleznev and V. E. Şhubin, FIZIKA I TEKHNIKA POLUPROVODNIKOV, Vol. 8, 1974.

4. Arkhipov, A. N., M. I. Yelinson, A. G. Zhdan, V. B. Sandomirskiy and A. A. Sigarev, FIZIKA I TEKHNIKA POLUPROVODNIKOV, Vol. 11, 1977.

5. Plotnikov, A. F., V. N. Seleznev, D. N. Tokarchuk and G. P. Ferchev, KVANTOVAYA ELEKTRONIKA, Vol. 4, 1977.

6. Agrafeṇin, Yu. V., V. Ye. Getalov, V. M. Zaletin, A. F. Kravchenko and A. S. Terekhov, MIKROELEKTRONIKA, Vol. 6, No. 4, 1977.

7. Svidzinskiy, K. K., ELEKTRONNAYA PROMYSHLENNOST', No. 6, 1973.

8. Senoshenko, O. V., I. Ye. Maronchuk and Yu. E. Maronchuk, MIKROELEKTRONIKA, Vol. 2, No. 3, 1973.

9. "Svoystva struktur metall-dielektrik-poluprovodnik" [The Properties of Metal-Dielectric-Semiconductor Structures], edited by A. V. Rzhanov, 1976.

10. Bobylev, B. A., A. F. Kravchenko and A. S. Terekhov, FIZIKA I TEKHNIKA POLUPROVODNIKOV, Vol. 6, 1972.

6521
CSO: 1870

PHYSICS

THERMAL RADIO RADIATION FROM CLOUDS

Moscow RADIOTEKHNIKA I ELEKTRONIKA in Russian No 9, 1978 pp 1792-1806

[Article by A. B. Akvilonova and B. G. Kutuza, received by the editors on 15 March 1978]

[Text] The results of theoretical and experimental research into radio radiation of clouds in the wave band of 0.3 to 10 cm are presented. The effect of various physical characteristics of clouds (temperature, water content, water reserve, moisture content) on the spectrum of brightness temperatures was studied based on model calculations. The nature of the dependency wave lengths on the zenith angle was studied. Calculations were made both for cases of measurements from the earth's surface as well as for the case of making measurements from aircraft. A technique for determining the integral parameters of the atmosphere (total mass of water vapor in the atmosphere and water reserve of the clouds) according to SHF radiometric measurements is presented. Estimates of the permissible errors of measurements of brightness temperatures at waves 0.8 and 1.35 cm at the required accuracy of parameters being determined are given. Experimental data obtained by measurements from stationary ground sites, from a laboratory aboard an aircraft and from the "Kosmos-243" satellite are presented.

Since Dicke and his associates measured radio thermal radiation of the earth's atmosphere [1, 2] for the first time in 1945, systematic research into its radiative and absorbent properties has been underway in many countries. At first interest in this research was primarily associated with problems of radio astronomical observations where the atmosphere at waves shorter than 3 cm created considerable interference to reception of radiation from cosmic sources and was limited to determining the radio characteristics of the free atmosphere. The theoretical works of Van Vleck [3, 4]

were of great importance for the formation of SHF radiometry of the atmosphere. The absorption spectrum of millimeter and centimeter waves in molecular oxygen and in water vapor was calculated in these works. These calculations were subsequently refined by S. A. Zhevakin and A. P. Naumov [5-7]. Experimental research of radio radiation of cloudless atmosphere in the SHF band was conducted in the 50's by S. A. Zhevakin, V. S. Troitskiy, A. Ye. Salomonovich, A. Straiton, D. Hogg and others [8-13].

At the IRE AN SSSR [Institute of Radio Engineering and Electronics of the USSR Academy of Sciences], SHF radiometric research of the atmosphere was begun in 1961 at the initiative and under the direction of A. Ye. Basharinov. In the process primary attention was focused on research of the radiative and absorbent properties of a heterogeneous atmosphere containing clouds and precipitation as well as on the elaboration of methods for determining meteorological parameters by measurements of radio characteristics of the atmosphere. This article presents the basic results of work performed on SHF radiation of a cloudy atmosphere, part of which was published in [29-43].

1. The diffusion effect in cloudy atmosphere in the SHF band is negligible. Under these conditions as well as under the assumption of a local thermodynamic equilibrium the radio brightness temperature of a stratus humilis atmosphere during an observation from the earth's surface can be presented in the form [9, 16]

$$T_{\text{я}}(\lambda, z) = \int_0^{\infty} T(h)\,\gamma_{\lambda}(h)\,e^{-\int_0^{h}\gamma_{\lambda}(h')\sec z\,dh'}\sec z\,dh, \qquad (1)$$

Where T (h) is the temperature of the atmosphere at altitude h; $\gamma_{\lambda}(h)$ is the total absorption coefficient; z is the zenith angle; λ is the wave length.

The total absorption coefficient in a cloudy atmosphere is computed from the molecular absorption in the oxygen and in the water vapor, as well as from the absorption in the small droplets of the clouds. The absorption in molecular oxygen depends on the temperature and the pressure. Information on this can be found, for example, in [6, 7]. The absorption coefficient in water vapor, in addition, has a dependency, close to linear on the absolute humidity [5, 17]. For the absorption factor in a water cloud the expression [18, 19]

$$\gamma_{\text{об}}(\lambda) = \frac{0{,}6\pi}{\lambda}\,\mathrm{Im}\left(\frac{\varepsilon_{\text{в}}-1}{\varepsilon_{\text{в}}+2}\right)w, \qquad (2)$$

(1)

Key: (1) c lo

is valid where $\varepsilon_{\text{в}}$ is the complex permittivity of water; and w is the water content of the cloud. The frequency dependence of water permittivity in a radio band is determined by the Debye formula:

$$\varepsilon_\infty = \varepsilon_0 + \frac{\varepsilon_s - \varepsilon_0}{1+(\lambda_s/\lambda)^2} - i\,\frac{\lambda_s}{\lambda}\,\frac{\varepsilon_s - \varepsilon_0}{1+(\lambda_s/\lambda)^2} \tag{3}$$

where

$$\lambda_s = 2\pi c \tau_p \frac{\varepsilon_s+2}{\varepsilon_0+2};$$

τ_p is the relaxation time of the water molecules; ε_s is the water permittivity at frequencies $\tau_p \ll 1/\nu$; ε_0 is the water permittivity at frequencies $\tau_p \gg 1/\nu$. The parameters ε_s, ε_0 and τ_p have been rather well investigated at temperatures higher than the melting point of ice [14, 15, 20, 21].

During measurements from aircraft the brightness temperatures of the system "atmosphere--underlying surface" is formed from the right ascending radiation of the atmosphere, the radiation of the underlying surface of the earth attenuated by absorption in the atmosphere, and radiation of the atmosphere reflected from the surface:

$$T_B(\lambda, \theta) = T_n \varkappa(\lambda, \theta)\, e^{-\tau(\lambda)\sec\theta} + \int_0^H T(h)\,\gamma_\lambda(h)\, e^{-\int_h^H \gamma_\lambda(h')\sec\theta\, dh'} \times \tag{4}$$

$$\times \sec\theta\, dh + R(\lambda, \theta)\, e^{-\tau(\lambda)\sec\theta} \int_0^\infty T(h)\,\gamma_\lambda(h)\, e^{-\int_0^h \gamma_\lambda(h')\sec\theta\, dh'} \sec\theta\, dh,$$

where T_n, $\varkappa(\lambda, \theta)$ and $R(\lambda, \theta)$ is the temperature, emissivity and reflection factor of the underlying surface respectively; H is the altitude of the aircraft above the surface;

$$\tau(\lambda) = \int_0^\infty \gamma_\lambda(h)\, dh$$

is the total vertical absorption; and θ is the angle road from the nadir.

2. Let us look at the effect of various physical characteristics of clouds on the radio frequency radiation of the atmosphere during observation from the earth's surface "from below" and from an aircraft "from above." Model calculations of brightness temperatures were performed for this purpose in the band of waves of 0.3 to 3.0 cm, excluding the region of resonance absorption of oxygen in the neighborhood $\lambda \sim 5$ mm. In selecting the models we used statistics on the temperature, humidity, water content, and altitudes of the upper and lower boundaries for stratus (St), stratocumulus (Sc), altostratus (As), and altocumulus (Ac) clouds [22-25], as well as for cumulus clouds of varying capacity [26, 27]. The basic characteristic of the cloud models are shown in Table 1.

Table 1. Basic Characteristics of Clouds

Cloud shape	warm half year	cold half year	Ac	As	Cuhum	Cumed	Cucong
Model No	1	2	3	4	5	6	7
Height of lower boundary, H_{1b}, km	1.6	0.71	3.5	4.0	1.1	1.1	1.1
Thickness, H, km	0.3	0.35	0.3	1.0	1.0	1.0	4.5
Temperature at lower boundary, T_{1b}, °C	4.6	-8.6	-7.8	-10.9	8	8	8
* Water reserve, W, kg/m^2	0.10	0.08	0.06	0.3	0.15	0.52	4.70
* Total mass of water vapor in the atmosphere, Q, g/cm^2	1.44	0.66	1.38	1.44	1.71	1.99	2.28

* By the water reserve of a cloud and the total mass of water vapor in the atmosphere is meant the quantity of water in liquid droplet and vaporous states respectively contained in a column of air with a base area of 1 m^2 and 1 cm^2.

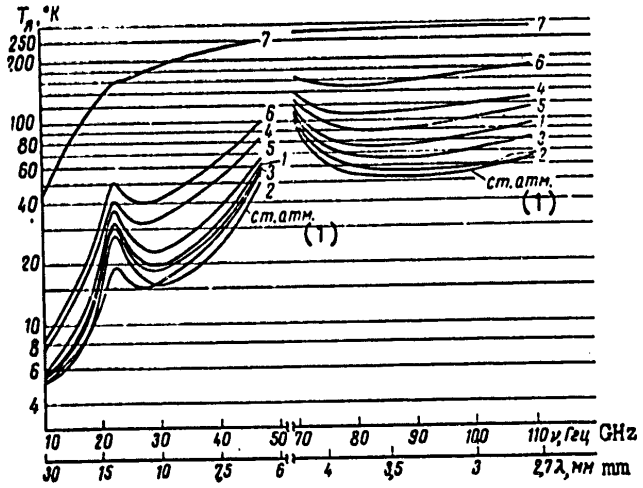

Figure 1. SHF spectra of the brightness temperature of a cloudy atmosphere during observation from the earth's surface in the direction of the zenith. 1-7 is the cloud model number according to Table 1.

Key: (1) standard atmosphere

Figure 1 shows the spectra of brightness temperatures of 7 types of clouds during observation to the zenith from the earth's surface. The figure also shows the spectrum of brightness temperatures for a standard clear atmosphere [28]. The strongest effect of the clouds is in the wave length band from 1 to 0.75 cm (v=30-40 GHz) and from 4 to 2.7 mm (v=75-110 GHz). In these spectral intervals the increment of brightness temperatures $\Delta T_{\text{я}}$ can reach 200° K for cumulus clouds, while for the stratus shaped clouds this value is considerably smaller and ranges from 2 to 60°K. At the frequencies $v \leq 15$ GHz only the extended cumulus clouds make a noticeable contribution to the brightness temperature. Thus at the frequency v=10 GHz the estimated value of $\Delta T_{\text{я}}$ for the Cucong [cumulus congestus] clouds was 42°K. The region of resonance absorption of water vapor in the neighborhood $\lambda \approx 1.35$ cm for stratus shaped clouds remains quite sensitive to change of the total mass of water vapor in the atmosphere which is quite evident from curves 1 and 2 in figure 1.

The estimated dependencies of increments of brightness temperature of the atmosphere at waves 0.33, 0.8, 1.5, 3, and 5 cm on the water reserve of clouds during observation to the zenith are shown in figure 2. In the linear range ($T < 30°$ K) the slope of the curves (logarithmic scale) for all waves is about the same. For millimeter waves the nonlinear range of variation in brightness temperature with the water reserve of the clouds begins at values greater than 1 kg/m^2.

The nature of the dependency of the brightness temperature of stratus shaped cloud cover on the zenith angle varies with the wave length and is determined primarily by the ratio between the absorption in the cloud and absorption in the oxygen and in the water vapor. In the long wave portion of the centimeter band full absorption in the atmosphere is less than 1 neper right up to zenith angles of 80° which provides for linear growth of the brightness temperature with sec z. However in the millimeter waves this dependency has another form. The curves shown in figure 3 show that at the wave 0.4 cm the brightness temperature of the clouds increases with the growth of the zenith angle, reaches maximum at angles 65-75°, and then monotonically subsides. At the greater angles, despite the fact that the fundamental absorption in the cloud is great, the contribution made by the cloud to the RF radiation of the atmosphere at the wave 0.4 cm becomes comparatively small due to the large absorption in the oxygen and in the water vapor.

During observation from aircraft the effect of clouds on the received RF radiation of the system "atmosphere--underlying surface" substantially depends on the type of underlying surface. Clouds create the greatest contrasts when measurements are made over a smooth water surface. Figure 4 shows the frequency relationships of increments of brightness temperature during observation to the nadir caused by the appearance of clouds. The calculations were made for a smooth sea surface at a temperature of 288.1°K and for the cloud models shown in Table 1. The increment values for stratiform cloud cover are similar both when observing "from below" and when observing "from above." The radio brightness contrast during observation "from above" of extended cumulus clouds are approximately twofold smaller than during the observation "from below."

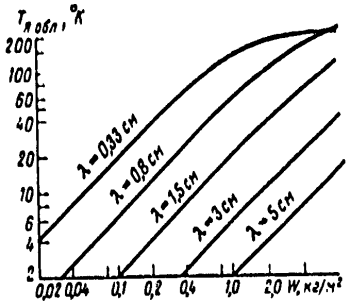

Figure 2. Brightness temperature of a cumulus cloud in direction of zenith as a function of lower boundary of cloud H_{lb} = 1.1 km, thickness 2.0 km

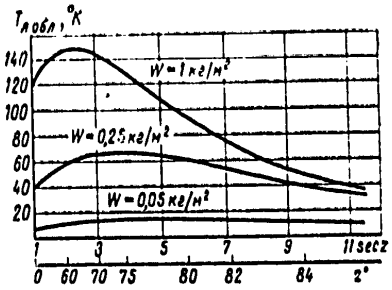

Figure 3. Brightness temperature of a stratus cloud T as a function of the secant of the zenith angle for three values of water reserve during observation from the earth's surface at wavelength of 0.4 cm.

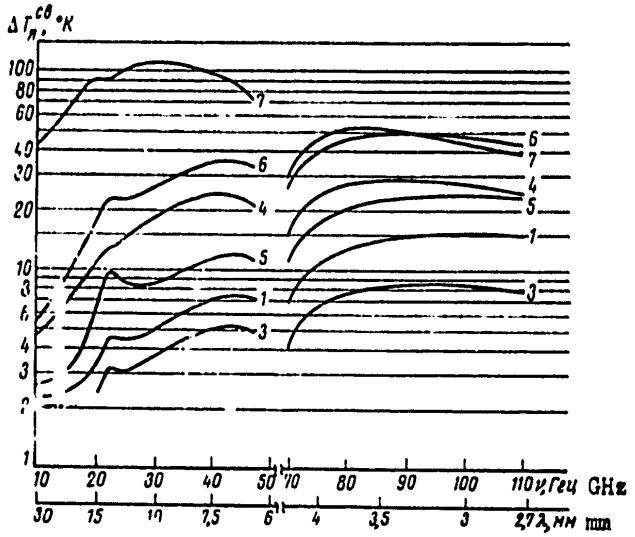

Figure 4. Spectra of increment of brightness temperature $\Delta T_{я}$ (v) of the system "atmosphere-underlying surface" due to clouds during observation from space in the direction of the nadir. 1, 3-7 is the cloud model number according to table 1; smooth sea surface

Droplet temperature varies with the altitude of the cloud. The temperature of the horizontal layer which divides the cloud into the upper and lower parts with equal values of water content may be used as the parameter

describing the effective temperature of the cloud. Data on the maximum deviations of brightness temperature of the system "atmosphere--ocean surface" with a change in cloud temperature by 5°K are shown in Table 2.

The calculations show that for stratiform clouds the effect of variations in the profile of the liquid-water content on the brightness temperature is negligible ($\Delta T_я < 0.1$°K). For clouds with vertical development this effect becomes noticeable at a thickness of 1.5 km or more. The maximum deviations in the brightness temperature through variations of the profile of the liquid-water content inside the cloud are observed with cumulus congestus clouds in a wave band of 1 to 1.5 cm, reaching values of 11°K during an observation "from below" and 5°K during observation "from above."

An increase in the total mass of water vapor due to the saturation of it in the cloud layer leads to an increase in the brightness temperature which is most noticeable in the region of resonance absorption $\lambda = 1.35$ cm. On a percentage basis the increase in $T_я$ for stratiform clouds is greater than for cumulus. Thus, for example, for stratus and stratocumulus clouds an increase in the water vapor (ΔQ=0.14 g/cm^2) increases the brightness temperature at the wave 1.35 cm by 1.4-2.1°K, which is 33-47 percent of the total contribution of the cloud. A cumulus congestus cloud may increase the moisture content of the atmosphere to 1 g/cm^2 which would lead to a change in the brightness temperature by 4-7.5°K, and compared to the contribution to $T_я$ of the water reserve this would be only 4-6 percent.

Colloidal-steady cloud formations may contain large droplets with a radius of $r > 30$ mkm, for which the conditions of a Rayleigh scattering are not met and the calculation of the absorption according to formulas (2) and (3) may lead to appreciable errors at the millimeter waves. For droplets with a radius of 45 mkm calculations according to the precise formulas of Mie and the relationship (2) already yield a discrepancy of 4-6 percent at the wave 0.2 cm. However taking into account the distribution of droplets according to size [22] this discrepancy would not exceed 1-3 percent except for cumulus congestus and cumulonimbus cloud cover where it may be appreciably large.

3. Measurements of radio radiation of a cloudy atmosphere were made in the wave band from 0.4 to 10 cm from stationary ground sites, aircraft and satellites. The ground experiments were used to study the mutual relationships among SHF spectrums of absorption and radiation of the atmosphere and physical parameters of clouds, as well as for working out the technique of aircraft and satellite measurements of the radio radiation of the atmosphere. Measurements of radiation characteristics of the atmosphere were made simultaneously at several waves in different sections of the spectrum; this technique is discussed in [30, 32]. Table 3 shows the basic characteristics of superheterodyne, Dicke radiometers developed under the direction of V. S. Ablyazov which were recently used to study the radiative properties of the atmosphere during observation from the earth's surface and from an aircraft.

Table 2. Deviations in brightness temperature ΔR (ν), caused by 5°K change in cloud temperature

Cloud shape and temperature	St, Sc; warm half year, T_{clo}=4°C	As, T_{clo}=-13°C	Cumed, T_{clo}= 0°C	Cucong, T_{clo} = =13°C
ν=22.235 GHz	0.4	2.1	2.4	6.7
ν=37.5 GHz	0.9	2.4	4.3	1.1
ν=90 GHz	0.5	2.0	0.6	0.05

Table 3. Basic characteristics of radiometers

Wavelength, cm	Sensitivity, °K	Frequency Reception Band, MHz	Time constant, sec
0.41	3	30	8
0.8	0.4	800	1
1.2-1.5	0.6	30	3.5
1.55	0.2	800	1
2.25	0.16	1000	1

Table 4. Mean and maximum values of $T_я$ for clouds of different shapes

Shape and temperature of clouds, °C		Cumed	Cucong	St, Sc; winter -10	St, Sc; summer 5
λ = 0.41 cm	$T_{я\ clo}$	50	90	20	35
	T^{max}_{clo}	140	160	35	70
λ = 0.82 cm	$T_{я\ clo}$	30	70	12	15
	$T^{max}_{я\ clo}$	120	162	20	35
λ = 1.6 cm	$T_{я\ clo}$	10	25	4	5
	$T^{max}_{я\ clo}$	40	67	7	11
λ = 3.3 cm	$T_{я\ clo}$	2.5	7.0	0.9	1.0
	$T^{max}_{я\ clo}$	11	20	1.5	2.5

In addition to this equipment radiometers with low noise amplifiers at input in the band of waves 3 and 10 cm with a sensitivity of 0.2 and 0.07°K respectively with a time constant of 1 sec were used in some periods.

The radio radiation of the clouds was detected from stationary points using a non-scanning antenna or with rotation of it in azimuth. During these experiments observations of the temperature, pressure and absolute humidity at the earth's surface were made regularly. In a number of experiments an aircraft furnished meteorological information and joint radar and radiosonde measurements were performed [30, 32, 35]. As an example figure 5 a and b shows the profiles of the brightness temperature of the atmosphere obtained during passage of cumulus clouds through a non-scanning antenna. The measurements were made on the "RT-22" radiotelescope of the FIAN SSSR [Physics Institute imeni P. N. Lebedev of the Academy of Sciences, USSR] [45]. In the first case (Figure 5a) the radiation of the clouds was recorded at the zenith angle of z = 60° simultaneously on waves 0.41, 0.82 and 1.6 cm and in the second (Figure 5b) at z=78° simultaneously on waves 0.82, 3.3 and 10 cm. The superimposition of the electrical axes of the antenna at these waves was achieved using a special exciter located at the focal point of a 22-meter mirror. For convenience of comparison the curves are normalized for maximum values and the intervals of averaging of the brightness temperatures lie within the range of 5 to 16 sec. Some difference between the profiles is caused by disturbance of the linear relationship between the brightness temperature and the water reserve which shows up in the millimeter band (see Figure 2). Clearly evident in these curves are the discontinuities of the radio radiation of the clouds which are primarily caused by the pulsations of the field of the liquid-water content and which disturbed the smooth change of brightness temperature during passage of the clouds. Cloud brightness temperature measurement errors are determined by the fluctuating threshold of sensitivity and stability of the gain factor of the radiometer as well as by errors in the measurement of parameters of the antenna. The accuracy of an individual reading of T_q of the clouds shown in Figure 5 was about 5 percent at waves 0.41 and 10 cm and 2-3 percent at the other waves.

Brightness temperature values of stratiform clouds increase as the zenith angle increases. For waves $\lambda \geq 0.8$ cm this increase is approximately proportional to sec z. With a cumulus cloud cover the dependency of the brightness temperature on the zenith angle shows up to a lesser degree. The increase of it is noticeable when z is varied from 0 to 60°. The maximum increases of T_q at waves 0.8 and 1.6 cm during passage of the cumulus clouds was recorded at the interval of angles of z from 60 to 80°. The mean and maximum values of brightness temperatures shown in Table 4 were obtained as a result of processing of the recordings of the radiation of clouds of various forms.

The data in Table 4 was obtained during observation of cumulus clouds at angles of z=60° and of the stratiform clouds in the direction of the zenith. Comparison of the experimental and calculated data on brightness temperatures of clouds shows satisfactory agreement of them. A direct comparison

of the measured values of $T_я$ and those calculated according to data from aerological sounding is not possible due to the great variability of the water reserve of the clouds in space and in time [31, 40-43], as well as the inertia of aerological methods. The spatial-time dependencies of the intensity of fluctuations of the radio brightness temperature of a cloudy atmosphere are discussed in [31, 43].

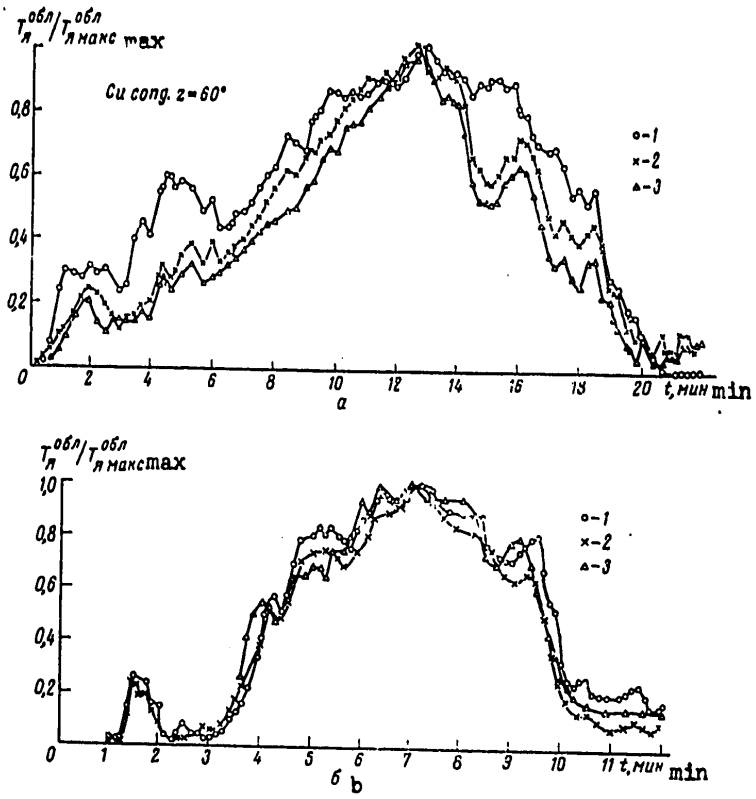

Figure 5. Profiles of increments of brightness temperature of the atmosphere, obtained during passage of cumulus clouds through a superimposed electrical axis of a non-scanning antenna. Reading was made relative to level of a clear sky; a--composite measurements on wavelengths 0.4, 0.8 and 1.6 cm, brightness temperature of a clear sky at these waves was 100, 38.5, and 22°K respectively, zenith angle 60°: 1--λ = 0.4 cm, $T_{я\,max}^{col}$ = = 160°K; 2--λ = 0.8 cm, $T_{я\,max}^{col}$ = 159°K; 3--λ = 1.6 cm, $T_{я\,max}^{col}$ = 69°K; b--same but on wavelengths 0.8, 3.3 and 10 cm, brightness temperature of a clear sky was 96, 23.6 and 20.5°K respectively: 1--λ = 0.8 cm, $T_{я\,max}^{col}$ = 79°K; 2--λ = 3.2 cm, $T_{я\,max}^{col}$ = 8.5°K; 3--λ = 10 cm, $T_{я\,max}^{col}$ = 0.7°K

4. The simultaneous measurements of absorption in a cloud at several waves makes it possible to derive information on the permittivity of the water. If we know the total absorption in the cloud simultaneously at 2 waves λ_1 and λ_2 along the same propagation path, the relationship of the absorptions for a thin cloud according to (2) will have the form

$$k(T_{clo}, \lambda_1, \lambda_2) = \frac{\lambda_2}{\lambda_1} \frac{\mathrm{Im}\left[\frac{\varepsilon_c(\lambda_1)-1}{\varepsilon_c(\lambda_1)+2}\right]}{\mathrm{Im}\left[\frac{\varepsilon_c(\lambda_2)-1}{\varepsilon_c(\lambda_2)+2}\right]}. \tag{5}$$

After conversions relationship (5) can be presented:

$$k = \frac{\lambda_2^2+4\pi^2c^2\tau_p^2}{\lambda_1^2+4\pi^2c^2\tau_p^2}. \tag{6}$$

Thus the cloud absorption ratio will be dependent on the parameter τ_p of the Debys formula which describes the relaxation time of the water molecules, if one of the long waves used is comparable in magnitude to the value $2\pi c\tau_p$, from which the following expression can be derived for the relaxation time of the water molecules

$$\tau_p = \frac{1}{2\pi c}\sqrt{\frac{\lambda_2^2-k\lambda_1^2}{k-1}} \tag{7}$$

This parameter of the Debys formula experiences the greatest variation with the temperature and determines the nature of the temperature dependence of the water permittivity under the conditions of super cooling $T_{clo} < 0°C$.

An experimental study of the effect of temperature on the spectrum of relative absorption in the cloud was done by observations of the radio radiation of the sun at the waves 0.41, 0.82 and 1.6 cm [32, 34]. The cloud absorption measurement accuracy depended primarily on the instability of the gain 0.41 cm, and 0.01 neper at the others. The observations were made during the presence of cumulus and stratocumulus cloud cover, and the thickness of it did not exceed 1-1.5 km. The effective temperature of the cloud during the experiment varied from 5 to -13°C and it was found from the data of aircraft or radiosonde aerological measurements. Figure 6 shows the derived experimental values of the relaxation time as a function of temperature, as well as calculated values of it during negative temperatures. One can see that a smooth increase in the parameter τ_p is observed with a decrease in temperature. From a comparison of experimental and theoretical values of τ_p the conclusion can be made that curve 5 derived by extrapolation of the data in [21] does not match the measured values. Curve 4 which is an extrapolation of data in [20] with positive temperatures lies below the experimental points although one cannot state with certainty that it contradicts the experimental data. The calculated values of the parameter γ_p derived

from the formula cited in [15] (curve 3) as well as through extrapolation of the data in [14] agree with the experimental data if one takes into consideration the errors in measurements of absorption and temperature of the cloud and the latter were estimated for 1-3°C. The experimental values of τ_p of supercooled water agree better with the following approximation relationship (curve 1):

$$\tau_p = \exp\left\{9{,}8\left(\frac{273}{273+T_{clo}}-0{,}955\right)\right\}\cdot 10^{-12},\ \frac{\text{сек.}}{\text{см}}. \tag{8}$$

In the domain of positive temperatures $T_{clo} > 0°$ C the values of τ_p computed from formula (8) do not differ by more than 7 percent from the data in [14] when $0° \text{ C} \leq T_{clo} \leq 40°$C and from the data in [15] and [20] when $0° \text{ C} \leq T_{clo} \leq 15°$C. For confident selection in favor of one of the approximations shown in Figure 6 research into absorptions in a cloud must be done at lower temperatures or the accuracy of measurements must be improved.

5. The theoretical possibilities of solving the inverse problems of SHF radiometric sounding of a cloudy atmosphere are based on the fact that a clear relationship exists between brightness temperature and meteorological parameters as well as that oxygen, water vapor and clouds have a distinct effect on the spectrum of radiation of the atmosphere. The problem of determining the integral parameters of a cloudy atmosphere has been discussed in [29, 30, 32-34].

When the absorption in the atmosphere is not too large ($\tau \leq 1$ neper), the integral relationship (1) may be written in the form

$$T_a(\lambda, z) = T_{cp}[1-e^{-\tau(\lambda)\sec z}], \tag{9}$$

where T_{cp} is the mean absolute temperature of the atmosphere. During observation from aircraft the expression for brightness temperature of the system "atmosphere-underlying surface" (4) will have the form

$$\begin{aligned} T_a(\lambda, 0) = {} & T_n \varkappa(\lambda, 0) e^{-\tau(\lambda)\sec\theta} + T_{cp}{}^{\uparrow}[1-e^{-\tau(\lambda)\sec\theta}] + \\ & + R(\lambda, 0) e^{-\tau(\lambda)\sec\theta} T_{cp}{}^{\downarrow}[1-e^{-\tau(\lambda)\sec\theta}], \end{aligned} \tag{10}$$

where $T_{cp}{}^{\uparrow}$ and $T_{cp}{}^{\downarrow}$ is the mean absolute temperature of the atmosphere during rising and descending radiation in the direction of the angle of view. If the temperature, emissivity and reflection factor of the underlying surface are known, then by the relationships (9) and (10) one can find the total absorption in the atmosphere which is associated with the integral meteorological parameters by the following relationship [29]:

$$\tau(\lambda_i) = \tau_{0_2}(\lambda_i) + K_p(\lambda_i) Q + K_w(\lambda_i, T_{\substack{обл \\ clo}}) W, \tag{11}$$

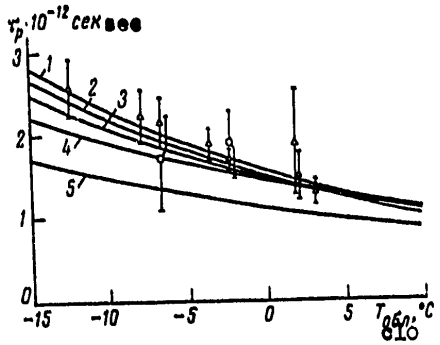

Figure 6. Experimental and theoretical values of relaxation time τ_p as a function of temperature. Curve 1 is calculated according to relationship (8). Curves 2, 4 and 5 were constructed by extrapolating experimental data on τ_p, obtained with positive temperatures in [14, 20 and 21] respectively. Curve 3 shows the values calculated according to [15]. The triangles depict the experiment at waves 0.41 and 0.82 cm; the circles depict the experiment at waves 0.82 and 1.57 cm.

Table 5. Permissible errors in measuring brightness temperatures at waves 0.8 and 1.35 $\delta T_я$ and effective temperature δT_{clo} when determining water reserve

Cloud shape	St, Sc; warm half year	As	Cumed	Cucong
Absolute error				
δW kg/m^2	0.05	0.1	0.2	0.2
$\delta T_я$ (0.8), °K	1.7	3.6	2.0	0.18
$\delta T_я$ (1.35), °K	4.6	10	14	4.3
δT_{col}, °K	20	11	3.1	1.3

Where τ_{O_2} is the total vertical absorption in the oxygen, $K_p(\lambda_i)$ and $K_w(\lambda_i, T_{clo})$ are the weighting absorption factors in the water vapor and in the water vapor and in the clouds respectively which depend in the general case on the upper-air distribution of the meteorological elements. Variations in the coefficient $K_p(\lambda)$ as a function of the profiles of the temperature,

pressure and humidity do not exceed 5 percent with the exception of the resonant transition in the vicinity of $\lambda = 1.35$ cm, where they may be somewhat large [44]. Variations in the coefficient $K_w(\lambda)$ as a function of the profile of the liquid-water content in the cloud at a given temperature do not exceed 1 percent for clouds with a thickness up to 1 km and 10 percent for extended cumulus clouds with a thickness of 5 km or more.

When measuring the total absorption at several wave lengths a system of equations (11) is formed which is linear with respect to the unknown parameters of total mass of water vapor and water reserve of the clouds, and nonlinear with respect to the unknown effective temperature of the cloud. Measurement of the total absorption in the atmosphere at 2 waves is sufficient to determine parameters Q and W when the effective temperature of the cloud is known. The working wave lengths should satisfy 2 evident conditions: the total absorption in the water vapor and in the cloud added together should form an appreciable quantity that can be measured with the required accuracy; the determinant of system (11) must differ considerably from zero:

$$D = K_p(\lambda_1)K_w(\lambda_2) - K_p(\lambda_2)K_w(\lambda_1).$$

The radio windows of 0.6-1.0 cm, 0.3-0.4 cm and 1.6-3 cm as well as the range of resonant absorption of water vapor 1.2-1.5 cm are the most suitable for solving this problem.

Instrument and methodological errors affect the accuracy of determining the integral parameters. Instrument errors include errors in measuring brightness temperatures and total absorptions; methodological errors include those in the selection of the weight factors K_p and K_w. The contribution of the errors in measuring absorptions $\delta\tau(\lambda_1)$ and $\delta\tau(\lambda_2)$ in the error in determining meteorological parameters Q and W can be estimated from the relationships

$$\frac{\delta Q}{Q} = \frac{\sqrt{[K_w(\lambda_2)\delta\tau(\lambda_1)]^2 + [K_w(\lambda_1)\delta\tau(\lambda_2)]^2}}{\Delta\tau(\lambda_1)K_w(\lambda_2) - \Delta\tau(\lambda_2)K_w(\lambda_1)} \qquad (12)$$

$$\frac{\delta W}{W} = \frac{\sqrt{[K_p(\lambda_2)\delta\tau(\lambda_1)]^2 + [K_p(\lambda_1)\delta\tau(\lambda_2)]^2}}{\Delta\tau(\lambda_1)K_p(\lambda_2) - \Delta\tau(\lambda_2)K_p(\lambda_1)}$$

where $\Delta\tau(\lambda) = \tau(\lambda) - \tau_{02}(\lambda)$. The errors in determining the total mass of water vapor and water reserve of the clouds are associated with the errors in measuring the temperature of the cloud by the following expressions:

$$\frac{\delta Q}{Q} = \frac{[K_p(\lambda_1)\Delta\tau(\lambda_2) - \Delta\tau(\lambda_1)K_p(\lambda_2)]\times}{D[K_w(\lambda_2)\Delta\tau(\lambda_1) - K_w(\lambda_1)\Delta\tau(\lambda_2)]},$$
$$\times\left[K_w(\lambda_1)\frac{\partial K_w(\lambda_2)}{\partial T_{об.}} - K_w(\lambda_2)\frac{\partial K_w(\lambda_1)}{\partial T_{об.}}\right]\delta T_{об.}$$
$$\frac{\delta W}{W} = \frac{1}{D}\left[K_p(\lambda_2)\frac{\partial K_w(\lambda_1)}{\partial T_{об.}} - K_p(\lambda_1)\frac{\partial K_w(\lambda_2)}{\partial T_{об.}}\right]\delta T_{об.}, \quad (13)$$

Table 5 shows the maximum errors in measuring the brightness temperature of the atmosphere and the effective temperature of the cloud which allow finding the value of the water reserve of the clouds with a given accuracy.

From table 5 it is evident that with the same errors in determining the parameter W the requirements for accuracy in measuring the brightness temperature at the wave 0.8 cm are higher than at the wave 1.35 cm and depend on the type of cloud cover. With 2 wave measurements the combination of waves 0.8 and 1.35 cm provides relatively high accuracy in determining the water reserve of stratiform and cumulus cloud covers at values of $W < 0.5$ kg/m^2.

In the case of cumulus congestus cloud cover a higher accuracy in determining parameter W is achieved if a longer wave, for example, the wave $\lambda = 2$ cm is selected instead of the wave 0.8 cm.

The accuracy in determining the meteorological parameters Q and W are also affected by the errors in finding the mean temperature of the atmosphere, the requirements for which are approximately by one order of magnitude less severe than for measurements of T_q. Additional errors occur when observation is made "from above." These are caused by the effect of variations of the temperature and reflection factor of the underlying surface [36]. The relative error in determining the total mass of water vapor $\delta Q/Q$ has a linear relationship with the errors in finding the coefficient K_p. For example, with variations in the coefficient K_p at 5 percent the value of $\delta Q/Q$ is 6-7 percent. In the process an additional error will be introduced into the cloud water reserve value that is being determined which is 1-4 percent depending on the value of the total mass of water vapor and absorption in the cloud.

6. Observations of descending radio radiation of the cloudy atmosphere were also made using a laboratory on board an aircraft. The laboratory contained SHF radiometers [42] in the 0.8, 1.35 and 2.25 cm wave length band. The flights were made in a number of areas in Central Asia, Siberia and the Far East during 1975-1977. Radiation from the upper hemisphere was received using horn antennas. The antennas for the 0.8 and 1.35 cm channels were directed to the zenith, while the third antenna was at a zenith angle of 75°. At the 2.25 cm wave the radiation was measured at 2 polarizations.

Measurements were taken on the aircraft at the same time of the outside air temperature and the height of the upper and lower boundaries of the clouds. Figure 7 shows the examples of the profiles of the radio brightness temperature at the 0.8 cm wave length for 3 types of clouds: Sc, Cucong and Cuhum. The flight was made at low altitude which was lower than the lower boundary of the clouds and aircraft speed was 100 m/sec. Spatial resolution was about 0.3 km. The level of radiation of a clear sky is shown by a dashed line. The profiles of the radio brightness temperatures basically describe the profiles of the water reserve of the clouds.

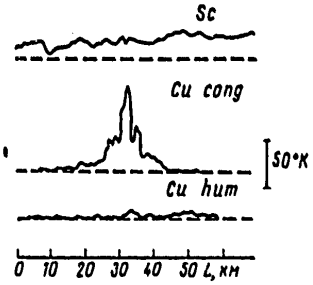

Figure 7. Profiles of radio brightness temperatures, obtained from an aircraft at wavelength of 0.8 cm for three types of clouds: stratocumulus (Sc), cumulus congestus (Cucong), and cumulus humilis (Cuhum). Radiation level of a cloudless sky is designated by the dashed line.

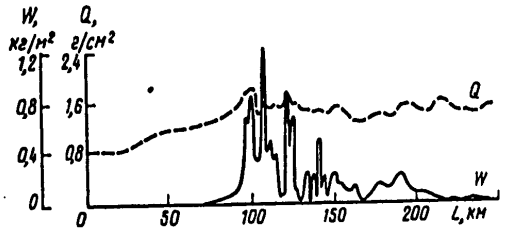

Figure 8. Data on the total mass of water vapor Q and water reserve of clouds W, obtained during aircraft experiments in the rear of an occluded cyclone with an intersection of a secondary cold front. 26 March 1975, flight Tashauz-Chardzhou.

The aircraft measurements make it possible to obtain the detailed structure of the field of humidity and water reserve of the atmosphere. Figure 8 shows the variation in the total mass of water vapor and water reserve of the clouds during a flight at the rear of an occluded cyclone with an intersection of a secondary cold front. The data was obtained in horizontal

flight at an altitude of 200 m in Central Asia. Three distinct sections can be identified in the graphs. The first section is cloudless. A transition from cold air to warm is observed in it. At a distance of about 90 km the air temperature changed from 20 to 25°C, while the value of the meteorological parameter Q increased from 0.85 to 1.6 g/cm^2. The second section is in the zone of the warm air. It has the sharply jagged shape of the profile of W and this is where the cumulus clouds were. A gradual breakup of the clouds with a decrease in their water reserve occurs in the third section. During measurement from the aircraft the error in determining the brightness temperature of the cloud at the 0.8 and 1.35 cm wave lengths was 0.6 and 0.9°K respectively. The minimum reported value of the water reserve of a cloud was 0.03 kg/m^2 and that of the total mass of water vapor was 0.05 g/cm^2. For the values of Q and W, which substantially exceeded these values, the errors are 10-15 percent.

An experiment on the "Kosmos-243" satellite (1968) showed the possibility of obtaining data on the integral parameters of the atmosphere above the sea surface [37-40]. Radiation leaving the system "atmosphere-underlying surface" was received by 4 radiometers in the direction of the nadir in the following sectors of the spectrum: λ_1=8,5 см; λ_2=3,4 см; λ_3=1,35 см и λ_4=0,8 см. The temperature of the ocean surface and its emissivity on short wave channels 3 and 4 were found by the values of the radio brightness temperature on long wave channels 1 and 2. Then the integral parameters of the atmosphere Q and W were determined using the technique described earlier. Figure 9 shows an example of the profiles of the brightness temperature at the wave lengths 0.8, 1.35 and 3.4 cm during the flight of the "Kosmos-243" satellite over the Pacific Ocean. The large values of brightness temperatures at wave lengths 0.8 and 1.35 cm, reaching 244 and 233°K respectively, as well as the noticeable brightening at wave lengths 3.4 cm ($\Delta T_{\text{я}}$ = 20°K) show that the satellite orbit projection intersected a large thick mass of clouds with large values of water reserve. The SHF radiometric measurements correlated well with the television and infrared images of the cloud cover. Data on the total mass of water vapor and water reserve of the clouds along the projection of the satellite "Kosmos-243" in the northern part of the Atlantic Ocean are shown in Figure 10. One can see very substantial variations in the meteorological parameters Q and W during intersection of the three frontal sections. The areas with thick cloud cover are characterized by increased values of moisture content. In this experiment the errors in determining the total mass of water vapor were 0.2-0.4 g/cm^2. At greater values of it the absolute accuracy of a single measurement of W is estimated to be 30-50 percent.

Conclusion

The results of the theoretical and experimental research performed establish the dependencies of the SHF spectrum of brightness temperatures of the atmosphere on water reserve, temperature, altitude, moisture and other physical parameters of clouds. They also demonstrated the possibility of determining the integral meteorological parameters of the atmosphere by

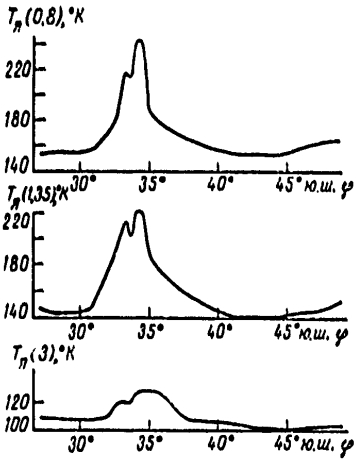

Figure 9. Profiles of the brightness temperature of the system "Atmosphere-Surface of the Ocean" at wavelengths 0.8, 1.35 and 3 cm along the projection of the orbit of the "Kosmos-243" satellite over the Pacific Ocean.

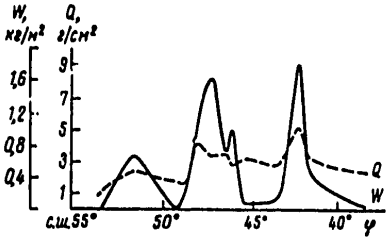

Figure 10. Data on the total mass of water vapor Q and water reserve of the clouds W, obtained during intersection by the "Kosmos-243" satellite of three frontal divisions over the Atlantic Ocean.

means of SHF radiometric sounding. Starting in 1965-1966 parallel research of radio thermal radiation of clouds was performed at the Main Geophysical Observatory imeni A. I. Voyeykov, the Central Aerological Observatory and other organizations and was directed basically at determining the relationship of radio brightness temperatures to meteorological parameters. The effectiveness of the SHF radiometric method for studying the cloudy atmosphere was confirmed by experiments performed on the "Nimbus-5" (1972), "Nimbus-6" (1975) and the "Meteor" (1975) satellites.

The authors are grateful to N. F. Kukharskaya for compilation of programs and calculations run on the computer.

Bibliography

1. R. H. Dicke , REV. SCIENT. INSTRUM., 1946, 17, 268.

2. R. H. Dicke , R. Beringer, R. L. Kyhl, A. B. Vane, PHYS. REV., 1946, 70, 340.

3. J. H. Van Vleck, PHYS. REV., 1947, 71, 413.

4. J. H. Van Vleck, PHYS. REV., 1947, 71, 425.

5. S. A. Zhevakin, A. P. Naumov, IZV. VUZOV MVO SSSR [Ministry of Higher Education, USSR], (RADIOFIZIKA), 1963, 6, 4, 674.

6. S. A. Zhevakin, A. P. Naumov, RADIOTEKHNIKA I ELEKTRONIKA, 1965, 10, 6, 987.

7. S. A. Zhevakin, A. P. Naumov, IZV. VUZOV MVSSO SSSR [Ministry of Higher and Secondary Special Education, USSR] (RADIOFIZIKA), 1967, 10, 9-10, 1213.

8. S. A. Zhevakin, V. S. Troitskiy, N. M. Tseytlin, IZV. MVO SSSR (RADIOFIZIKA), 1958, 1, 2, 13.

9. S. A. Zhevakin, V. S. Troitskiy, RADIOTEKHNIKA I ELEKTRONIKA, 1959, 4, 1, 21.

10. A. Ye. Salomonovich, O. M. Atayev, IZV. VUZOV MVO SSSR (RADIOFIZIKA), 1960, 3, 4, 606.

11. D. G. Hogg, R. A. Semplak, BELL SYSTEM TECHN. J., 1961, 40, 1331.

12. D. G. Hogg, J. APPL. PHYS., 1959, 30, 9, 1417.

13. C. Tolbert, A. Straiton, BRIT. J. APPL. PHYS., 1959, 29, 5, 776.

14. J. A. Saxton, PHYS. SOC. AND ROY. METEOROL. SOCL, London, 1946, pp 292-320.

15. V. I. Rozenberg, "Rasseyaniye i oslableniye elektromagnitnogo izlucheniya atmosfernymi chastitsami" [Scattering and Attentuation of Electromagnetic Radiation by Atmospheric Particles], Gidrometeoizdat, 1972, 348.

16. K. Ya. Kondrat'yev, "Luchistyy teploobmen v atmosfere" [Radiant Heat Exchange in the Atmosphere], Gidrometeoizdat, 1956.

17. A. H. Barrett, V. K. Chung, J. GEOPHYS. RES., 1962, 67, 11, 4259.

18. K. S. Shifrin, "Rasseyaniye sveta v mutnoy srede" [Light Scattering in a Turbid Medium], GTI, 1951.

19. G. Van de Khyulst, "Rasseyaniye sveta malymi chastitsami" [Light Scattering by Small Particles], translated from English, IL, 1961.

20. C. H. Collie, J. B. Hasted, D. M. Ritson, PROC. PHYS. SOC., 1948, 60, pt 2, 338, 145.

21. M. M. Magat, J. CHEM. PHYSIQUE, PHYSICOCHIMIE BIOLOGIQUE, 1948, 45, 4-5, 93.

22. Ye. M. Feygel'son, "Luchistyy teploobmen i oblaka" [Radiant Heat Exchange and Clouds], Gidrometeoizdat, 1970, 230.

23. I. P. Polovina, "Vozdeystviya na vnutrimassovyye oblaka sloistykh form" [Effects on Internal Stratiform Clouds], Gidrometeoizdat, 1971, 215.

24. L. S. Dubrovina, TRUDY VNIIGMI-MTsD [All-Union Scientific Research Institute of Hydrometeorological Information], 1974, Issue 7, pp 3-11

25. R. A. Devyatova, TRUDY GIDROMETEOROL. TSENTRA SSSR, 1974, Issue 148, pp 73-90.

26. M. S. Shmeter, "Fizika konvektivnykh oblakov" [Physics of Convective Clouds], Gidrometeoizdat, 1972, 231.

27. F. Ya. Voyt, I. P. Mazin, IZV. AN SSSR, FIZIKA ATMOSFERY I OKEANA, 1972, 8, 11, 1966.

28. Yu. A. Glagolev, "Spravochnik po fizicheskim parametram atmosfery" [Handbook on Physical Parameters of the Atmosphere], Gidrometeoizdat, 1970.

29. A. Ye. Basharinov, S. T. Yegorov, M. A. Kolosov, B. G. Kutuza, TRUDY GGO [Main Geophysical Observatory imeni A. I. Voyeykov], 1968, issue 222, 153-158.

30. A. Ye. Basharinov, B. G. Kutuza, TRUDY GGO, 1968, issue 222, 100-110.

31. N. I. Ananov, A. Ye. Basharinov, K. P. Kirdyashev, B. G. Kutuza, RADIOTEKHNIKA I ELEKTRONIKA, 1965, 10, 11, 1941.

32. A. Ye. Basharinov, B. G. Kutuza, "Trudy 3-go Vsesoyuznogo soveshchaniya po radiolokatsionnoy meteorologii" [Works of the Third All-Union Conference on Radar Meteorology], Gidrometeoizdat, 1968, 96-106.

33. A. E. Basharinov, B. G. Kutuza, BULL. AMER. METEOROL. SOC., 1968, 49, 5, p5 2, 597.

34. A. Ye. Basharinov, B. G. Kutuza, IZV. VUZOV MVSSO SSSR (RADIOFIZIKA), 1974, 17, 1, 52.

35. A. Ye. Basharinov, A. G. Gorelik, V. V. Kalashnikov, B. G. Kutuza, IZV. AN SSSR, FIZIKA ATMOSFERY I OKEANA, 1970, 6, 5, 526.

36. B. G. Kutuza, L. M. Mitnik, A. M. Shutko, TRUDY GIDROMETEOROL. TSENTRA SSSR, 1969, issue 50, pp 86-93.

37. A. Ye. Basharinov, S. T. Yegorov, A. S. Gurvich, DOKL. AN SSSR, 1969, 188, 6, 1273.

38. A. M. Obukhov, A. Ye. Basharinov et al., KOSMICHESKIYE ISSLEDOVANIYA, 1971, issue 1, 66.

39. A. B. Akvilonova, B. G. Kutuza, L. M. Mitnik, IZV. AN SSSR, FIZIKA ATMOSFERY I OKEANA, 1971, 7, 2, 139.

40. A. B. Akvilonova, M. S. Krylova, B. G. Kutuza, L. M. Mitnik, TRUDY TSENTR. AEROLOG. OBSERVATORII, 1972, issue 103, 73-81.

41. A. B. Akvilonova, A. Ye. Basharinov et al., IZV. AN SSSR. FIZIKA ATMOSFERY I OKEANA, 1973, 9, 2, 187.

42. V. S. Ablyazov, A. B. Akvilonova et al., "Radiofizicheskiye issledovaniya atmosfery" [Radiophysical Research of the Atmosphere], Gidrometeoizdat, 1977, 204-207.

43. S. P. Gagarin, B. G. Kutuza, IZV. AN SSSR, FIZIKA ATMOSFERY I OKEANA, 1977, 13, 12, 1307.

44. A. P. Naumov, IZV. AN SSSR, FIZIKA ATMOSFERY I OKEANA, 1968, 4, 2, 170.

45. P. D. Kalachev, A. Ye. Salomonovich, RADIOTEKHNIKA I ELEKTRONIKA, 1961, 6, 3, 422.

8545
CSO: 8144/0518

PHYSICS

UDC 621.378:535.4

AMPLIFYING DYNAMIC HOLOGRAMS[1]

Minsk ZHURNAL PRIKLADNOY SPEKTROSKOPII in Russian Vol 28 No 6, Jun 78 pp 992-996

[Article by Ye.V. Ivakin, A.M. Lazarus, I.P. Petrovich, and A.S. Rubanov]

[Text] The recording of a dynamic hologram in a solution of polymethine dye on the basis of saturation of amplification has been experimentally carried out. The dependence of the diffraction effectiveness on the pumping power and the recording field is investigated. It is shown that it is possible to increase the sensitivity by one or two orders over the bleachable media. The main experimental patterns are qualitatively confirmed by calculations.

The known methods for recording and reproducing wave fields are based on the absorption of light energy. This applies to both photoemulsions and to nonsilver light-sensitive materials. In dynamic holography, when bleachable recording mediums with a short information storage time are used [3], the recording and (or) reading of a hologram can be accompanied by optical amplification of the light beams. In this case the hologram is a substance with spatial modulation of the amplification factor.

Among the extensive class of bleachable substances for the recording of amplifying holograms, the most promising ones are solutions of complex organic compounds [4], which make it possible to achieve a high amplification factor value. When excited in the absorption area (Figure 1a) the substance is

---

[1]Presented at the 2d All-Union Conference on Holography (Kiev, 1975) and the 8th All-Union Conference on Coherent and Nonlinear Optics (Tbilisi, 1976) [1,2].

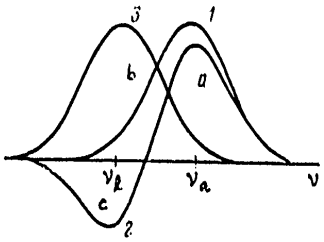

Figure 1. Absorption (1,2) and luminescence (3) spectra of a dye solution: 1. undisturbed; 2. in a powerful pumping field.

bleached, while amplification appears (Figure 1c) inside the boundary of luminescence (Figure 1b). Recording of the wave front in band a leads to spatial modulation of the substance's optical and spectroscopic properties: the absorption coefficient's hologram is recorded in the absorption area (a), while that of the amplification factor is recorded in the luminescence area (b).

In [4] the authors realize one of the variants of a dynamic hologram in which amplification is used at the reproduction stage. The recording medium was a thin layer of polymethine dye solution. The dynamic lattice was registered by the emissions of a monopulsed laser with a wave length corresponding to the dye's absorption band. Diffraction of the sounding beam in the amplification band was observed to occur simultaneously with registration of the lattice. In this case there was amplification of both the sounding and diffracted beams. Under the conditions of the experiment reported in [4], the value of diffraction effectiveness D was more than 200.

In this article we discuss the possibility of using the phenomenon of amplification saturation in the recording of dynamic holograms. In this case, the process of recording the hologram in the inverse medium is accompanied by amplification of the interfering waves' intensity and the simultaneous appearance and amplification of additional diffracted light beams (self-diffraction in the amplifying medium).

Figure 2 is a schematic diagram of the experimental setup. A solution of polymethine dye #4568 was placed in container 1, which has clear ports (for the prevention of spurious oscillation). The initial transmission T_p^0 (λ_p = 694 nm) of a layer of thickness d = 1 mm is less than 10^{-2} (because of the small value of T_p^0, an exact measurement was not made). The center of the dye's absorption band corresponds to wave length λ_a = 682 nm, while the center of the luminescence outline corresponds to λ_l = 694 nm. Amplification appeared in the dye layer under the effect of emissions (λ_p = 694 nm) from monopulsed ruby laser 2, which has a phototropic shutter. Maximum bleaching of the layer corresponded to transmission T_p (λ_p = 694 nm) $\sim$ 0.2 at an energy density of 2 j·cm^{-2}. Simultaneously, part of the emissions of laser 2 were shunted off by mirror 3 and used to pump

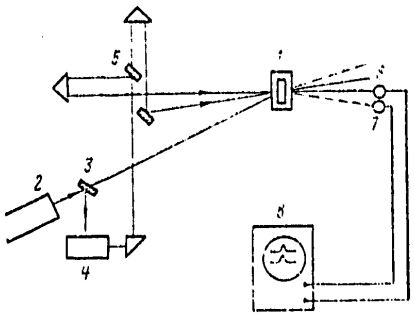

Figure 2. Optical circuit for recording dynamic hologram in the inverse medium.

liquid laser 4, which uses a solution of the same dye and operates on wave length λ_c = = 730 nm. The generation spectrum was narrowed to 0.3 nm by adding a dispersing element to the resonator.

In order to form the amplifying hologram, the emissions from source 4 were split (with the help of light-splitting device 5) into two beams of approximately equal intensity that were then directed into the plane of container 1. The beam-splitting method insured combination of the mode structure and path difference compensation. When propagating in the inverse medium, the interfering waves were amplified and caused a spatially nonuniform (with a period Λ = 100 μ) reduction in the population of the excited state. As a result of this, the amplifying lattice on which the incident waves were diffracted was recorded in the medium.

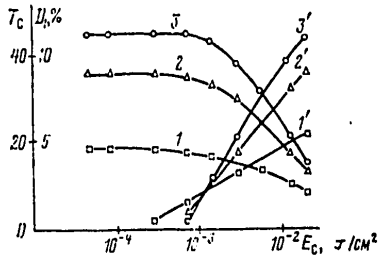

Figure 3. Layer amplification T_c (1-3) and diffraction effectiveness D_1 (1'-3') as functions of pumping energy E_p and recording field E_c; E_p = 0.4 (1,1'), 0.9 (2,2'), 2 (3,3') j/cm^2.

The results of an experimental measurement of the effectiveness of self-diffraction D_1 (the ratio of the intensity of the emissions diffracted in the first order to the intensity of the original beam) and amplification of the dye layer (hologram) T_c are given as functions of the energy of the interfering beams, for three different pumping intensity values, in Figure 3. The intensities of the diffracted beams forming the hologram were measured with the help of photoreceivers 6 and 7 and oscillograph 8 (Figure 2). The linear amplification T_c on the 730 nm wave length was 20, 35 and 40. The maximum self-diffraction effectiveness D_1 reached ~10 percent in the experiment. As the intensity of the interfering beams increased, so did the diffraction effectiveness. This increase was most clearly expressed for high pumping energy values.

As is obvious (Figure 3), the amplifying mediums' sensitivity during the recording of holograms is higher than in the bleachable substances. In the case of bleachable dyes, diffraction effectiveness on the order of 1 percent is reached when the density of the interfering beams' radiation is $E_c \sim (0.5\text{-}1)\cdot 10^{-1}$ j·cm^{-2}. Under the conditions of this experiment, the use of the amplification effect made it possible to increase the sensitivity substantially and to push the value of E_c to $\sim 10^{-3}$ j·cm^{-2}. In connection with this, the sensitivity decreased slightly as the pumping energy increased.

A detailed theoretical analysis of the features of self-diffraction in the inverse medium would be quite complicated. However, the possibility of increasing the sensitivity when using amplifying mediums for hologram registration can be illustrated in the following manner. It follows from Figure 3 that the appearance of diffracted beams (indicative of the recording of the interference field) corresponds to the transition from the linear to the nonlinear amplification area. This fact makes it possible to formulate approximate theoretical estimates of the dependence of sensitivity on the dye's properties and the power of the pumping wave that are based on an examination of the features of the light beam's propagation in the amplifying medium. For our calculations we will start with the equation describing the change in the flow when it interacts with the excited dye [6]:

$$\frac{dI_c}{dz} = -\frac{1+\Gamma_\rho I_\rho}{1+\alpha_c I_c + \alpha_\rho I_\rho} k_c^0 I_c, \tag{1}$$

where

$$\begin{aligned}
\Gamma_\rho &= \frac{B_{12}(\nu_\rho)\tau}{c}\left\{e^{\frac{hc}{kT}(\nu_c-\nu_\rho)} - e^{\frac{hc}{kT}(\nu_c-\nu_c)}\right\};\\
\alpha_\rho &= \frac{B_{12}(\nu_\rho)\tau}{c}\left\{1 + e^{\frac{hc}{kT}(\nu_c-\nu_\rho)}\right\};\\
\alpha_c &= \frac{B_{12}(\nu_c)\tau}{c}\left\{1 + e^{\frac{hc}{kT}(\nu_c-\nu_c)}\right\};\\
k_c^0 &= h\nu_c N B_{12}(\nu_c);\quad \nu_c = \frac{1}{2}(\nu_a+\nu_\rho);
\end{aligned} \tag{2}$$

B_{12} = Einstein coefficient; τ = lifetime of the dye in the excited state; c = speed of light; N = density of the molecules; T = temperature of the medium; $I_p(\nu_p)$ and $I_c(\nu_c)$ = pumping intensity in the absorption band and light beam intensity in the amplification area.

In accordance with (1), the relationship between the dimensionless intensities upon emerging from the layer (z = d) is

$$\xi = \frac{\alpha_c I_c(d)}{1 + \alpha_\rho I_\rho(d)} \tag{3}$$

which determines the degree of amplification saturation. We will characterize the transition to nonlinear amplification by the value $\xi = \xi_y < 1$. The threshold intensity of the wave as it enters the layer (I_c^{thr}) that is necessary for hologram recording will then be defined as

$$I_c^{thr} = \xi_y (1 + \alpha_\rho I_\rho^0 T_\rho)/\alpha_c T_c, \tag{4}$$

where I_p^0 = intensity of the pumping wave as it enters the layer. Since amplification saturation is assumed to be only slight in the entire layer, T_c can be derived from equation (1) by ignoring the nonlinear dependence of the absorption and amplification coefficients on I_c:

$$\ln T_c = \frac{k_c^0}{k_\rho^0}\left\{\ln T_\rho\left(1 - \frac{\Gamma_\rho}{\alpha_\rho}\right) - \frac{\Gamma_\rho}{\alpha_\rho}\ln T_\rho^0\right\}. \tag{5}$$

In the same approximation, pumping wave transmission is determined from the transcendental equation

$$(1 - T_\rho)\alpha_\rho I_\rho^0 = \ln T_\rho - \ln T_\rho^0. \tag{6}$$

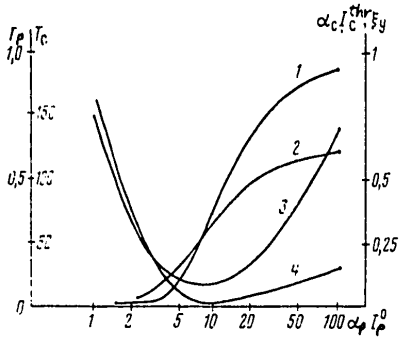

Figure 4. Dependence of pumping transmission T_p (1), layer amplification T_c (2) and threshold intensity of the recording field $\alpha_c I_c^{thr}$ (3,4) on pumping intensity $\alpha_p I_p^0$. $T_p^0 = 10^{-3}$ (1-3) and 10^{-4} (4).

Figure 4 shows the results of the calculation of pumping wave transmission T_p, amplifying flow transmission T_c and the threshold intensity $\alpha_c I_c^{thr}$ that determines the medium's sensitivity, all as functions of $\alpha_p I_p^0$. Calculations were made for $T_p^0 = 10^{-3}$ and 10^{-4}. The values $k_c^0/k_p^0 = 0.07$ and $\Gamma_p/\alpha_p = -10.1$ correspond to the conditions of the experiment described above.

The existence of an optimum for the amplifying layer's sensitivity, which for the given parameters corresponds to the value $(\alpha_p I_p^0)_{opt} \sim 10$, follows from the calculative data (see Figure 4, curves 3 and 4). This result is natural and is caused by the competition between the increase in amplification and the decrease in the value of the effective parameter of nonlinearity

$$\alpha_c' = \frac{\alpha_c}{1 + \alpha_\rho I_\rho^0 T_\rho} \tag{7}$$

as pumping intensity $\alpha_p I_p^0$ increases. For small values of $\alpha_p I_p^0$, the increase in amplification is predominant, because in this case α_c^* decreases comparatively slowly. In the area of values $\alpha_p I_p^0 > (\alpha_p I_p^0)_{opt}$, amplification converges on saturation with respect to pumping, while α_c^* decreases in proportion to $1/(\alpha_p I_p^0)$.

The experimentally observed decrease in sensitivity (see Figure 3) as pumping increases is apparently related to the excess of $\alpha_p I_p^0$ over the optimum value.

Within the framework of this approach, let us correlate sensitivity to hologram recording on the basis of the mechanisms of amplification saturation and absorption. By analogy with (3), we assume that hologram recordings in the absorption band are achieved in connection with the transition to nonlinear transmission of the layer at the value $\alpha_t I_t^{thr}(z = 0) = \zeta_t < 1$. Assuming equality of the parameters $\zeta_t \simeq \zeta_y$, the gain in sensitivity during the transition from absorption to amplification can be estimated from the relationship

$$\frac{I_t^{thr}}{I_c^{thr}} = \frac{\alpha_c}{\alpha_t} \frac{T_c}{1 + \alpha_p I_p^0 T_p}. \qquad (8)$$

In the area of the absorption and luminescence bands' maximums, α_c and α_t are approximately identical. For parameter values corresponding to those in Figure 4, $\alpha_c/\alpha_t \simeq 0.8$. In this case, it follows from (8) that there is an increase in sensitivity in the area of the optimum (see Figure 4) by one or two orders in comparison with a recording in the absorption band, which agrees qualitatively with the result of the experiment.

Additional Notes: After this article was published, the authors worked on improving the experiment described in it. For this purpose, they succeeded in matching the generated wave length of laser 4 (λ = 720 nm) with the center of the circumference of amplification of the registering layer 1 (a solution of #4568 dye from which the impurities have been removed). In this case, the layer's linear amplification T_c (λ = 720 nm) was $\sim 10^3$. As should have been expected from (8), the sensitivity gain in comparison with the absorbing layers was more than 10^3, while the energy's threshold density $E_c^{thr} \simeq 2 \cdot 10^{-5}$ j·cm^{-2}. During the experiment, it was observed that D_1 and T_c were not dependent on E_c in the section of substantial saturation. In connection with this, the value of D_1 reached $\sim$12 percent. The given experimental results agree with the theoretical estimates given in the article.

BIBLIOGRAPHY

1. Ivakin, Ye.V., Petrovich, I.P., and Rubanov, A.S., MATERIALY II VSESOYUZNOY KONFERENTSII PO GOLOGRAFII (Materials of the 2d All-Union Conference on Holography), Kiev, 1975, Vol 2, p 18.

2. Ivakin, Ye.V., Lazaruk, A.M., Petrovich, I.P., and Rubanov, A.S., TEZISY DOKLADOV VIII VSESOYUZNOY KONFERENTSII PO KOGERENTNOY I NELINEYNOY OPTIKE (Summaries of Reports Given at the 8th All-Union Conference on Coherent and Nonlinear Optics), Tbilisi, 1976, Vol 2, p 382.

3. Stepanov, B.I., Ivakin, Ye.V., and Rubanov, A.S., DAN SSSR (Proceedings of the USSR Academy of Sciences), Vol 196, 1971, p 567.

4. Ivakin, Ye.V., Petrovich, I.P., Rubanov, A.S., and Stepanov, B.I., KVANTOVAYA ELEKTRONIKA (Quantum Electronics), Vol 2, 1975, p 1556.

5. Stepanov, B.I., and Gribkovskiy, V.P., UFN (Progress of Physical Sciences), Vol 95, 1968, p 45.

11746
CSO: 8144/0477

SCIENTISTS AND SCIENTIFIC ORGANIZATIONS

UDC 681.132.65

SECOND INTERNATIONAL SCHOOL OF SEMICONDUCTOR ELECTROOPTICS 'CETNIEWO-1978'

Moscow KVANTOVAYA ELEKTRONIKA in Russian Vol 5 No 11, Nov pp 2503-2506

[Article by P. G. Yeliseyev and M. A. Herman]

[Text] The Second International School of Semiconductor Electrooptics "Cetniewo-1978" (named after the sports base on whose territory the participants were housed and where the lectures were given) was held at Wladislawowo (not far from Gdansk, Poland) from 6 through 14 May 1978. The first school, as reported previously [1], was held at the same location in October 1975. The organizers of the school are the Polish Academy of Sciences (Institute of Physics of the Polish Academy of Sciences at Warsaw) and the Polish Physical Society.

The international school assembled more than 200 students from 13 countries who heard 23 lectures on various problems of semiconductor electrooptics, mainly concerning radiation sources. Specialists working actively in electrooptics appeared at lectors. Soviet science, occupying the leading position in semiconductor electrooptics, was most widely represented -- seven lectures from the academic institutes of Moscow, Leningrad and Kiev. The lectors also included representatives of Poland, GDR, Japan, Great Britain, the United States, Canada, Brazil, France, Sweden, West Germany and Italy.

The lectures were divided into the following sections:

physical phenomena in electrooptical materials and devices (four lectures);

technological problems (four lectures);

electrooptical devices (six lectures);

injection lasers (six lectures);

optical communications and integrated optics (three lectures);

The lectures were read in sequence in the same hall so that the students could visit all of them. Since the time allocated for each lecture was almost 2 hours and since the lecture itself comprised 1-1.5 hours, there were good opportunities for discussion of the problems touched on and for explanation of questions which arose. The library, containing copies of the texts of all lectures, was made available to the students.

The director of the Institute of Physics of the Polish Academy of Sciences, Corresponding Member of the Polish Academy of Sciences Professor E. Kolodzeiczak, chairman of the program committee of the school, opened the work of the school. Member of the Presidium of the Polish Physical Society Doctor A. Kuyevskiy and Chairman of the Wladislawowo City Council S. Sarafin greeted the participants. The regular work of the school was then begun with the lecture of the Corresponding Member of the USSR Academy of Sciences, winner of the Lenin Prize Professor Zh. I. Alferov "Heterostructures in Semiconductor Electronics."

As indicated by the experience of the past few years, the idea of using heterojunctions in semiconductor devices was exceptionally fruitful, specifically with regard to electrooptical devices. Heterostructures -- combinations of one or several heterojunctions and p-n junctions in a unified multilayer system -- became the basis for new types of radiation sources and detectors: heterolasers, heterowaveguides and heterophotodiodes. New trends in electrooptics are being developed -- integrated optics, image converters and amplifiers, optical memory systems and so on. The contribution of Soviet scientists was of decisive significance in these fields. The lecture of Zh. I. Alferov (Physicotechnical Institute imeni A. F. Ioffe of the USSR Academy of Sciences) contained a survey of the advances in development of electrooptical and other semiconductor devices based on A.GaAs/GaAs heterostructures, whose technology is more developed. Expansion of the range of applications of heterostructures is of important practical significance. A decisive step was made recently in this direction which made it possible to create many new heterostructures. The essence of this new stage in development of semiconductor electrooptics consists in the use of multicomponent solid solutions within the framework of which a wide range of ideal pairs of semiconductor materials can be accomplished which are suitable for joining in heterojunctions. The lecture of P. G. Yeliseyev (Physics Institute imeni P. N. Lebedev of the USSR Academy of Sciences) "Type III-V Quaternary Systems for Coherent and Noncoherent Radiation Sources" was devoted to the problem of creating new heterostructures. The development of the world's first new heterolasers based on GaInPAs/InP, GaInAsSb/GaSb and AlGaAsSb/GaSb systems, which cover a wide spectral range of IR radiation, in the USSR was specifically reported in this lecture.

The Soviet delegation also presented the following lectures: "The Quantum Efficiency of Light Diodes on Binary Heterostructures: Theory and Experimental Investigations" (D. Z. Garbuzov, FTI [Physicotechnical Institute] imeni A. F. Ioffe); "Photodetectors and Radiation Converters Based on Heterostructures" (V. I. Korol'kov, FTI imeni A. F. Ioffe); "MNOS Systems for

Optical Reversible Memory Devices in Computers" (Yu. M. Popov, FIAN [Physics Institute imeni P. N. Lebedev of the USSR Academy of Sciences), "GaAlAs Heterostructures in Integrated Optics" (Ye. L. Portnoy, FTI imeni A. F. Ioffe); and "Electroluminescent Image Converters and Amplifiers" (S. V. Svechnikov, Institute of Semiconductors of the Ukrainian SSR Academy of Sciences).

Timely developments were presented in the theoretical and experimental aspects in these lectures. Specifically, methodical problems of determining the internal quantum yield of radiative recombination in AlGaAs heterostructures were considered in the lecture of D. A. Garbuzov. Improving the characteristics of photodetectors by using heterojunctions and development of new types of photodetectors and converters (selective photodiodes, electroluminescent photoresistors, solid-state converters and so on) were described in the lecture of V. I. Korol'kov. New promising MNOS structures (metal-nitride-oxide-semiconductor) as reversible data carriers for optical memory devices were presented by Yu. M. Popov. The use of heterostructures with Bragg reflectors in the integrated optics component base was discussed by Ye. L. Portnoy. He reported, for example, about continuous injection heterolasers with Bragg reflectors developed at FTI imeni A. F. Ioffe.

Corresponding member of the Ukrainian SSR Academy of Sciences S. V. Svechnikov talked about efficient image amplifiers based on multilayer structures in which the photosensitive material is CdSSe and the scintillating material is ZnS:Mn. Image intensity in contrast amplification of 200 was achieved on a mockup with illumination of 10^{-3} lux.

A number of lectures was presented by the hosts of the school, Polish specialists. Academician of the Polish Academy of Sciences L. Sosnovski gave a detailed survey of the characteristics of the most important narrow-band semiconductors in a lecture on the topic "Type IV-VI Semiconductors as Materials for Infrared Electrooptics." Research associate of the Institute of Physics of the Polish Academy of Sciences, Doctor M. A. Herman gave a lecture entitled "The Coherence of Semiconductor Laser Emission" and a research associate of the same institute Doctor T. Bryshkevich gave a lecture entitled "The Electroepitaxy of Compound $A^{III}B^{V}$ and Its Application in the Technology of Electrooptical Devices."

A detailed survey of the advances of Polish electrooptics and of the production of electrooptical devices was given in the talk of Doctor B. Mroziyevich, director of the Institute of Electronic Technology (ITE), which is part of the Polish Electroindustrial Company Unitra. During the past 3 years the institute has achieved significant success in development and production of electrooptical devices. New light diodes, digital displays, photodetectors and optrons have been introduced into mass production. New models of powerful GaAs:Si light diodes, GaAs:Zn light diodes for fiber-optics communications lines and silicone avalanche photodiodes, specifically, have been developed. Green light diodes based on GaInP have apparently appeared in mass production for the first time in worldwide practice.

Fundamental investigations, for example, in the field of the radiative mechanism of recombination in compensated GaAs:Si and AlGaAs:Si semiconductors are being carried out extensively.

The lecture of Doctor D.-I. Nishidzawa (University of Tohoku, Sendai, Japan) "Method of Stoichiometric Crystallization of III-V Compounds for Light Diodes and Injection Lasers" aroused special attention among the lectures. Investigations directed toward optimization of the liquid-phase epitaxy (ZhFE) mode of GaP, GaAs and other electrooptical materials were generalized in the lecture. The novelty of these investigations is that, unlike the generally accepted approach when only pure hydrogen is controlled during ZhFE in the gaseous phase over the liquid phase, an optimum value of the partial pressure of the volatile components of the compound (for each temperature) is selected and maintained in the given case. This procedure provide reproducible production of the crystallographic and electrophysical parameters of the compound and, which is very significant for the technology of radiation sources, apparently provides minimum deviation from stochiometry in the solid phase. This in turn improves the radiative characteristics of the materials by reducing the point defect concentration.

Doctor T. Nishinaga (Tokyo Technological Institute, Japan), in his lecture, illuminated another technological aspect of ZhFE -- the causes and methods of preventing nonplanarity of the epitaxy front. His lecture was entitled "The Morphology of the Crystallization Front and Inhomogeneities in Impurity Distribution During Multilayer Liquid-Phase Epitaxy."

The greatest attention in the lectures was devoted to the theory of injection lasers and to their fundamental properties. These problems were considered in the lectures of Doctor M. Pilkun (Stuttgart University, West Germany) "Investigations of Optical Amplification and Its Saturation in Semiconductor Lasers," of Doctor M. Adams (University of Southhampton, Great Britain) "A Unified Approach to Theoretical Problems of Injection Lasers," of H. Bachert (Central Institute of Optics and Spectroscopy, Berlin, East Germany) "Investigating the Possibility of Controlling the Spectral Behavior of Injection Lasers," of Doctor K. Unger (Leipzig University imeni K. Marx, East Germany) "The Statistical Approach in Study of the Effect of Strong Alloying and Mixing of Type III-V Compounds on the Electrooptical Properties of These Materials" and of Doctor H. E. Ripper (Physics Institute of Campinas University, Brazil) "Injection Laser Modes." One important theoretical problem of interpretation of the dynamics of generation in band injection heterolasers was touched on in several lectures and was outlined in more detail in the lecture of Doctor G. H. Thompson (Standart Telecommunication Laboratory (STL), Great Britain) "Heterolasers With Band Geometry and the Effects of Optical and Electronic Restriction." The increased interest in the problems of the dynamics of band heterolasers is related to the fact that lasers of this type are ideal sources for fiber waveguide communications lines. They are exceptionally compact, simple, easily matched with waveguides without intermediate optics and permit direct (internal) modulation of radiation over a wide frequency band. However, some anomalies,

specifically, discontinuities in the output characteristics related to instability of the generation channel, were detected in planar band heterolasers. Narrower band structures and the use of lateral optical and electronic restriction may be employed to eliminate these undesirable phenomena. For example, these types of lasers with a wide band structure of 2 microns were developed in the laboratory of STL.

A survey of the problems occurring in development of optical communications systems was given in the lecture of Doctor J. Diamond (Bell Northern Research Laboratory, Ottawa, Canada) "The Characteristics of Electrooptical Devices for Optical Communications Systems." Attention was turned here, specifically, on the significant success in optimization of spectral matching of the source and fiber waveguide. Actually, due to development of heterolasers based on the GaInPAs/InP quaternary system, the band of wavelengths of 1.0-1.5 microns became accessible for application in optical communications and the conditions of signal propagation are much better in this band than in the previously developed band near 0.8 micron. This true not only in lesser attenuation of emission, but also in a smaller value of the phase velocity dispersion passing through a minimum at a wavelength of approximately 1.3 microns. Restrictions on the line capacity on the part of dispersion of the material are essentially negligible near this wavelength. Heterolasers for this wavelength based on the GaInPAs/InP system, accomplished for the first time in the Soviet Union, are being investigated intensively in many laboratories of the world. Directly connected to development of fiber-optics communications lines, some problems and investigations on waveguide optics were considered in the lecture of Doctor B. Crosinniani (Central Institute of Mail and Television, Italy) "Mode Dispersion in an Optical Fiber With Regard to Mode Coupling."

Problems of degradation are also related to a range of problems of the practical application of heterolasers. Extensive introduction of heterolasers in an optical communications system is being delayed by the inadequate service life of serial models. Moreover, as was reflected in the lectures of Doctor G. H. Thompson and J. Diamond, laboratory service-life tests provide the basis to assume that this problem has been completely resolved since service-life values on the order of 10^4 hr in the continuous mode can be achieved at elevated temperatures. These results indicate that this level of durability will also become accessible for mass production in the near future.

The detailed processes which cause degradation of heterolasers were discussed in the lecture of Doctor H. Wulhaus (Optical Information Systems of the Exxon Company, United States) "Generation of Dislocations in Electrooptical Materials and Their Behavior During Optical Excitation." Methods of electronic microphotography permit expansion of the detailed structure of accelerated degration foci (so-called dark line and spot defects). Luminescent topography makes it possible to follow the growth kinetics of these defects. Doctor H. Wulhaus showed a movie in which the evolution of degration foci is shown in real time. Experiments indicate

the important role which mechanical stresses and dislocations in heterostructures play in acceleration of the degradation process.

Problems concerning the properties of deep luminescent centers in widezone materials were illuminated in the lectures of Doctor H. G. Grimmeis (Technological Institute, Lund, Sweden) "Deep Impurities in Semiconductors and Their Role in Electrooptical Devices" and of Dr. F. Ozel (National Center for Telecommunications Research (CNET), France) "The Use of Strongly Alloyed Rare-Earth Materials in Electrooptical Devices." Brief surveys of advances in various laboratories given outside the regular lectures by representatives of Poland, France, Great Britain, Canada and Japan aroused great interest.

Zh. I. Alferov, who expressed the common opinion about the exceptional importance and undoubted success of the Second International School of Semiconductor Electrooptics, gave a talk at the concluding session in the name of the participants with gratitude to the organizers of the school. Doctor M. A. Herman, chairman of the organizing committee of the school, gave some concluding words. He reported that the proceedings of the Second International School will be published in English under the title "Semiconductor Optoelectronics" (Proceedings of the Second International School on Semiconductor Opto-Electronics "Cetniewo-1978," edited by M. A. Herman, Polish Scientific Publishers, Warszawa, 1979) and will be distributed to the participants during the first half of 1979.* It is planned to hold the Third International School of Semiconductor Electrooptics at Cetniewo in 1981.

---

*Send orders to the address: ORWN (Osrodek Rozpowszechniania Widawnictw Naukowych) PAN, Palac Kultury i Nauki, Warszawa, Poland.

BIBLIOGRAPHY

1. Eliseyev, P. G. and M. A. Herman, KVANTOVAYA ELEKTRONIKA, Vol. 3, 1976.

6521
CSO: 1870

PUBLICATIONS

PERFORMANCE OF OPERATING SYSTEMS

Moscow KAK RABOTAYUT OPERATSIONNYYE SISTEMY (How Operating Systems Function) in Russian 1978 signed to press 15 Jun 78 pp 2-5, 191-192

[Annotation, foreword and table of contents from book by E. A. Trakhtenberg, Nauka Press 22,900 copies, 182 pages]

[Text] The book describes the principal functions of operating systems, their structure and their mode of operation. It discusses the kinds of these systems, their reactions to signals received from external devices, the computational situation and the manner in which the computer resources are taken into account, and the sequence of implementation of tasks is determined.

Foreword

The first computer employing electronic circuits to perform arithmetic and logic operations appeared in 1945. Since then, and until the present, computers have passed through three stages of development or, as the saying goes, three generations. Each computer generation differed from its predecessor in the components of its assembly, in its design and in its software.

The first-generation computers were of the vacuum tube kind. The number of tubes reached several thousand and they often broke down, so that computer reliability was low. The operating speed of these computers also was low. Essentially, they were large arithmometers. The computer then included an arithmetic device, a control device, a memory and several external devices. Computers of this kind virtually lacked any software except perhaps subroutine libraries. Programs for these computers were written in instruction codes or in primitive mnemocodes. During that period the concept of the "operating system" had not yet even existed.

The second-generation computers, which appeared in the 1950s, were already built from discrete semiconductor elements. Their reliability and operating speeds increased markedly, and their dimensions decreased. A large number of electromechanical memory devices and input/output devices had appeared. In operating speed these computers were markedly inferior to electronic processors and hence, to reduce processor idling, computer design was adjusted for

the introduction of interruption systems, memory protection and special apparatus for the control of external devices which made it possible to develop multiprogram systems. The computers were provided with algorithmic-language and code translators, sophisticated subroutine libraries and service systems assuring the adjustment of programs and solution of problems. The first operating systems, assuring packet, single-program and multiprogram operation, had appeared. The first series of joint-program machines were developed. The instruction system and the software of all the machines in a series of this kind was either the same or a component part of senior models with respect to junior models. Models in a series differed chiefly in productivity and direct-access memory volume. The more "senior" a model was, the greater its potential was.

Lastly, computers began to be designed on the modular principle. That is, they could be connected to varying numbers and types of external equipment, varying volumes of direct-access memory, or special units could be attached to the control device and arithmetic device, and so on.

The third-generation computers which appeared in the 1960s are based on integrated circuits, and their reliability and operating speeds are still higher while their dimensions are still smaller. In this connection, the hardware potential of computers has markedly increased, and their software has developed extraordinarily to where its cost has begun to exceed greatly the cost of the equipment upon which it operates. The development of series of computers has become the norm. The productivity of a junior model in the series may sometimes differ by a factor of tens of times from the productivity of the senior model.

The design of third-generation computers is characterized by both the further development of the hardware devised in the second generation as well as designing of new hardware. This primarily applies to hardware support for operating systems, including the development of microprogram control, addressing and input/output systems combined with fairly complex exchange devices termed channels. A typical example of the set of program-compatible computers of the third generation is the series of YeS computers.

The principal feature of the software of third-generation computers is the availability of sophisticated operating systems.

Operating systems are complex ensembles of programs controlling the computational process. They have relieved the programmer of a large part of the exhausting and laborious work connected with the programming "cuisine," and they have assured computer control. But unfortunately, their "control apparatus" has proliferated and the information links have become numerous and confusing.

This book is devoted to these unique and interesting control systems. It describes the nature of the operating systems, the manner of their response to the requirements of users, and to the signals received from various external

devices as well as to the operational situation arising in the course of computations. The book also describes how these systems allow for and distribute computer resources, programs and data files, how they determine the sequence of implementation of various tasks, and why they expend on "themselves" a substantial part of computer operating time.

The book may be of interest to specialists working with computers as well as to readers interested in computer methods of control.

Contents

	Page
Foreword	3
Chapter I. Introduction to Operating Systems	6
Classification and Design Principles of Operating Systems	6
Basic Functions and Structure of Operating Systems	13
Operating Features of Real-Time Operating Systems	21
Operating Features of Operating Systems in Computer Networks	30
Chapter II. Organization of Exchange With External Memory Devices	41
External Memory Devices	41
Distribution of Information on Carriers	48
Organization of Data in External Memory Devices	54
Data Exchange Control	63
Buffer Control	68
Virtual Memory	73
Chapter III. Preparing Users' Programs for Implementation	91
Program Modules	91
Assembling the Modules and Organizing Their Linkages	93
Program Loading	103
Libraries	107
Chapter IV. Description of Task and Its Preparation for Implementation	110
Description of Tasks	110
Preparation of Task for Implementation	117
Sample Program Selection Algorithm for Solution According to the Scalar Criterion	129
Sample Program Selection Algorithm for Solution According to the Vectorial Criterion	137
Chapter V. Controlling the Computational Process	147
Initiation and Completion of Tasks	147
Interruption System	151
Organization of Responses to Interruption	165

Time Service..... 176
Dialog With the Operator..... 178

Instead of a Conclusion..... 180

Bibliography..... 187

1386
CSO: 1870

UDC 621.396.96 (078.5)

THE THEORETICAL PRINCIPLES OF RADAR

Moscow TEORETICHESKIYE OSNOVY RADIOLOKATSII in Russian 1978 signed to press 12 May 78 pp 2-4, 604-607

[Annotation, foreword and table of contents from the book by A.A. Korostelev, N.F. Klyuyev, Yu.A. Mel'nik, A.A. Veretyagin, V.A. Gubin, V.Ye. Dulevich, Yu.S. Zinov'yev and A.V. Petrov, Sovetskoye Radio Publishers, 18,000 copies, 608 pages]

[Text] A systematic presentation of the principles of radar, a description of radar signals, questions of the synthesis of devices for detecting signals and measuring their parameters, and procedures for estimating target positions or the parameters of its motion based on measurement data are given in the book.

The presentation employs the statistical theory of space-time filtering: the initial signal is the electromagnetic field in the aperture of the antenna, while the radar itself is treated as a single space-time filter or correlator. The theory of the dynamic search and detection of signals is presented, as well as the various devices for processing them, including digital, optical and holographic ones. The theoretical fundamentals of the statistical synthesis of tracking meters are presented, and their curcuit designs, both analog and digital, are given. Methods of protecting against active and passive jamming are analyzed, including polarization methods and MTI circuits. Data is given on Lidar and thermal radar systems.

The book is intended for students in the radio engineering specialties of the higher educational institutes, and can also serve as a textbook for graduate students, engineers and scientific workers. Some 212 figures, 11 tables and 116 bibliographic citations.

Foreword to the Second Edition

Since the publishing of the first edition of the book, "The Theoretical Principles of Radar", the theory and engineering of radar havemoved far ahead. However, the new achievements in radar have not been adequately reflected in teaching literature. In this regard, the authors set themselves the goal

in reworking the book of methodically working out and presenting the theoretical principles of radar, including new sections, from unified scientific and procedural viewpoints. This required such a substantial revision of the material, that the revised edition offered to the readers here is in essence an entirely new book, both as regards contents and the method of presentation.

The basic directions of the revision reduced to the following.

1. The presentation of the material is based on the statistical theory of space-time filtering developed in recent years. This has permitted a description of the processes in the antenna and in the remaining receiving channel radar for a signal in the form of an electromagnetic wave as a function of time and space, from unified viewpoints. The description of the optimal space-time structures is given as applied to radars with phased and synthesized antenna arrays, working with both a reflected and a thermal signal, as well as applied to optical-holographic devices for signal processing.

2. The characteristics of resolving power, precision and uniqueness of the measurements are treated as a applied to any measurable parameter or set of parameters, which are then given specifically, something which has permitted curtailing the volume of the material through the elimination of repetitious calculations and discussions.

3. Dynamic signal search and detection theory is presented, which most completely describes the potential capabilities of radars having phase antennas and which are controlled by digital computers.

4. The statistical synthesis of tracking meters (automatic tracking systems) for a measurable process in the general case, encoded in the signal being received, is treated for the first time in textbook literature. Such an approach has allowed a more in-depth description of the properties of tracking meters in general and their specific designs, both analog and digital.

5. A description of optical and holographic signal processing methods is included, and more attention is devoted to digital processing.

6. The characteristics of radar signals, in particular the polarization characteristics, as well as methods of processing and selecting signals based on the utilization of these characteristics, are presented in a more thorough fashion.

7. A description of laser radar methods, employing laser radiation, is included, and the information on radiothermal radar observation is expanded, including a treatment of the questions of generating thermal images using synthesized antennas.

The personal theoretical and procedural developmental work of authors, as well as experience in the lectures they have given were widely used in

writing the book. In working on the book, the authors have made an effort to see that in terms of its scientific and procedural level, it meets the standards for a textbook for the higher educational institutes of the radio engineering profession. Also given in the book is material intended for use in the diploma project. It can be useful to engineers, graduate degree candidates and scientific workers studying new problems in radar.

The book was written by a large collective of authors under the general editorship of Professor V.Ye. Dulevich, and he wrote chapters 2 and 14. Chapters 1, 4 and 5 (with §5.3 and §5.4), and 9-13 were written by A.A. Korostelev, where 9.3 was written in conjunction with A.V. Petrov, chapters 3, 6-8 and §5.3 were written by N.F. Klyuyev, chapters 15, 19, §5.4, 17.1, 17.4 and the last section of §2.3 by Yu.A. Mel'nik, chapter 16 by V.A. Gubin, chapter 17 (with the exception of §17.1 and 17.4) by A.A. Veretyagin, chapter 18 by Yu.S. Zinov'yev and chapter 20 by A.V.Petrov.

The authors consider it their pleasant duty to express their gratitude to Professor S.Ye. Fal'kovich and the faculty of the department, headed up by Professor A.G. Saybelem, for their valuable remarks and requests which were made in editing the manuscript, as well as their gratitude to readers who expressed their opinion on the first edition of the book.

Table of Contents

Foreword to the First Edition 3

Chapter 1. General Information on Radar 5
1.1. Basic definitions 5
1.2. The classification of radar stations (systems) 7
1.3. The principles of measuring coordinates and their derivatives 11
1.4. Methods or measuring coordinates 16
1.5. The generalized structural configuration of radar systems 18
1.6. The design specifications of radar stations 21

Chapter 2. Radar Targets and the Characteristics of Return Signals 24
2.1. Producing radar return signals 24
2.2. Radar targets of the simplest configuration 31
2.3. The statistical characteristics of radar returns 36
2.4. Complex and group targets 48
2.5. Spatially distributed targets 50
2.6. Surface distributed targets 53

Chapter 3. Optimal Methods of Receiving Radar Signals 56
3.1. Evaluating reception quality 56
3.2. Optimal detection methods 59
3.3. Optimal methods of measuring signal parameters 63
3.4. The statistical characteristics of fluctuating interference 66
3.5. The optimal reception of radar signals in noise 68
3.6. Digital methods of detecting pulse signals 86
3.7. Calculating the output voltage of an optimum receiver by the complex envelope method 88
3.8. The effectiveness of optimum signal detection methods in the presence of fluctuating interference 91
3.9. Signal detection for the case of incomplete a priori data on the statistical characteristics of radar signals and interference 104

Chapter 4. The Space-Time Theory of Radar Signal Reception 109
4.1. The space-time description of the received radar signal(wave) 109
4.2. The space-time correlation function 113
4.3. The potential precision and resolving power when measuring a single parameter of a wave (signal) 117
4.4. The potential precision and resolving power for the case of the joint measurement of several signal parameters 128
4.5. The optimal receiver as a matched space-time filter or correlator 136
4.6. Space-time equivalency 145

Chapter 5. Radar Signal Processing Devices 152
5.1. Electronic analog devices for signal processing 152
5.2. Optical-acoustical analog devices for signal processing 157
5.3. Digital devices for processing pulse signals 168
5.4. Displays 171

Chapter 6. Target Search and Detection 181
6.1. General information on scanning methods 181
6.2. Types of sequential scanning of space 185
6.3. Target detection during radar scanning 189
6.4. Optimization of radar scanning 203

Chapter 7. Range Measurement 215
7.1. Methods of Range Measurement 215
7.2. The utilization of signals with a complex waveform in range measurement 223

7.3. Range measurement errors 233

Chapter 8. Radial Velocity Measurement 236
8.1. The basic relationships for the Doppler effect 236
8.2. The measurement of radial velocity with an unmodulated signal 240
8.3. Radial velocity measurement errors 244
8.4. The joint measurement of range and velocity 248

Chapter 9. Measuring Angular Coordinates and Angular Velocities 253
9.1. The potential direction finding precision and azimuthal resolving power 253
9.2. Amplitude and phase methods of direction finding 260
9.3. Direction finding by the analysis of a signal envelope 267
9.4. Synthesized antennas arrays 274
9.5. Measuring angular velocities 281

Chapter 10. The Design Principles of Tracking Meters 287
10.1. The structural configuration of a tracking meter 287
10.2. Descriminators 293
10.3. The extrapolator 302
10.4. The optimal structure of an extrapolator and tracking meter as a whole 311

Chapter 11. Range Tracking Meters 321
11.1. The functional schematic of a range tracking meter 321
11.2. The elements of analog range tracking meters 323
11.3. The circuits of analog range tracking meters 331
11.4. The elements of digital range tracking meters 337

Chapter 12. Velocity Tracking Meters 344
12.1. The specific features of the functional schematic of a velocity tracking meter 344
12.2. Analog circuits of velocity tracking meters 347
12.3. Digital discriminators 350
12.4. Digital frequency synthesizers 353

Chapter 13. Bearing Tracking Meters 360
13.1. The structure and classification of bearing tracking meters 360
13.2. Angular discriminators 362
13.3. Rotation synthesizers 369
13.4. The circuits and components of monopulse bearing tracking meters 378

13.5. Single channel bearing tracking meters with conical scanning 389
13.6. The digital logging of angular coordinates 392
13.7. Bearing tracking meter errors 395

Chapter 14. Radar Range 398
14.1. The radar observation range in free space 398
14.2. The radar observation range for the case of active transponding 402
14.3. The influence of ground returns on radar range 403
14.4. The influence of the earth's curvature on radar range 410
14.5. The influence of atmospheric refraction on radar range 412
14.6. The influence of electromagnetic wave attenuation in the atmosphere on radar range 416

Chapter 15. Atmospheric Errors in Radar Measurements 420
15.1. The influence of the atmosphere on the propagation velocity of radar waves and the signal waveform 420
15.2. Systematic errors in range measurement 425
15.3. Systematic errors in the measurement of the elevation angle 431
15.4. Systematic errors in the measurement of velocity 435
15.5. Random atmospheric errors in measurements 438

Chapter 16. Active Jamming and Methods of Combatting It 442
16.1. General information on active jamming 442
16.2. The spatial-power engineering relationships for radar surveillance and their suppression by active jamming 446
16.3. Methods of protecting radars against active jamming 453

Chapter 17. Protecting Radar Stations Against Passive Jamming 460
17.1. Protection methods 460
17.2. The physical principles behind Doppler methods of moving target indication 464
17.3. The effectiveness of MTI systems with period interlace compensation 474
17.4. The principles of polarization gating 484

Chapter 18. Optical Radar 495
18.1. The physical principles of optical direction finding 495
18.2. The scattering properties of targets and the characteristics of reflected signals in the optical band 503

18.3. The statistical characteristics of the signal and noise at the output of a photodetector 509
18.4. The optimal reception and the detection characteristics of a pulsed, incoherent optical radar system 514
18.5. The effective range of optical radar systems 520
18.6. Measuring the motion parameters of objects 521

Chapter 19. Radiothermal Radar 529
19.1. The characteristics of radiothermal radiation 529
19.2. The reception of radiothermal signals 541
19.3. Radiometer circuits 547
19.4. The space-time processing of radiothermal signals 551

Chapter 20. The Secondary Processing of Radar Measurement Results 567
20.1. The tasks of secondary processing 567
20.2. The identification of trajectories 571
20.3. The precision in the determination of the position and velocity vector of a target from measurement data 574
20.4. Determining the Parameters of trajectories from the data of redundant measurements 581
20.5. The specific features of the determination of the trajectories of maneuvering targets and nonmaneuvering objects 593

Bibliography 598

Subject Index 602

8225
CSO:1870

PUBLICATIONS

UDC 539.23+548.55

TRANSITION REGIONS IN EPITAXIAL SEMICONDUCTOR FILMS

Novosibirsk PEREKHODNYYE OBLASTI EPITAKSIAL'NYKH POLUPROVODNIKOVYKH PLENOK in Russian 1978 signed to press 29 Apr 78 pp 2, 272

[Annotation and table of contents from the book by L.N. Aleksandrov, Nauka Publishers, Siberian Department, 2,300 copies, 272 pages]

[Text] The physical laws governing the processes which occur with the formation and epitaxial growth of films and which cause the appearance of a transition region at the interface of the substrate and the film are treated in this book. The elimination or reduction of these regions is particularly important for semiconductor films in connection with their use in microelectronic, acoustical-optical, laser and other devices. The process of film growth is treated theoretically on the basis of probability statistical and kinetic methods. The influence of the chip-substrate (mismatching of the lattices and the moduli of elasticity, the orientation and processing of the surface, dopant-diffusion), the role of the growth processes (nucleus formation, the change in the microrelief of a surface, the distribution of the doping agents, the dynamics of dislocations), the influence of changes in the initial phase (the nonsteady-state nature of the modes, auto-alloying through a gas or liquid phase, the change in the growth conditions) are shown sequentially. Actual ways of eliminating transition regions in epitaxial structures are shown and experimental results are given which were obtained in the leading research centers in our country and abroad.

The monograph is intended for scientific workers and engineers, as well as for students of the higher educational institutes and graduate degree candidates specializing in the growth of crystals and films, solid state physics, semiconductor physics and semiconductor electronics.

Table of Contents

Foreword 3

Chapter I. The Epitaxial Films of Semiconductors and Transition Regions 6

1. The thickness inhomogeneity of epitaxial films, the transition region and dimensional effects 6
2. Germanium epitaxial films, methods of obtaining them and their properties 14
3. Gallium arsenide epitaxial films, methods of obtaining them and their properties 30
4. New film semiconductor materials in microelectronics 47
5. Polycrystalline silicon films in microelectronic devices 58

Chapter II. General Laws Governing the Growth of Epitaxial Films and the Formation of the Transition Region 67

1. A thermodynamic and kinetic treatment of epitaxial growth of semiconductor films 67
2. The statistical theory of the initial crystallization stage 73
3. The kinetics of the initial stage of layered epitaxial growth of films and the formation of the transition region 80
4. The influence of substrate surface orientation on the effective growth rate of an epitaxial film and the formation of a transition layer 85
5. Simulating the growth of the epitaxial films of semiconductors on an electronic digital computer 92
6. The interaction of screw dislocations with interphase boundaries in a substrate-film-transition region structure 97
7. The mechanism of film growth in the liquid phase epitaxy method 106

Chapter III. The Formation of a Transition Region and the Decisive Role of the Substrate 115

1. The preparation of the substrate surface for the epitaxial precipitation of films 116
2. The action of a substrate during heteroepitaxial deposition of films 122
3. The diffusion of impurities from the substrate in into the film 135
4. The influence of the change in substrate properties during heating 148

Chapter IV. The Formation of a Transition Region During the Growth of Films 154

1. The epitaxial growth of semiconductor films 154
2. The distribution of impurities and structural defects during the growth of films 166

3. Homoepitaxial growth of the films of an atomatically pure surface 177
4. The heteroepitaxial growth of silicon and germanium films 188
5. The formation of a transition region during the heteroepitaxial growth of cadmium sulfide films 202

Chapter V. The Formation of a Transition Region During a Change in State of the Initial Phase 212
1. The formation of a transition region during changes in the gaseous phase 212
2. The formation of a transition region during changes in the vacuum or liquid phase 228

Chapter VI. Ways of Decreasing the Transition Region in Epitaxial Structures 239

Bibliography 248

8225
CSO:1870

END